THE ROLE OF BIOMECHANICAL CUES IN MECHANOTRANSDUCTION AND BREAST CANCER METASTASIS

THE ROLE OF BIOMECHANICAL CUES IN MECHANOTRANSDUCTION AND BREAST CANCER METASTASIS

By

ARJUN RAHA, B.Tech

A Thesis Submitted to the Department of Mechanical Engineering and the School of Graduate Studies of McMaster University in partial fulfilment of the requirements of the Degree of Master of Applied Science

Masters of Applied Science — McMaster University

Department of Mechanical Engineering — Hamilton, Ontario, Canada

TITLE: The Role of Biomechanical Cues in Mechanotransduction and Breast Cancer Metastasis

AUTHOR: Arjun Raha

B.Tech (Biotechnology)

McMaster University, Hamilton, ON

SUPERVISOR: Dr. Fei Geng

NUMBER OF PAGES: xiv, 109

Lay Abstract

Breast cancer is the most common cause of cancer related deaths in women particularly when it spreads to the brain. The brain is composed of many different sub-locations comprised of different proteins that can change the tissue's stiffness. Breast cancer can detect these changes and become more aggressive in its growth using a combination of proteins such as yes associated protein (YAP) and Piezo1. How these proteins interact in the context of breast to brain cancer metastasis however is poorly understood. This project examined the effects of surface stiffness, on YAP, and Piezo1 activity to understand how breast cancer and brain cells react to changes in surface stiffness. Results showed that on stiff surfaces YAP activity affects cancer cell migration. Also, human brain tissue was found to vary in stiffness depending on the region examined. Future investigations may shed light on therapies that could take advantage of learnings in this area to better target the spread of breast cancer.

Abstract

Breast cancer metastasis to the brain is one of the most lethal forms of metastases. Metastasis is regarded as a non-random process governed by several biomechanical factors including tissue stiffness. As brain tissue is ultrasoft and extremely heterogeneous compared to breast cancer primary sites; how are breast cancer cells able to colonize the vastly different microenvironment of the brain? As a key protein of the Hippo pathway, YAP is regarded as a mechanotransducer that is sensitive to changes in substrate stiffness. Its biochemical activity is intertwined with Piezo1, a mechanosensitive ion channel activated through plasma membrane deformation. To impact cellular function, YAP enters the nucleus and binds to the TEAD transcription domain triggering downstream expression of proteins involved in cell motility, wound healing, and metastasis. In this work, triple-negative breast cancers (TNBC) were shown to experience greater migration rates on stiff surfaces compared to soft PDMS substrates. Concurrently, cells showed YAP nuclear localization in a stiffness dependent manner. Then, mechanical characterization of human brain tissue was performed to characterize the stiffness heterogeneity in the brain associated with region specific metastasis. Five to six regions of the brain from two different patients showed similar patterns of stiffness heterogeneity with the anterior regions being generally stiffer than posterior regions. As Piezo1 is directly linked with detecting changes in biomechanical stimuli, it was used as a readout of surface

stiffness to examine if cells in the brain could detect different regional stiffnesses. Comparisons of grey and white matter showed no significant difference in Piezo1 expression. As a drug screening framework, molecular dynamic simulations were performed to evaluate drug efficacy on well-characterized inflammatory mediators that are implicated in metastasis. These findings contribute to understanding the gap in knowledge surrounding the interplay between tissue stiffness and YAP mechanotransduction in the context of breast-to-brain metastasis.

Acknowledgements

With utmost gratitude, I want to thank my supervisor and mentor, Dr. Fei Geng. I could not have asked for a more open-minded and supportive professor to work with. His contributions through research ideas, career development advice, funding, and overall enthusiasm and passion for research have made my Master's experience truly enjoyable. I would also like to sincerely thank my co-supervisor Dr. Bill Wang for his mentorship on all things related to brain biomechanics. It was never a dull moment when he came to campus, particularly when squishing brains in ABB.

Thank you to all past and present members of the Geng Lab for their support in my research and as friends. Special thanks to Dr. Saeed Mohammadi who has been one of my closest friends and mentors in the lab. I appreciate our regular chess matches which have probably kept me sharp throughout my Master's. I'm incredibly grateful to Bonnie Chen who worked with me on the cancer research project and helped me get settled in the Geng Lab when I first started. A sincere thank you to Angela Sun, Minji Hong, Jatheeshan Raveenthiran, and Yuning Wu for your contributions to this work and your commitment to spending long hours in the lab working with me. Also, a huge thank you to Zhi Su for humoring me on some of the tougher days.

I don't know how I would have managed this journey without the support of my family. Thank you to my dad who has inspired me to enjoy the process of learning and asking questions that have truly shaped my personality

as a researcher and more importantly as a person. Thank you to my first lab instructor, my mom, for showing me just how similar lab work and cooking are and engraining good lab practices in the kitchen long before I even step foot in a lab. To my emotional support sister… thank you for being my best friend!

Finally, I want to express my immense gratitude to my friends of the "Mills Crew", "Hamilton Mandems", and "Everyday …" group chats for your support in life and by extension my Master's journey.

Table of Contents

List of Figures and Tables

List of Abbreviations and Definitions

BSA	Bovine serum albumin
DAPI	4′,6-Diamidino-2-phenylindole dihydrochloride
DMEM	Dulbecco's Modified Eagle Medium
ECM	Extracellular matrix
EMT	Epithelial-to-mesenchymal transition
FA	Focal adhesion
FFS	Fluid shear stress
FITC	Fluorescein isothiocyanate
GsMTx-4	Grammostola spatulate mechanotoxin 4
H&E	Hematoxylin and eosin
HA	Hyaluronic acid
HER2	Human epidermal growth factor receptor 2
IF	Immunofluorescent
LATS1/2	Large tumor suppressor 1/2
MCF-7	Michigan Cancer Foundation-7, a breast cancer cell line
MSC	Mesenchymal stem cells
N/C	Nuclear-cytoplasmic
O-GlcNac	O-linked -N-acetylglucosamine
PBS	Phosphate buffered saline
PDMS	Polydimethylsiloxane
TAZ	Transcriptional coactivator with PDZ-binding motif
TEAD	Transcriptional enhanced associate domain
TNBC	Triple-Negative Breast Cancer
YAP	Yes-associated Protein

Declaration of Academic Achievement

Arjun Raha contributed to the writing, experimental design, literature research, conducting of experiments, data analysis, interpretation of results, and figure generation for all chapters of this thesis

Dr. Fei Geng contributed to experimental design, writing, interpretation of results, and revision of all chapters of this thesis.

Dr. Bill Wang contributed to experimental design, procurement of brain specimens, and data interpretation in Chapters 3 and 4

Dr. Sheila Singh and her lab for their collaboration and assistance in procuring brain specimens

Dr. Aftab Taiyab for providing mouse retina specimens and guidance regarding histological staining

Wei Chen performed experiments and contributed to experimental design in Chapter 2

Dr. Saeed Mohammadi assisted in data analysis in Chapter 2

Angela Sun performed experiments in Chapter 2

Lily Zhong performed experiments in Chapter 2

Jatheeshaan Raveenthiran assisted in data analysis in Chapter 3

Minji Hong performed experiments in Chapter 4

Yuning Wu performed experiments in Chapter 4

Chapter 1

Chapter motivation and overview

The motivation behind this chapter is to provide a literature review of topics related to this project. Topics discussed in the introduction provide background information that serves as the basis for this research. Note that there may be overlap between information discussed as part of the introductions of this chapter and subsequent chapter introductions. Materials and methods are also included in this chapter that pertain to work done in all chapter of this thesis.

Introduction

1.1 Breast cancer metastasis

Cancer metastasis is the process by which cancer cells move from their initial location of incidence and travel to other parts of the body through the bloodstream or the lymphatic system [1], [2]. All breast cancers begin in the terminal duct lobular units (functional unit of the breast) of the collecting duct [4]. Metastatic breast cancer, however, typically spreads to the liver, brain, bones, or lungs [3]. In such instances, the newly established tumor is known as a secondary or metastatic tumor which is made up of breast cancer cells rather than the cells of the organ where the cancer has colonized. During this process breast cancer cells must break away from the primary tumor, enter the bloodstream, and survive a period of time in circulation before they extravasate and seed

themselves at a distal organ [2]–[4]. There are two high-level contributors to such metastases, the cancerous cells themselves (seeds), and microenvironment that they inhabit (soil) [5]. From the “seed” or cellular perspective, genetic mutations and subsequent alterations in metabolic activity are considered the hallmarks of cancer [8]–[11]. From the “soil” or microenvironment perspective, chemotactic signals, mechanical forces, and extracellular matrix composition are some of the key factors which govern breast cancer metastasis [12]. As such, the distribution of metastasis is considered a non-random process and each tumor type shows a distinct pattern of metastasis to specific vital organs, termed “organotropism” [5], [13]. The phenomenon of organotropism is a complex and dynamic area of research with recent focus on how the distal microenvironment influences metastasis [5], [7].

1.1.1 Mechanism of metastasis

The classical steps that characterize most metastases include (1) local invasion of cancer cells at the primary site, (2) intravasation, (3) survival in circulation, (4) extravasation, (5) and finally colonization of a distal secondary site [2], [14]. At the primary site, cancer cells initiate local invasion through morphological and phenotypical conversions such as epithelial to mesenchymal transition (EMT), the collective amoeboid transition (CAT), and the mesenchymal to amoeboid transition (MAT) [15]. Importantly, these morphogenetic changes are quite plastic as cancer cells may adopt different invasive morphologies based on their local microenvironment [16]–[18]. As local invasion progresses cancer cells eventually begin to enter the bloodstream, a process known as

intravasation [19]. Breast cancers leverage EMT to intravasate as it endows them with increased motility and permeability through endothelial barriers [20], [21]. In circulation, circulating tumor cells (CTC) are exposed to several selective pressures such as lack of anchorage, shear stress, exposure to reactive oxygen species, and immune cells [21], [22]. During intravasation, the shear stress experienced by cancer cells can also trigger EMT endowing them with the ability to modulate their morphogenetic properties to survive in circulation [22]. Some cancer cells also survive by entering a dormant state but retain their viability to ultimately grow into metastatic lesions [23]. Once tumor cells have reached the secondary site, they must emerge from a dormant state and/or alter their phenotype to bypass the endothelial layer once again [23]. This reverting of phenotype is known as a mesenchymal-epithelial transition (MET), a process that allows tumor cells to adhere to the endothelial wall and proliferate to eventually form a secondary metastasis [23], [24]. Factors such as mechanical properties, biochemical, and cellular signalling all influence the extravasation and colonization process [18]. The metastatic process however is considered highly inefficient [25] which is why the combination of oncogenic, epigenetic, and microenvironmental factors play a critical role in facilitating metastases and their locations.

1.1.2 Triple-negative breast cancer

Breast cancer is a clinically heterogeneous disease with different versions and pathologies stemming from benign to highly aggressive phenotypes [4]. One subtype is triple-negative breast cancer (TNBC) which accounts for 15-20% of all breast cancers

[26]. Triple-negative breast cancer is classified via the absence of three typical biomarkers observed in other forms of breast cancer: (1) the estrogen receptor (ER), (2) the progesterone receptor (PR), and (3) the human epidermal growth factor receptor 2 (HER2). Compared to other breast cancer TNBC shows higher proliferation, invasion, and metastasis particularly to bone, brain, and lungs [26], [27]. Typically, the disease presents itself as a high-grade-infiltrating ductal carcinoma identified through imaging techniques such as mammograms, ultrasounds, MRI, and/or biopsies [28]. TNBC also has various subtypes that encompass differences in genomic expression, histopathology, copy number, and mutational variations that govern the cancers' behaviour and the location of metastasis [29]–[31]. Overall, TNBC poses the worst prognosis compared to other types of breast cancer with greater migratory behaviour and a higher likelihood of early distal metastasis [27], [32], [33].

1.1.3 Breast cancer metastasis to the brain

Disseminated breast cancer cells can colonize a few different secondary sites, however, their colonization in the brain is regarded as the deadliest metastasis [3]. Typically, variants of TNBC such as MDA-MB-231-Br and MDA-MB-435 have a higher tropism for the brain compared to other breast cancer subtypes [34]. Patients with TNBC have a shorter time window to brain metastasis compared to other breast cancers, suggesting the innate ability of TNBC to adapt to the brain microenvironment [27]. TNBC also exhibits greater similarity to cancer stem cells (CSC) compared to other breast cancers which suggest they can manipulate their phenotype to adapt to the foreign

"soil" of the brain [35]. Preferential metastasis to the brain shows unique gene expression profiles [35] that up-regulate key enzymes and growth factors such as cyclooxygenase (COX2), HBEGF which is a ligand for epidermal growth factor (EGFR), and α2,6 sialyltransferase ST6GALNAC5 [33], [36]. This results in enhanced adhesion, invasion, and proliferation abilities to assist in brain colonization [33], [36].

Breast cancers can also manipulate the extracellular matrix in the brain microenvironment ultimately changing the tissue's mechanical properties [38]. Cancerous tissue obtained from brain metastases of breast cancer highly expressed hyaluronic acid (HA) which is a major component of the brain ECM [39]. HA is known to interact with the CD44 receptors on metastatic breast cancer cells which results in increased secretion of HA synthase leading to metastasis [40]. These ECM changes may be another contributing factor to the "toxic cycle" of cancer progression as breast cancers can re-organize the foreign ECM and adapt to grow on surfaces unique from their native microenvironment [41], [42]. Minimal data exist regarding the tumor-ECM interaction in brain metastases thus the search for putative markers that modulate the brain metastatic niche is critical in understanding the disease.

Brain metastasis has become increasingly common among patients who receive chemotherapy or targeted molecular therapies such as Herceptin (Trastuzumab) [34]. This is mainly because most chemotherapeutic agents do not cross the blood-brain barrier meaning the brain effectively becomes a sanctuary for breast cancer cells [34].

1.2 Biomechanical cues related to cancer metastasis

Biomechanical cues such as cell ECM stiffness, shear stress, and compressive stress play an important role in shaping cancer cells for metastasis and distal colonization [44]. The connection between tissue level biomechanics and their effect on biochemical signalling is mediated through a series of mechanosensitive molecules [45]–[48]. The growth of primary tumors creates solid stress which induces tensional force in and around the tumor microenvironment [49]. This paired with the activation of neighboring stromal cells that exhibit high contractility creates extracellular matrix anisotropy and stiffening, a feature correlated with tumor malignancy [44]. This process is best characterized as a feedback loop where increased tractional forces exhibited by tumors cells cause ECM reorganization resulting in oncogene activation and subsequent tumor cell proliferation [50]. In some instances, the stiffness of the ECM at a distal site can be altered before cancer cell invasion suggesting that compatible tissue biomechanics might be a precursor to metastasis [38], [51], [52]. As such, tissue stiffness is an important biomechanical property that is related to cancer metastasis.

Cancer cells also experience shear stress in lymph, blood circulation, and via interstitial flow within the tumor [53]. Increasing evidence suggests that low fluid shear stress (FSS) stimulates the activation of a series of cytokines and mechanosensitive molecules including IFF-2, VEGEF, ROCK, and Cav-1, triggering downstream biochemical signalling that promotes invasion and metastasis [50]–[52]. This is particularly relevant in the context of tumor extravasation as shear stress enhances cancer cell adhesion to inflamed endothelial cells through YAP, Abl1, and Lck-mediated

pathways [54]. In response to shear stress, breast cancers acquire mesenchymal stem-cell-like potential that promotes EMT transition, a well-characterized precursor to many metastases [55]. This demonstrates how shear stress can modify cell phenotypes which may aid in distal colonization. Similarly, shear stress can also activate YAP/TAZ and/or Wnt-β-catenin signalling to promote cancer cell migration and proliferation [53]–[55]. Additionally, TNBC that is mechanically preconditioned through shear stress shows tropism to the skull and brain demonstrating the role of biomechanics in distal metastases [54], [58]. Thus, shear stress is regarded as another biomechanical cue that can modulate both metastatic and organotropic properties of circulating cancer cells.

Compressive force is another biomechanical cue that contributes to tumor growth and invasion [59], [60]. Such forces arise in instances of uncontrolled growth in a confined space and cancer cell extravasation through tight cell-cell junctions [59], [61]. “Leader cells” are observed to arise when intratumoral compressive stress forces a subset of tumor cells to extend filopodia at the leading edge of a cell sheet [59]. This is accompanied by cytoskeletal organization showing elongated microtubules in the direction of migration [59]. As such, interstitial compression on tumors cells is thought to initiate “leader cell” formation and an invasive morphology [59]. Importantly, plasma membrane deformation in such instances triggers activation of migratory and pro-oncogenic pathways [62]–[64]. *In vivo* induced compression (comparable to pressure in growing tumors) over 1-month triggers β-catenin translocation from adherent junctions to the nucleus which is implicated in hyperplasia and tumorigenesis [65]. The resulting solid stress creates greater interstitial pressure and hypoxia triggering EMT which is correlated

with invasive phenotypes in cancer [61], [66]. Similar to ECM stiffness and shear stress, the level of solid stress cancer cells experience from compression produces analogous cellular responses [61]. Broadly, these include cellular stress fiber formation, increased expression of adhesion complexes, and EMT showcasing a common phenotype in response to biomechanical cues [61]. Thus, understanding the role of proteins that transduce one form of mechanical stimulus may simultaneously shed light on their implications in other mechanical cues.

1.2.1 Role of substrate stiffness in cancer progression

Tissue stiffening is a classic characteristic of solid tumors and in some instances is reflective of cancer progression [67], [68]. One of the major contributing factors to the local stiffening of cancerous tissue is the reorganization of ECM proteins such as collagen, fibronectin, hyaluronan, and other fibrous proteins and proteoglycans [68]–[70]. As the ECM becomes stiffer, cancers cells exert greater tractional forces and assume a tensile morphology through activated stress fibers which have downstream implications on cell adhesion, proliferation, and metastasis [71], [72]. This agrees with data showing the invasive front of human breast cancers is stiffer compared to adjacent normal stroma [68]. Note that collagen alignment also plays a role in guiding cancer cell migration, however, the density and level of crosslinking of ECM proteins are also elevated which correlates to greater substrate stiffness [73], [74].

The brain is the softest tissue in the body [75], [76], and like breast cancers, primary brain cancers such as glioblastomas (GBM) show comparable growth patterns on

stiff substrates showcasing increased metastatic potential [77], [78]. This pattern of growth might also allude to similar mechanotransduction features between the two cancer subtypes given the propensity of breast-to-brain metastasis. For example, primary brain cancers produce dense Tenascin-C and hyaluronic acid networks resulting in ECM stiffening [78]. This correlates with increased GBM invasion and integrin-based adhesion suggesting that glioblastomas can modify their microenvironment to create biomechanically favorable growth mediums [38], [71]. Brain tropic breast cancer MDA-MB-231-Br cells also seem to be less perturbed by the relatively soft substrate stiffnesses of the brain compared to their native ECM [79]. Specifically, migration and proliferation rates of brain tropic TNBC cell lines are increased on soft substrates compared to typical MDA-MB-231 cells [79]. This suggests that brain tropic TNBC might have adapted mechanotransduction features that enable growth on brain mimetic stiffnesses [79], [80]. At the macroscopic level, however, the effect of tissue stiffness is less clear with contradictory evidence correlating tissue stiffness and metastasis [81], [82]. This begs the question whether cells display an analogous response to stiffness at the tissue scale compared to single cells. Given the sparsity of research regarding mechanotransductive adaptation employed by brain tropic breast cancers [79], studying glioblastomas may provide clues regarding the adaptation required for brain metastasis [83], [84].

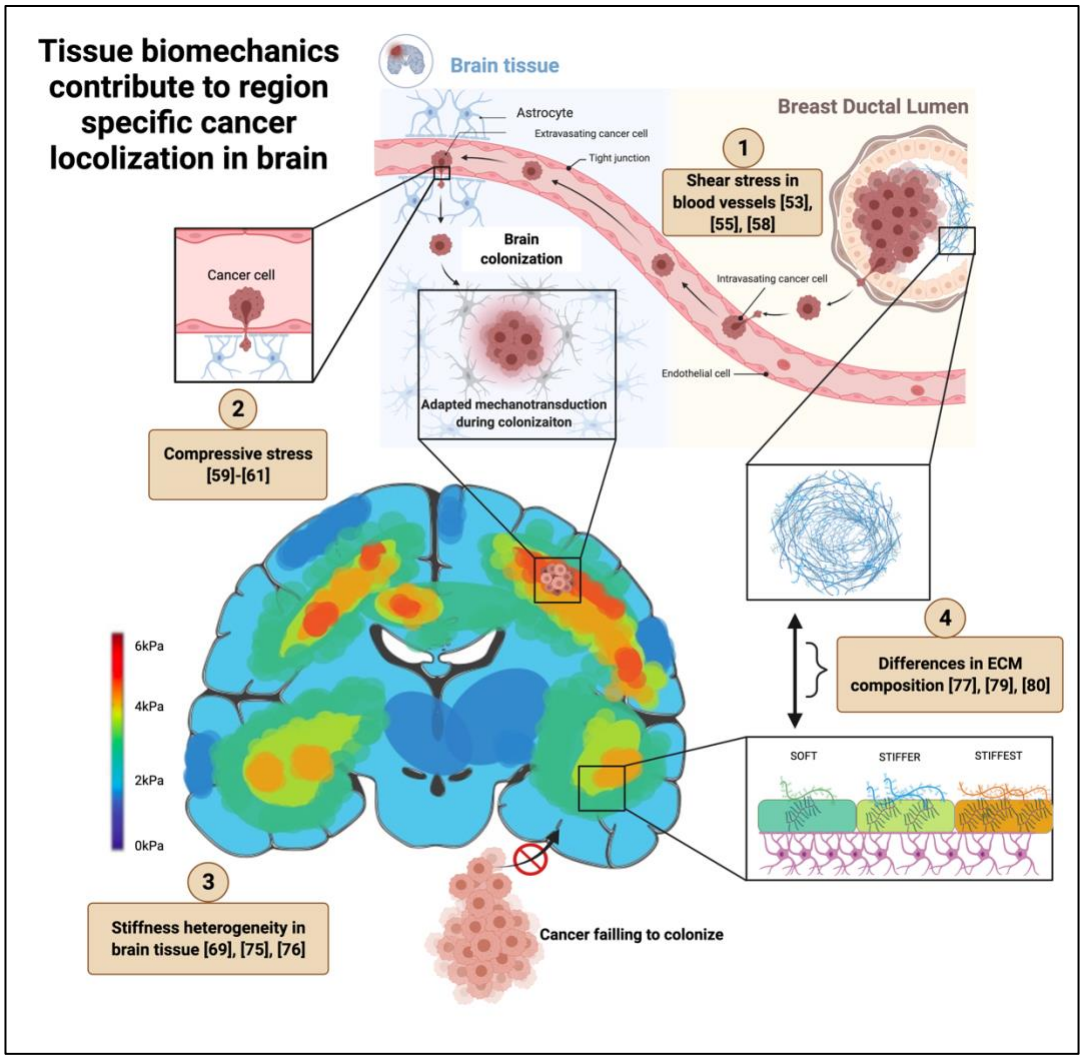

Figure 1: Summary of biomechanical cues in breast to brain cancer metastasis. **(1)** During extravasation breast cancer cells experience shear stress from entering the bloodstream. This can lead to the acquisition of mesenchymal stem cell-like potential that promotes EMT. As such, cancer cells gain the ability to drastically adapt their physiology to colonize an array of distal organs and even develop chemoresistance. **(2)** Breast cancers also experience compressive stress during passage across the endothelial barrier and via cell-cell contact during uncontrolled growth in confined tissue architecture. These compressive forces can drive gene expression that favours proliferation and ultimately induce a metastatic phenotype. **(3)** Further, breast cancers with a propensity for metastasis are extremely adaptable with the ability to grow on various substrate stiffnesses. Brain tropic breast cancers also seem to prefer relatively a soft substrate which is unique from many other metastatic cancers. **(4)** Finally, the differences in ECM composition contribute to both biomechanical differences between primary and secondary sites but

also induces cancer adaptations to favour colonization. As such, there is evidence to suggest that the biomechanical forces may shape their propensity for metastasis to specific organs and even sub-locations within the tissue. Figure created with BioRender.com.

1.3 Mechanotransduction in cancer progression

Mechanotransduction is the process cells use to sense and convert mechanical stimuli from their environment into biochemical signals that guide intracellular changes such as ion concentrations, and activation of signalling pathways [85]. Cells form discrete multiprotein complexes called focal adhesions (FA's) that aid in mechanosensing of stiffness and other mechanical cues to the cytoskeleton [85]. As such, FA's act as the main hub of cell-ECM interactions showing analogous organization in response to surface stiffness, cellular stretching, and cellular density [85]. Evidence shows that FA expression results in activation of mechanosensitive transcription factors YAP/TAZ [86], [87] demonstrating how mechanical cues can regulate intracellular trafficking. Elosegui-Artola et al.(2017), propose a connection between FA activity, cytoskeletal tension, and YAP translocation showing that the application of force opens nuclear pores through cytoskeleton reorganization and facilitates YAP nuclear entry [88]. This mechanism could regulate other mechanosensitive transcription regulators such as β-catenin, as the mechanical strain upon tissues and membrane deformation from tumor growth facilitate its' nuclear entry [89], [90]. Given that YAP and β-catenin are key regulators of the Hippo and Wnt signalling pathways (pathways that facilitate organ growth, cell migration, and angiogenesis), perturbations in mechanotransduction as observed in cancers may alter their activity in response to mechanical stimuli [47], [86], [91], [92].

Thus, further understanding the mechanotransduction cascade in cancer may uncover potential therapeutic targets.

1.4 Role of Piezo proteins in mechanotransduction

Various types of cells including cancer can transduce physical stimuli into biochemical signals using the Piezo family ion channels [63], [93]. Piezo1 and Piezo2 are the two main isoforms and are evolutionarily conserved in animals, plants, and protozoa [94]. These channels are activated by membrane deformation which occurs when cells experience physical forces through shear stress, substrate stiffness, osmotic pressure, and confinement [95]. When active, the channels open, allowing for calcium influx thus transducing mechanical forces into biochemical signals [64]. The homotrimer structure of Piezo proteins consist of three propeller-like blades situated on the extracellular region of the plasma membrane, a single extracellular cap, an intracellular anchor, three intracellular beam regions, and a pore conducting path [96]. Briefly, the blades of Piezo1 sense the deformation in the cell membrane, creating a force that is intracellularly transmitted [64], [97]. The intracellular beams act to amplify the force imparted on the blades like a lever-based apparatus that pull on the central pore, opening the cap, and triggering calcium ion flux [64], [96], [97]. Calcium is associated with many signalling pathways involved in cancer metastasis such as angiogenesis, cell migration, intravasation, and proliferation [64], [98]. Disruption of calcium homeostasis is known to enhance hallmarks of cancer such as apoptosis, cell migration, invasion, and metastasis [93]. Upon stretching or wounding, the fast proliferation response generated by epithelial

cells was shown to be unambiguously dependent on Piezo1 function [63]. One theory is that Piezo1 interacts with extracellular signal-regulated kinase 1 (ERK1), a calcium-activated kinase that plays a role in controlling the G2/M transition in cell proliferation [63], [93]. Considering that proliferative pathways are hijacked by cancer cells; Piezo proteins may serve as a promising therapeutic target for limiting uncontrolled growth [99]–[101].

1.4.1 Piezo channels in breast cancer

Both isoforms of the Piezo family contribute to the migration and metastatic capability of breast cancer [102], [103]. Piezo1 is considerably increased in MCF7 cell lines, a model of primary invasive ductal carcinoma compared to the non-invasive subtype MCF10A [102]. Using non-specific blockers for Piezo channels like tarantula toxin *Grammostola spatulate* mechanotoxin 4 (GsMTx-4), the migration of MCF7 cells can be inhibited [102]. Patients with high levels of Piezo1 mRNA expression in primary tumors show a shorter overall survival time demonstrating the oncogenic role of Piezo1 in this version of breast cancer [102]. Given that other types of breast cancer likely share similar functional pathways utilized for proliferation and metastasis Piezo1 may serve as a potential therapeutic target in inhibiting more than one subtype of invasive breast cancer.

Similarly, Piezo2 has also been implicated in modulating breast cancer migration. Piezo2 is shown to be over-expressed in triple-negative breast cancer MDA-MB-231-BrM2, which is known to metastasize to the brain [103]. Activation of Piezo2 is shown to

generate Ca^{2+} influx which regulates cytoskeleton remodelling through the RhoA-mDia pathway and knockdown of Piezo2 subsequently decreases the metastatic potential to the brain [103]. Using their MDA-MB-231-BrM2 model Pardo-Pastor et al. suggest that the mobilization of Fyn kinase and subsequent activation of calpain may be a mechanism that contributes to RhoA activation which ultimately modulates proliferation, invasion, and metastasis [103]. Piezo2 expression was also found to be positively correlated with estrogen receptor (ER) status but negatively correlated with triple-negative status of breast cancer [104]. Patients with triple-negative breast cancer typically have low expression of ER receptors which correlates with lower Piezo2 expression compared to ER-positive cancer subtypes [104]. Low Piezo2 expression is correlated with a poorer prognosis and inhibition of Piezo2 correlates with dysregulation of the Hedgehog signalling pathway responsible in part for cell adhesion, proliferation, and migration [104]. For this reason, Piezo2 might serve as a prognostic marker in breast cancer progression.

1.4.2 Piezo channels in glioblastomas

Glioblastomas (GBM) are the most common form of brain cancer which originates from glial cells [105]. In a Drosophila model, Chen et al. examined the role of Piezo channels in the tumor microenvironment [106]. Their results demonstrate that stiffer tumors upregulate Piezo1 activity, thus enhancing mechanotransduction events and further exacerbating GBM development and cancer cell proliferation [106]. The underlying mechanism is hypothesized to foster the Ca^{2+}-dependent assembly of focal

adhesions triggered through stretch activation of Piezo1 leading to integrin-FAK signalling [106]. Given that FAK assembly is involved in cytoskeleton polymerization and cell motility, Piezo1 over-activation because of stiffer substrates may generate a feed-forward mechanism that contributes to cancer metastasis [106]–[108]. Further, Piezo2 knockdown has been reported to increase apoptosis, reduce cell proliferation, and angiogenesis in nude mice [109]. It is thought that Piezo2 is related to Ca^{2+}dependant overexpression of Wnt11 which is secreted by endothelial cells [109]. This boosts their angiogenic potential via β-catenin dependant signalling, hence Piezo2 downregulation in tumor endothelial cells results in inhibition of glioma tumor growth with reduced migration and invasion [109]. As such, Piezo1 and Piezo2 may play different roles in glioblastomas, however, both isoforms might be leveraged to adapt mechanotransduction for invasion within the brain.

1.5 Role of YAP in mechanotransduction

Yes-associated protein (YAP) is a key transcription factor in the Hippo signaling pathway. It functions in cooperation with transcriptional coactivator PDZ-binding motif (TAZ), to regulate cell proliferation, organ development, and stem cell self-renewal [110], [111]. Given these processes are dependent on the physical properties of the ECM and mechanical forces, YAP/TAZ are functionally required to sense mechanical cues through mechanotransduction [112]. Most YAP regulation occurs through the hippo pathway mediated by large tumor suppressor 1 (LATS1), and LATS2 which are inhibitors of YAP/TAZ [111]. They phosphorylate YAP which primes it for cytoplasmic retention

and subsequent degradation [111]. YAP/TAZ appear to act as nuclear relays of mechanical signals exerted by ECM rigidity and cell morphology [112]. This mechanism requires Rho GTPase activity and tension of the actomyosin cytoskeleton but is independent of the Hippo/LATS cascade [113]. It is also proposed that cell fate induced by stiff ECM and cell stretching should activate YAP, while a soft ECM and compact cell area should render it inactive [113]. Note that in either instance membrane deformation and cytoskeletal tension play a pivotal role in initiating and transducing force to YAP which then regulates downstream biochemical signals [113] [88], [114]. Interestingly, MSC differentiation to osteocytes is inhibited on stiff substrates when YAP is inhibited, while adipocyte differentiation which is not normally seen on stiff substrates becomes possible through YAP inhibition [113]. This suggests that perturbations in YAP mechanotransduction may allow cells to proliferate in atypical microenvironments providing a link to possible mechanisms for organotropic cancer adaptations [46], [91], [115].

1.6 Connecting YAP modifications and mechanical cues in metastasis

Traditionally, phosphorylated YAP (pYAP), is sequestered in the cytoplasm and primed for proteasomal degradation and subsequent down-regulation for β-catenin and Wnt signalling [113], [114]. In such instances, cells take a less invasive phenotype with lower proliferation and migration rates [46], [113]. O-GlcNacylation is the addition of sugars onto serine or threonine hydroxyl moieties and is an important protein

modification as it regulates the intracellular localization of YAP [116]. Aberrantly increased O-GlcNacylation has emerged as a cause of hyperactivation of YAP in cancer cells [117]. This is thought to disrupt YAP's interaction with upstream kinase LATS1 preventing YAP phosphorylation and degradation [116]. In contrast to pYAP, glycosylated versions of YAP (O-GlcNac-YAP) initiate nuclear translocation resulting in activation of TEAD transcriptional activity and subsequent proliferation and tumorigenesis [116]. The formation of actinomycin stress fibers has been shown to upregulate LATS activity, YAP nuclear entry, and increased proliferation, while the opposite effect occurs when stress fiber formation is inhibited [118]. It is known that mechanical cues such as surface stiffness induce the formation of stress fibers which are also correlated to a metastatic phenotype [61], [68], [71]. It is unclear whether YAP in such instances is O-GlcNacylated, however considering the correlations between mechanical cues, stress fiber formation, LATS activity, and YAP modification the glycosylation status of YAP may play a supporting role in facilitating this mechanotransduction cascade [87], [91]

1.7 Role of Wnt/β-catenin in mechanotransduction

It is well established that ECM stiffness plays a significant role in regulating cell morphology and behaviour [68], [119], [120]. Wnt/β-catenin signalling is another mechanotransduction pathway in addition to Hippo mechanisms driven by YAP/TAZ which can be activated through mechanical strain [89], [90]. β-catenin has two functions: (1) it mediates cell-cell adhesions through cadherins complexes required for structural

integrity and functional polarization of tissue structures; (2) it serves as a transcription factor of the canonical Wnt signalling pathway [121]. Stiff ECMs have been shown to activate several members of the Wnt/β-catenin pathway seemingly driven by integrin and FAK assembly [120]. Stem cell lineage is largely driven by integrin-β-catenin interactions where stiffness modulation can induce bone marrow MSCs to take on neuronal lineage when cultured on brain mimetic stiffnesses (1-2kPa) [120]. β-catenin is shown to play a similar role to YAP in some instances as it tethers Piezo channels to the actin cytoskeleton, thus converting mechanical tension into ion influx required for tissue homeostasis [122]. Perturbations in Wnt/B-catenin shuttling is linked to many diseases including cancer [47], [123]–[126]. As such, investigating the role of B-catenin and its interaction with the ECM and transcription factors like YAP may help to elucidate overlapping mechanisms for mechanotransduction and new targets for disease therapeutics.

1.7.1 β-catenin involvement in metastasis

Through its dual function, B-catenin contributes to cadherin-mediated cell-cell adhesion, and it determines the transcription output of the Wnt signalling pathway [121]. During malignant progression, epithelial cancer cells dissolve their cell-cell adhesion and gain invasive features [121] hence β-catenin is considering a contributing protein in cancer metastasis [121]. In mouse mammary carcinoma, complete knockdown of β-catenin function leads to massive apoptosis of mammary tumor cells, while loss of β-catenin's transcriptional activity resulted in a reduction of primary tumor growth, tumor

invasion, and metastasis [121]. Thus, targeting β-catenin in its role as a transcription factor could be a possible therapeutic target for various cancers [127]. Given that cancer-associated fibroblasts (CAFs), contribute to both ECM degradation and remodelling which are precursors to metastasis [128], Liu et al. accessed the effect of B-catenin inhibition on CAF related ECM remodelling [129]. They found that collagen fiber thickness, alignment, and connectivity were all reduced, and CAFs had significantly less contractile activity when β-catenin was inactivated [129]. Further, the pro-migratory role of β-catenin is also demonstrated as inhibiting its activity slows the migration front in scratch assays [129]. As such, it is hypothesized that β-catenin plays an important role in ECM remodelling, and inhibiting its activity suppresses communication between the ECM and intracellular trafficking events [127]–[129]. This effect also transfers over to other signalling pathways as β-catenin ablation affects YAP nuclear translocation and subsequent downstream effectors involved in metastasis [129]. This crosstalk between Wnt/β-catenin activity and YAP in the Hippo pathway suggests certain redundancies and combinatory effects of both transcription factors in mediating metastasis [130], [131].

1.8 Summary

The microenvironmental factors that play a role in breast cancer metastasis have received relatively little attention compared to genetic and epigenetic contributors. TNBC is one of the most aggressive subtypes of breast cancer and its metastasis to the brain indicates a poor prognosis. This form of metastasis exposes cancer cells to drastically different microenvironments which have different ECM compositions and stiffnesses.

How long are breast cancer cells able to adapt to such a drastically different microenvironment? Drawing comparisons between breast and brain cancer such as similar growth patterns on stiff substrates, sensitivity to ECM components like HA, HER2 expression, and genetic/epigenetic homology could help uncover the adaptations required for specific metastases. Still, little is known about how cancer cells adapt their mechanotransduction to such cues in favour of metastasis. Certain mediators of mechanotransduction such as YAP and β-catenin are known to be activated in metastasis and respond to biomechanical cues. Their activity, overlap, and interaction with other mechanotransduction proteins such as the Piezo family of transmembrane ion channels might shed light on how tissue biomechanics impact intracellular trafficking. Nuclear localization of YAP is associated with TEAD transcriptional activity which triggers angiogenesis, increased proliferation, and metastasis. Given that YAP localizes to the nucleus when cells are cultured on stiff substrates and when YAP is O-GlcNac modified a possible connection might exist between YAP glycosylation status and mechanotransduction. While YAP contributes to many processes related to mechanotransduction and cancer metastasis, β-catenin is another protein that behaves similarly in the Wnt signalling pathway. Its dual role and membrane adhesion protein and transcription factor allow it to interact directly with mechanical cues from ECM and transduce these signals to the nucleus. YAP and β-catenin are thought to play a cooperative role in breast cancer however the nature of this interaction in breast to brain cancer metastasis remains elusive. Here, it is proposed that tissue stiffness regulates the

expression of mechanosensitive proteins such as Piezo1, triggering glycosylation of YAP, and mediating its localization to the nucleus which initiates the metastatic cascade.

1.9 Thesis objectives

The objective of this master's thesis is to investigate the interplay between substrate stiffness, Piezo mediated mechanotransduction, and its connection to YAP signalling in hopes of demonstrating a mechanism with therapeutic targets for breast cancer metastasis. This research divides these overarching objectives into smaller objectives which are investigated in the following chapters and summarized in a conclusion. Chapter 2 aims to showcase how the tools and experimental systems were established to tackle the overarching objective of this research including information such as method validation, and system troubleshooting. Chapter 3 showcases the level of stiffness heterogeneity in biological tissues like the brain which is known to be a lethal site of metastasis for breast cancer. This chapter also discusses the biomechanical model used and associated challenges with mechanical testing of biological tissue. Finally, Chapter 4 outlines how the heterogeneity in stiffness at the tissue scale is transduced by the cells using mechanotransduction biomarkers

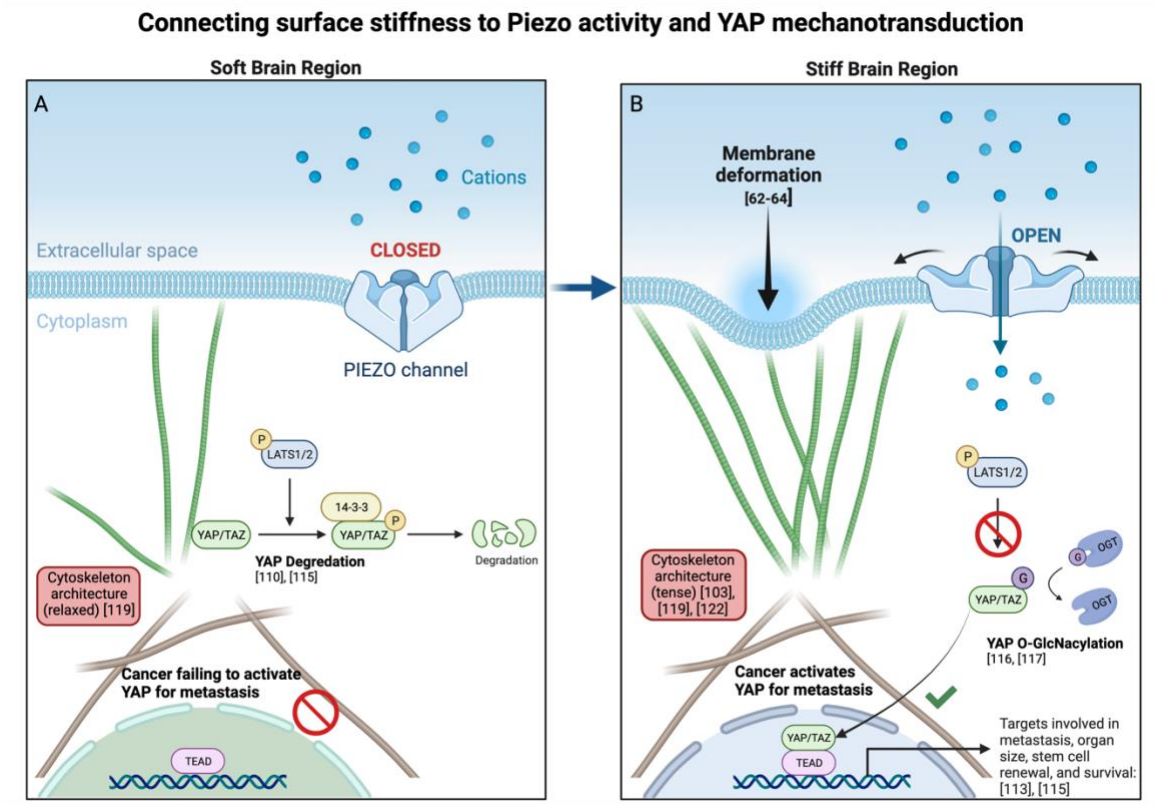

Figure 2: Proposed interplay between surface stiffness, Piezo channel activity, and YAP mechanotransduction. (A) On soft surfaces, the cell membrane experiences minimal deformation through cytoskeletal tension which translates to Piezo channels remaining closed and inhibited influx of cations. Piezo1 is known to be upstream of YAP however the exact nature of their interaction is still unclear. When YAP is allowed to be phosphorylated it is primed for cytoplasmic degradation. (B) In contrast, when membrane deformation occurs, Piezo channels become active allowing cation influx. This is correlated with YAP activation and nuclear entry which may be mediated by an O-GlcNacylation process via the enzyme O-GlcNac transferase (OGT). Once in the nucleus, YAP can bind to TEAD transcription domains and activate pathways involved in metastasis, organ size, cell stemness, and survival. Figure created with BioRender.com

1.10 Note to reader

The materials and methods section as well as some data from chapter 2 are cited from published work with permission under the author's rights from the respective journal.

Materials and Methods

1.11 PDMS fabrication

PDMS is fabricated via the addition of two components, an elastomer base (component A) and a curing agent (component B) both of which are transparent liquids. The elastomer base contains linear PDMS pre-polymers with two vinyl end groups that react with the component B multifunctional crosslinker leading to a three-dimensional crosslinked network. The resulting reaction is a hydrosilylation reaction that is well characterized and reported in literature [132]. Since PDMS is hydrophobic surface treatment is required to allow cell attachment hence oxygen plasma treatment and an extracellular matrix coating are applied [86].

Polydimethylsiloxane (PDMS) (Sylgard® 184, Dow Corning) base and crosslinker were mixed at three different ratios (by weight) of 1:5, 1:10, and 1:20 as described previously (Park et al., 2010). Mixtures were poured onto prepared 24- well plates (Thermo Fisher Scientific), cured at room temperature overnight (Figure 3). Resistance to deformation is defined by Young's elastic modulus, E, obtained by applying a tensile force (stress) to a sample with a defined cross-sectional area and measuring the relative change in length (strain). PDMS stiffness was measured by microindentation using a Biomomentum Mach-1 system (Biomomentum Inc) as described previously (Ireland et al., 2020). The base reagent is known to contain 0.5% xylene, 0.2% ethylbenzene, 60% dimethyl vinyl terminated dimethylsiloxane, 30–60% dimethylvinylated and trimethylated silica and 1–5% tetra (trimethylsiloxy) silane. Crosslinking agent contains 0.19% xylene, 0.1% ethylbenzene, 55–75% dimethyl, methylhydrogen siloxane, 15–35%

dimethylvinyl-terminated dimethyl siloxane, 10–30% dimethylvinylated and trimethylated silica and 1–5% tetramethyl tetravinyl cyclotetrasiloxane. The standard ratio for PDMS preparation is 1:10 as per the instruction of PDMS supplier Dow Corning. 1:5 and 1:20 ratios were chosen to extend PDMS stiffness ranges to identify the responses of breast cancer to matrix stiffness[1].

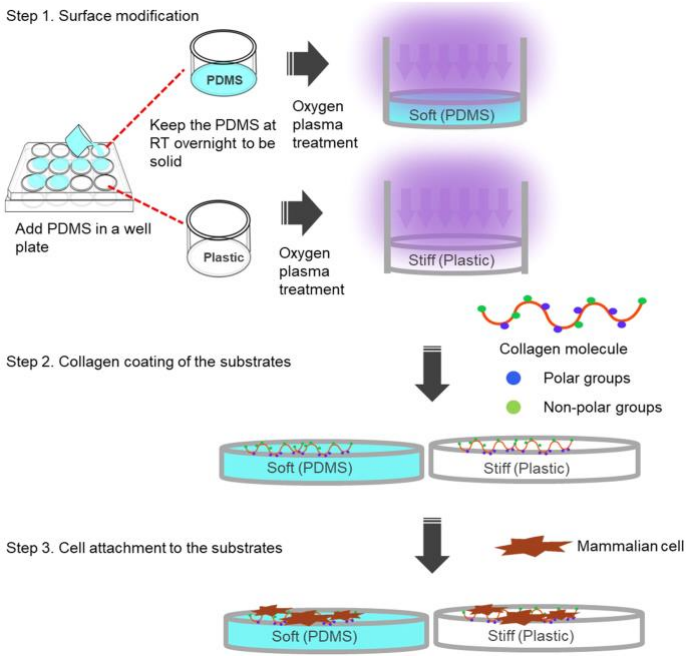

Figure 3: The preparation of PDMS and plastic substrates for mammalian cell culture[1].

1.12 Mechanical testing

1.12.1 PDMS testing

In preparation for testing three stiffnesses of PDMS were prepared by mixing different ratios of crosslinker to base (1:5, 1:10, and 1:20) in a 24 well plate

[1] Chen, W., Park, S., Patel, C., Bai, Y., Henary, K., Raha, A., Mohammadi, S., You, L, & Geng, F. (2021). The migration of metastatic breast cancer cells is regulated by matrix stiffness via YAP signalling. Heliyon, 7(2), e06252. https://doi.org/10.1016/J.HELIYON.2021.E06252

(Supplemental Figure 1) (Fig. S1). According to manufacturer instructions and literature, the ratio is proportional to the stiffness of the substrates [133]. To examine if the height of the sample was implicated in the stiffness, two masses of PDMS were also prepared in 1g and 2g quantities which created different heights between the samples once cured. The Mach-1 compression machine (Biomomentum Canada) with uniaxial indentation mode was used to characterize the material stiffness (Fig. S2, S3). Initially, the load cell with 1.5N capacity was calibrated using the manufacturer specified calibration weight. Using a spherical indenter with a 2mm diameter the height of the PDMS was then measured by taking an initial height of an empty well (height of zero) by lowering the indenter slowly until the instance force was detected. At this point, the height and load were set to zero and the process was repeated in a well with PDMS. The height difference was recorded as the sample thickness. Parameters such as the amplitude of indentation (10% of sample height), sample height, and velocity of indentation (1% of sample height in mm/s) were inputted into a pre-set compression test sequence and the machine was allowed to carry out the single indentation test. Once complete the sample height, and indenter geometry was inputted into the Mach-1 analysis software. A poison ratio of 0.3 was set for the Youngs modulus calculation as the material is assumed to behave elastically [134]. Young's modulus values were recorded, and subsequent data analysis was performed in Graphpad prism using student's t-test to compare mean stiffness values between groups.

1.12.2 Tissue testing

1.12.2.1 Tissue preparation

NOD SCID gamma mice (approx. 5 weeks old; male) were deeply anesthetized by intraperitoneal injection of Avertin© (tribromoethanol; 0.02ml/g of 1.25% solution). Once anesthetization was confirmed with loss of toe-pinch reflex, mice were decapitated with surgical scissors. An incision was made down the midline of the scalp from the neck to between the eyes. The skin of the head and face was pulled from posterior to anterior on either side of the head, exposing the skull. Removing the skin would usually remove the eyes from the sockets, after which the optical nerve was severed with surgical scissors, and the eyes transferred to ice-cold 4% paraformaldehyde (PFA). If removing the skin did not remove the eyes from their sockets, they were carefully removed by inserting one arm of narrow forceps into the socket behind the eye and gently prying out. Following eye removal, a small (approx. 3mm) incision was made with surgical scissors at the skull posterior, from the middle of the foramen magnum. Starting at this incision, sections of the skull were gradually removed by prying off small sections with forceps until the entire brain was exposed. Once exposed, the brain was gently removed from the skull by inserting forceps under the anterior of the brain and prying out of the skull while severing cranial nerves. The brain was then placed in ice-cold PBS.

Fresh human brain specimens were taken from two donors: (1) a 58-year-old male with right temporal glioblastoma treated with resection, chemotherapy, and radiation, who succumbed to disease progression; (2) a 78-year-old female with bilateral frontal

glioblastoma that never received treatment and passed away. Regions of the Cortex, Basal Ganglia, Thalamus, Caudate head, Pons, Cerebellum, Cervical spinal cord, and Corpus callosum were harvested by Dr. Bill Wang. Some areas of the cortex were sub-sampled including grey matter, white matter, and the grey-white matter junction. All tissues were placed into ice-cold PBS and collected within 12 hours post-mortem. All mechanical testing was performed 24hrs post-mortem.

1.12.2.2 Tissue compression testing

Mechanical testing was performed using the Microtester from CellScale (Fig. S5). The apparatus uses a piezo-electric actuator (0.1μm resolution) to compress samples with force resolution down to 10nN. The tester also uses a high-resolution CCD imaging sensor to track the displacement of the sample and cantilever beam deflection throughout the testing procedure. Appropriate cantilever beam diameters were selected based on the type of compression testing performed (0.2032mm for quasi-static compression, 0.5588mm for stepwise-ramp compression). In preparation, a 3mm biopsy punch was used to extract cylindrical cores of brain tissue which were loaded onto the testing stage and flooded with PBS. The sample was positioned under a 6mm x 6mm metal platen which was attached to the appropriate cantilever beam. The platen and cantilever were lowered to contact the brain specimen ensuring that the platen contact was flush against the sample. Using the high-resolution camera, the height and average sample width were measured and recorded in the software SquisherJoy.

Two types of compression tests were performed on the various regions of the brain including a quasi-static compression and stepwise-ramp compression. The quasi-static compression consisted of a gradual compression of the tissue up to 10% strain over ten minutes. Stepwise ramp compressions consisted of cyclic loading of the tissues at 2.5%, 5%, 7.5%, and 10% strain. The compression profile is as follows: (1) 20 second compression up to a given strain, (2) 10 second "hold" period where the platen remains at a constant displacement and the average force is measured, and (3) 20 second recovery period where the sample is de-compressed. Young's Modulus was obtained by plotting the stress vs strain curve in Matlab and taking the slope of the elastic region (2.5% compression) for quasi-static compressions. The relaxation modulus was obtained by curve fitting the region of stress relaxation from 7.5% stepwise compression. A Zener model was applied to correctly fit the stress relaxation behaviour of the tissue using the following equation: $\sigma(t) = \varepsilon_{7.5\%} * (\alpha e^{-bt}) + \sigma_e$ where $\sigma(t)$ represented the stress (in Pa) at time t during the relaxation period. $\varepsilon_{7.5\%}$ was a constant representing the percent strain during the hold phase (i.e., constant strain of 7.5% of tissue height). The model solved for the constant α, the maxwell decay component b, composed of a spring and dashpot in series, and σ_e which is the equilibrated stress value at 7.5% strain respectively. The data was analyzed in GraphPad prisms utilizing a one-way ANOVA to access the differences between mechanical parameters in different brain regions.

1.13 Gap closure assay

1 x105 MCF-7 and MDA-MB-231 cells were seeded on PDMS and plastic substrates on 24 well plates. Cells were grown to form a confluent monolayer in the wells before wounding. A sterilized pipette tip was used to generate wounding across the cell monolayer, and the debris was washed with PBS. At varying intervals, the cells migrating into the wounded area were visualized and photographed at 0 and 24 h under an inverted microscope (IX51S1F-3, Olympus). The distance between the cell front was measured at 0 h and 24 h time-points using ImageJ. To measure the average healing speed inside the wound area at each timepoint, the following equation was used as described previously (Pijuan et al., 2019). v (µm/h) = [Distance initial time (µm) – Distance final time (µm)]/Total time (h)[1]

1.14 Immunofluorescence staining

1.14.1 YAP Immunofluorescence Staining

For the analysis of YAP nucleus localization, MCF-7 cells or MDA-MB-231 cells were fixed with 4% paraformaldehyde and permeabilized in 0.1% Triton X-100. Then, the cells were washed with PBS and blocked with 5% PBS-BSA at 4°C overnight. Then the cells were incubated with mouse anti human YAP monoclonal antibody (Santa Cruz Biotechnology) followed by fluorescein isothiocyanate (FITC)-conjugated goat anti-mouse secondary antibody (Sigma-Aldrich). Cell nuclei of each sample were stained with 4′,6-Diamidino-2-phenylindole dihydrochloride (DAPI, Thermo Fisher Scientific) and imaged on Olympus inverted phase contrast and fluorescence microscope (IX51S1F-3,

Olympus). For paxillin immunofluorescence, mouse anti-human paxillin monoclonal antibody (Thermo Fisher Scientific) was used[1].

1.14.2 Tissue preparation

Mouse eyes were fixed in 4% PFA at room temperature for 24hrs before transferring to 70% ethanol. Brain tissues samples were fixed in 10% neutral buffered formalin (NBF) for 72 hours at 4C before transferring to 70% ethanol. All tissues were sectioned and placed into tissue cassettes and subsequently embedded in paraffin wax. Mouse eyes were sliced into 4μm sections using a microtome from Leica Biosystems and brain tissue was sectioned into 6μm sections and mounted onto microscope slides. The mounted sections were then heated at 37℃ for 24 hours before proceeding with immunofluorescent staining.

1.14.3 Tissue staining

All tissue slides were deparaffinized by washing them in a series of 100% xylene and ethanol gradients (100%, 95%, 70%) before a final rinse in distilled water. Antigen retrieval was performed by incubating sections in 10mM sodium citrate at 85-90℃ for 20 minutes. Following this, the sections were allowed to cool at room temperature submerged in the hot sodium citrate for another 20 minutes. The sections were then blocked using 5% normal donkey serum (NDS) in 1X PBS for 1 hr at room temperature in a humidified chamber. Primary Piezo1 antibody was diluted 1:50 in 1X PBS before applying to tissue and incubating at 4℃ overnight. Sections were then washed twice using 1X PBS before applying AlexaFluro 568 donkey anti-rabbit IgG (H+L) secondary

antibody (A10042, Thermo Fisher Scientific) at 1:200 in 1.5% NDS and allowed to incubate for 1hr at room temperature. The sections were then washed three times in 0.1%PBST with a tinfoil cover to prevent light unwanted light exposure. Finally, 30-40μl of ProLong Gold mounting media with DAPI (P36931, Thermo Fisher Scientific) was applied after which the slides were stored at 4℃ in preparation for imaging. All images were analyzed using Image-J based on the area fraction of intensity of positive staining.

1.15 Colonization Analysis

CellProfiler (www.cellprofiler.org) was used to quantify YAP nuclear/cytoplasmic intensity in immunofluorescence images and YAP/DAPI colocalization was measured via the correlation between the intensities of green and blue channels on a pixel-by-pixel basis across an entire image. The Cell Profiler colocalization pipeline was carried out to calculate the correlation and colocalization (Manders Coefficient) between the pixel intensities[1].

1.16 Immunoblotting

Protein lysates were combined with equal volume of Laemmli sample buffer (cat# 1610737, Bio-rad) containing β-mercaptoethanol and SDS which aids in denaturing and linearizing proteins. The sample was heated to 90°C for 10 minutes to complete the denaturation process required for size separation. Proteins were then separated via SDS-PAGE on Bio-Rad Mini PROTEAN TGX gels submerged in premixed electrophoresis running buffer (100 mM Tris, 100 mM Tricine, 0.1% SDS, pH 8.3) (1610732, Bio-Rad). Then, samples were run through the stacking gel using 15 mA of current for 15 min

followed by an increased current of 35 mA for 45 min for the separating gel (Figure 4**)**. The gel was then placed into a blotting sandwich (Figure 5) and proteins were transferred to a nitrocellulose membrane pre-soaked in transfer buffer (1x Tris-Glycine, 20% methanol). The transfer process required 100 mA of current for 1hr to force protein migration from the gel to the membrane. The membrane was then blocked with 5% bovine serum albumin (BSA) in PBST for 15 min on a rocking platform before primary antibodies were dissolved in 3% BSA in PBST and applied to the membrane. Primary antibodies were incubated with the blot at 4℃ overnight. A summary of dilution factors for antibodies is listed in Table 1. All blots were washed nine times, 3 minutes each, with 0.1% PBST before applying secondary antibodies dissolved in 3% BSA in PBST. Secondary antibodies were incubated at room temperature for 2hrs after which HRP substrate was applied, and the blots were imaged on a C-digit blot scanner using Image Studios Lite visualization software (Li-COR Biosciences). All images were analyzed in ImageJ for signal intensity.

Table 1: Primary antibodies for immunoblotting and respective dilutions

Protein Target	Primary Antibody-Dilution Factor	Secondary Antibody – Dilution Factor
YAP	Anti YAP (14074S, Cell Signalling Technologies) – 1:1000	Goat Anti-Rabbit-HRP (ab6721) – 1:1000
β-catenin	Anti β-catenin (D10A8) – 1:1000	Goat Anti-Rabbit-HRP (ab6721) – 1:1000
Piezo1	Anti Piezo1 (NBP1-78537) – 1:500	Goat Anti-Rabbit-HRP (ab6721) – 1:1000
β-actin	Anti β-actin (A5441, Sigma-Aldrich) – 1:2000	Goat Anti-Mouse-HRP (12-329 Millipore) – 1:5000

1.16.1 Protein input preparation from cell pellet

Protein lysates were obtained by scraping cells from a culture flask, or via tissue homogenization. Scraped cells were suspended in 1.5ml of 1X PBS and centrifuged at maximum speed (14 800rpm or 21 000xg) for six minutes to create a cell pellet. Excess PBS was then discarded. Cell pellets were then lysed with appropriate lysis buffer (50 mM Tris-HCl, 150 mM NaCl, 1% Triton X-100, and 5 mM EDTA) supplemented with one cOmplete™ Protease Inhibitor Cocktail tablet (cat# 04693124001, Hoffmann-La Roche Limited) per 7ml volume. The protein concentration was determined using Pierce BCA protein assay kit (thermal fisher scientific).

1.16.2 Protein input preparation from tissue

Snap frozen (-80℃) tissue was weighed out to 100-200mg and wrapped in tinfoil. Tissue samples were then placed in liquid nitrogen and briefly pulverized using a pestle and mortar. The ground tissue was then placed into a pre-chilled round bottom falcon tube and RIPA buffer was added ensuring a 1:5 ratio of tissue to buffer. Using a motorized tissue homogenizer (Kinematica GmbH) the sample was homogenized for approximately 20 seconds and then transferred to a 4℃ chilled 1.5ml microfuge tube. The sample was centrifuged at 4℃ for 8 minutes at 500xg to separate crude homogenate from the protein fraction. The supernatant was then transferred into a new microfuge tube and stored at -80℃. Protein concentration was determined using Pierce BCA protein assay kit (thermal fisher scientific).

1.17 Immunoprecipitation

To create the purification complex 20μl GammaBind Plus Sepharose beads (Cytiva, 17088601) were first washed with 50μl of lysis buffer (50 mM Tris-HCl, 150 mM NaCl, 1% Triton X-100 and, 5 mM EDTA) supplemented with one cOmplete^{TM} Protease Inhibitor Cocktail tablet (cat# 04693124001, Hoffmann-La Roche Limited). Next either, RL-2 (Thermo Fisher Scientific, MA1-072 10ug) or CD110.6 (9875S Cell Signalling, 1:200) antibodies were added to the beads and the total suspension volume was brought up to 250μl using lysis buffer with protease inhibitor. The mixture was placed on a rotator for one hour at 4°C to form the purification complex. The beads are coated in with a resin that has an affinity for Fc regions of antibodies thus allowing for ease of binding to form a bead-Ab complex. After incubation, the mixture was centrifuged for 30 seconds at a half speed (7.4x1000 rpm) to pellet the bead-Ab complex. The complex was washed twice with 500μl of wash buffer (0.01% PBST) before adding 200-300μg of cell lysate. The volume was then brought up to 500 µl using lysis buffer with protease inhibitor. Samples were placed on the rotator for two hours at 4°C to form a bead-Ab complex to bind to the target antigen (Ag). Note that RL-2 and CTD110.6 target O-GlcNacylated proteins. Samples were then pelleted at half speed for 30 seconds and washed three times with wash buffer. Target antigens were then eluted using 15μl Laemmli sample buffer and boiled at 90℃ for 10 minutes to preserve proteins for western blotting.

1.18 Molecular dynamics simulation

Crystal structures of well know inflammatory proteins ACE2 and TLR9 were downloaded from PubChem and docked using Autodoc Vina, a free open-source package to evaluate binding affinities of compounds and their targets for predictive pharmacology applications. The docked output structures from molecular docking of TLR9 and ACE2 were converted to pdb files through PyRx (https://pyrx.sourceforge.io/) & BIOVIA Discovery Studio Visualizer (https://discover.3ds.com/discovery-studio-visualizer-download) using the confirmation of either CQ or HCQ that had the lowest vina result value (Model 1) along with the protein without the ligand serving as controls. Charmm-gui's solution builder (https://www.charmm-gui.org/?doc=input/solution) was then used to create the cubical water box, fitted to the protein complex, the force field, and protonation states. Charmm-gui was also used to add counter ions to make the system electrically neutral before each molecular dynamic simulation. NAMD software (https://www.ks.uiuc.edu/Research/namd/) was then used to run the equilibration step using canonical NVT and NPT ensembles at a stable temperature of 300 K and pressure of 1 bar. The production step followed using canonical parameters optimized through Charmm-gui. Once all files were made, VMD software (https://www.ks.uiuc.edu/Research/vmd/) was used to visualize the molecule and run the simulation by loading the input file of the protein or complex and loading the production

dcd file into it. With VMD's RMSD trajectory tool, RMSD graphs were produced with RMSD (nm) on the *y*-axis and time on the *x*-axis[2].

[2] Yu W, Bai Y, Raha A, Su Z and Geng F (2022) Integrative *In Silico* Investigation Reveals the Host-Virus Interactions in Repurposed Drugs Against SARS-CoV-2. *Front. Bioinform.* 1:763540. doi: 10.3389/fbinf.2021.763540

Chapter 2: Investigating stiffness dependency on YAP mechanotransduction in breast cancer

Chapter motivation and overview

To investigate the different elements of this thesis project several experimental phases were required to establish the link between breast cancer mechanotransduction, substrate stiffness, and brain metastasis. The first step was to characterize a substrate suitable for probing mechanotransduction events in breast cancer. For this reason, non-cytotoxic PDMS substrate was fabricated at different crosslinking ratios to create varying substrate stiffnesses [135]. A collagen coating was applied as an ECM layer after which the stiffness of the substrate was measured using the Biomomentum Mach-1 mechanical tester [135]. Given that YAP is considered a pivotal regulator in the mechanotransduction cascade [87], [115] and metastasis several experiments were carried out to examine the role of YAP in cancer cell migration, and intracellular localization. Additionally, western blotting was performed to capture the relative intensity of YAP between TNBC MDA-MB-231 and less metastatic MCF7 cells. Immunoprecipitation was performed to access YAP O-GlcNacylation as this is thought to competitively inhibit its phosphorylation thus preventing cytoplasmic degradation and possible nuclear entry [116]. Recall that nuclear entry of YAP is associated with increased migration, proliferation and stemness, and metastasis [87], [113], [115]. Finally, a drug screening framework using molecular

dynamic simulations was developed for accessing the effect of repurposed drugs against biomarkers that are upregulated in cancer.

Introduction

Cancer metastasis is a multistep process that requires activation of numerous microenvironmental and biochemical signals. Extracellular matrix stiffness is a well-known risk factor that influences intracellular mechanisms such as YAP localization, focal adhesion (FA) alterations, and cytoskeletal tension [81]. These mechanisms can trigger an invasive phenotype endowing cancer cells with the ability to colonize distal microenvironments such as the brain [3], [38], [136]. Thus, it is critical to understand the mechanisms that trigger invasive phenotypes to be able to develop therapies against metastatic breast cancer. As a signalling hub of mechanotransduction, yes associated protein (YAP) is responsive to changes in substrate stiffness [114], [115]. The intracellular localization of YAP is generally known to be within the cytoplasm or nucleus [113]. Nuclear localization of YAP is known to trigger its binding to transcriptional enhanced associated domain (TEAD) which is responsible for activating pathways of proliferation, wound healing, and metastasis [87], [115]. Typically, during cytoplasmic sequestration YAP is phosphorylated which primes it for degradation however nuclear localization may be regulated through its O-GlcNacylation [137], [138]. As triple-negative breast cancer is known to be highly metastatic understanding the interplay between stiffness and YAP intracellular trafficking may help us derive therapies that target mechanotransductive molecules that inhibit cancer progression.

Results

2.1 PDMS mechanical characterization

Mechanical testing was performed on three different formulations of PDMS 1:5, 1:10, and 1:20 ratios of crosslinker to base as well as two different thicknesses of PDMS. Results demonstrate that the modulus of elasticity (stiffness) decreased as increasing amounts of elastomer base are added[1]. This agrees with literature data showing a direct proportionality between stiffness and crosslinker to base ratio [133].

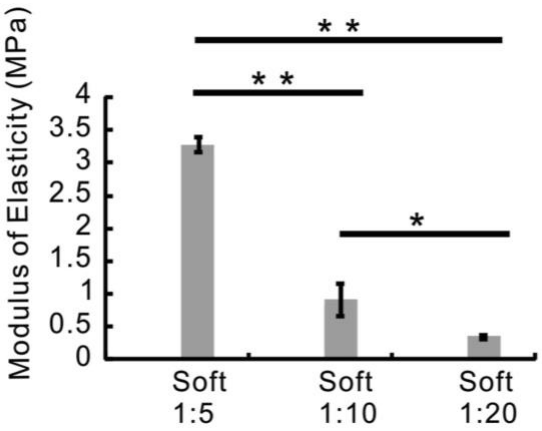

Figure 4: The determination of modulus of elasticity of three types of PDMS substrates[1].

Regarding the thickness of PDMS and its effect on stiffness two different thicknesses relating to 1g and 2g of samples were also tested via indentation. The amplitude of indentation was set to 0.39mm and 0.9mm for the 1g and 2g samples respectively (10% of sample height). Additionally, the velocity of indentation was set to 0.0039mm/s and 0.09mm/s for the 1g and 2g samples respectively (1% of sample height). Indentation testing showed that stiffness values of fabricated PDMS were comparable to literature values [133]. Exact values are reported in supplemental Table 1 (Table S1). Further, the

thickness of the substrates seems to have a partial effect on the elastic modulus where ratios of 1:5 and 1:10 of crosslinker to elastomer base produced significant differences in the stiffness but do not deviate greatly from literature. As such, either mass of PDMS can be used for mammalian cell culture.

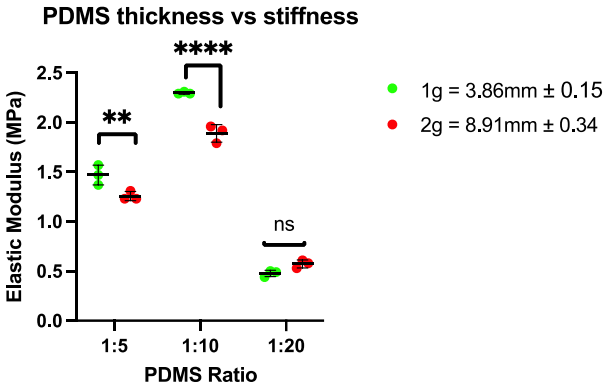

Figure 5: Elastic modulus measurements of PDMS at different stiffnesses using 1g and 2g quantities of substrate. **p $< \mathbf{0.0035}$, **** $\mathbf{p < 0.0001}$.

2.2 Triple-negative breast cancers acquire migratory advantage on stiff matrix compared to non-metastatic counterpart

Using the different PDMS stiffnesses, our group first established that proliferation rates of breast cancer cells are increased on stiffer substrates [86]. Given that YAP is also upregulated on stiff substrates [113] a scratch assay was performed to probe migration dependency on YAP expression and substrate stiffness (Figure 6A). Non-metastatic MCF-7, TNBC MDA-MB-231 cells, and Hs 578T cells were transfected with YAP siRNA (siYAP) to knockdown YAP expression and plated on various stiffnesses as previously characterized in section 2.2. Note that the stiff substrate in figure 6 refers to cells cultured on plastic culture plates. Results demonstrated that siYAP cells had

significantly slower healing speed than untreated cells on the same stiffness (Figure 6B). Also, cells grown on plastic showed the greatest difference in healing speed compared to cells growth on soft PDMS substrates. In contrast, across the different stiffnesses there was no significant different in healing speed when MCF7, MDA-MB-231 and Hs 578T cells were transfected if siYAP (Figure 6B)[1].

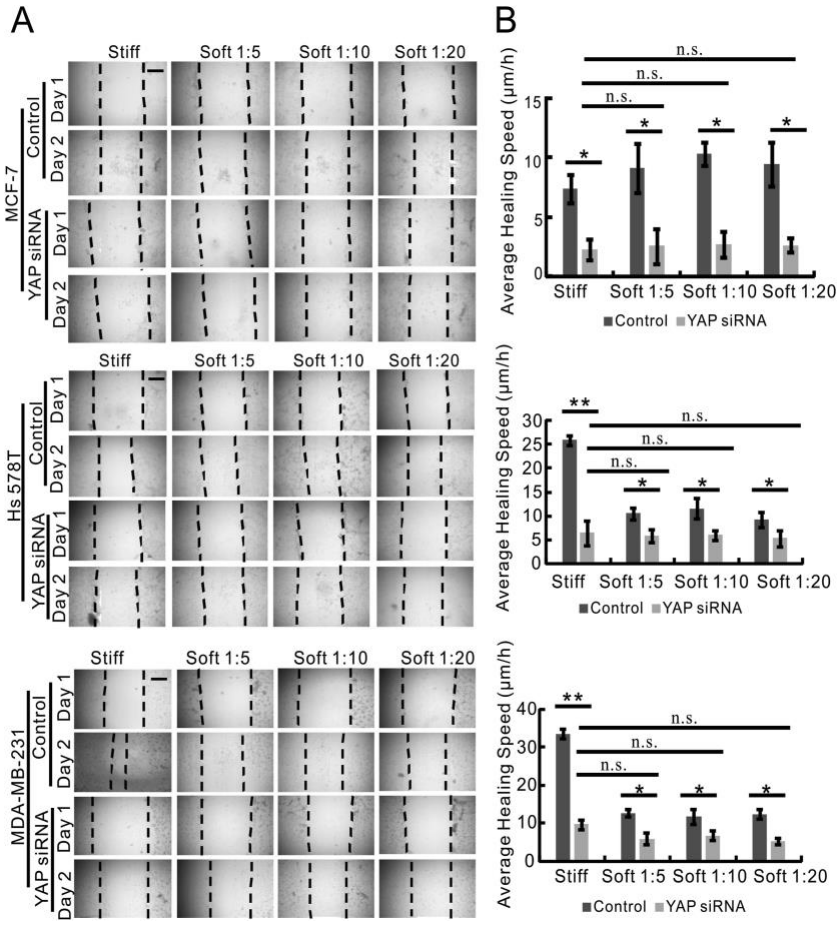

Figure 6: Migration of metastatic breast cancer cells was promoted by stiff matrix in a YAP-dependent manner. (A) Time-lapse microscopy images of gap closure of MCF-7, Hs 578T and MDA-MB-231 cells that were cultured on stiff (plastic) or soft (PDMS) substrates (Soft 1:5, Soft 1:10, Soft 1:20) at 0 h (Day 1) and 24 h (Day 2) after scratch was created. The dotted lines define the area lacking cells. Scale bar, 100 μm. (B) The quantification of Gap Closure Assay in Figure 3A using ImageJ. The average healing speed (μm/h) of MCF-7 (top graph), Hs 578T (middle graph) and MDA-MB-231 cells (bottom graph) was shown. Data were represented as means ± SD (n = 3). ∗P < 0.05[1].

2.3 YAP shows greater nuclear localization in TNBC migratory cells

YAP nuclear localization is associated with increase proliferation and metastasis [113]–[115]. To better understand the implication of matrix stiffness on YAP nucleocytoplasmic shuttling, an intracellular localization analysis was performed on MCF7 and MDA-MB-231 cells [86]. These cells were plated on stiff (plastic), and soft (PDMS) substrates and their respective YAP activity was monitored. Fluorescent microscopy of YAP (Figure 7A green channel) and DAPI (Figure 7A, blue channel) was performed. The Manders coefficient served as the readout of colocalization of the two channels (figure 7B). On the soft PDMS YAP was mainly localized outside the nucleus in both cell types while the stiff plastic substrate showed even intracellular distribution (Figure 7B). In both cell types, YAP and DAPI show greater colocalization as indicated by a larger Manders coefficient when cultured on stiff plastic (0.9) compared to soft PDMS (0.7) (Figure 7B)[1].

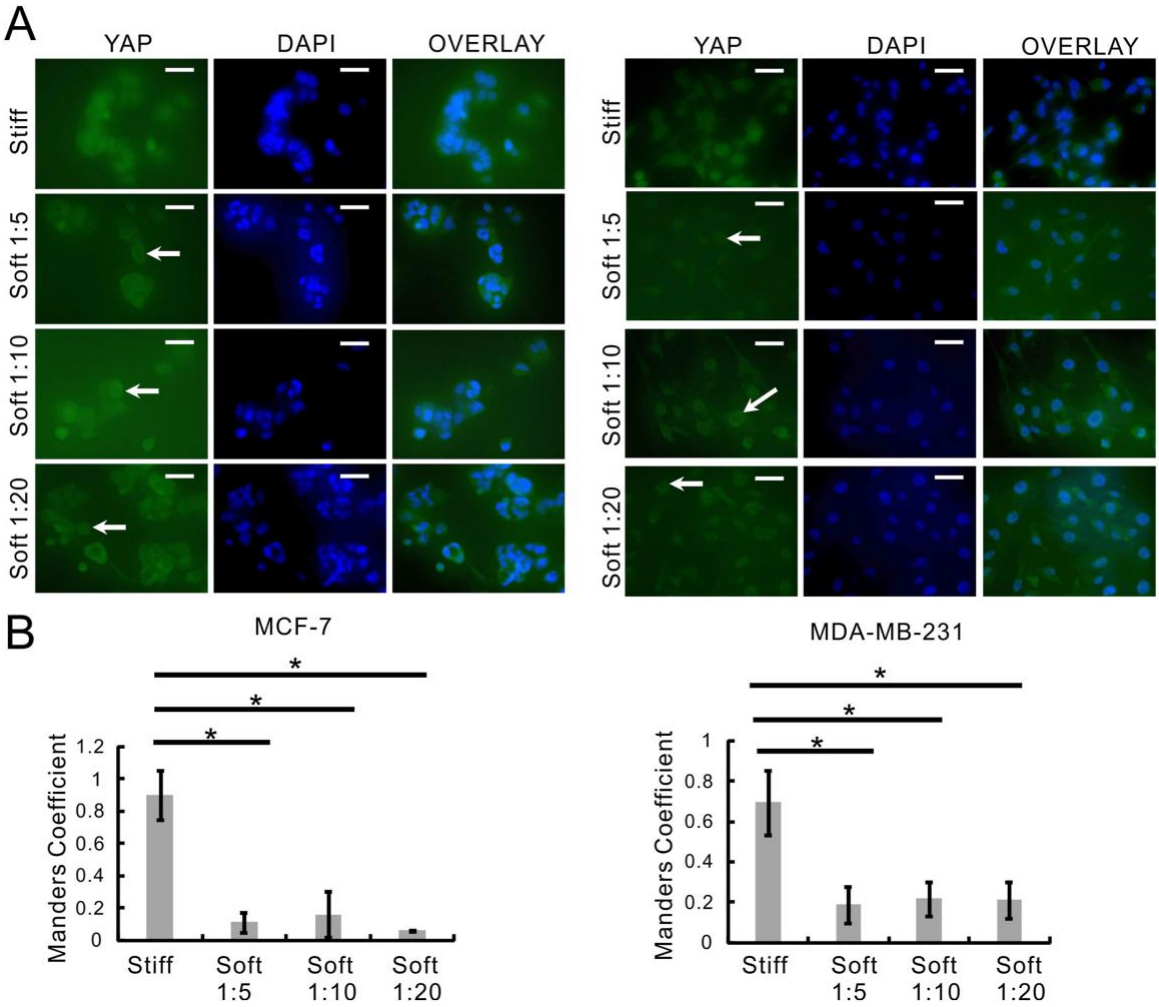

Figure 7: Both metastatic and non-metastatic cancer cell lines exhibited increased YAP nuclear entry in response to stiff matrix. (A) MCF-7 and MDA-MB-231 cells were cultured on stiff (plastic) or soft (PDMS) substrates (Soft 1:5, Soft 1:10, Soft 1:20) and then YAP subcellular localization in those cells was analyzed by immunofluorescence staining. The cells showing nuclear exclusion of YAP were highlighted by arrowheads. Field-of-views were selected randomly under each condition and photographed at a magnification of 40 ×. Scale bar, 10 μm; (B) Colocalization analysis of YAP and DAPI in the cells from Figure 4A were analyzed using CellProfiler. Data were represented as means ± SD (n = 3). ∗$P < 0.05$[1].

2.4 Focal adhesions are regulated by matrix stiffness in TNBC

To further probe the expression of YAP in response to matrix stiffness mRNA expression analysis was conducted in MDA-MB-231 given the innately low YAP expression in MCF7 cells (Figure 8A). The results show little difference in YAP mRNA expression and its target gene CTGF between the different stiffness conditions. Thus, YAP expression might not be significantly increased in the range of stiffnesses examined here. Further, as MDA-MB-231 cells and Hs 578T cells acquired higher migratory potential their respective FA dynamics were examined using paxillin staining. FAs are the hub of cell-ECM interactions thus greater migratory behaviour was thought to also increase FA expression. Perinuclear staining as well as defused cytoplasmic staining was observed in triple negative breast cancer cell lines while MCF7 cells showed only perinuclear staining[1].

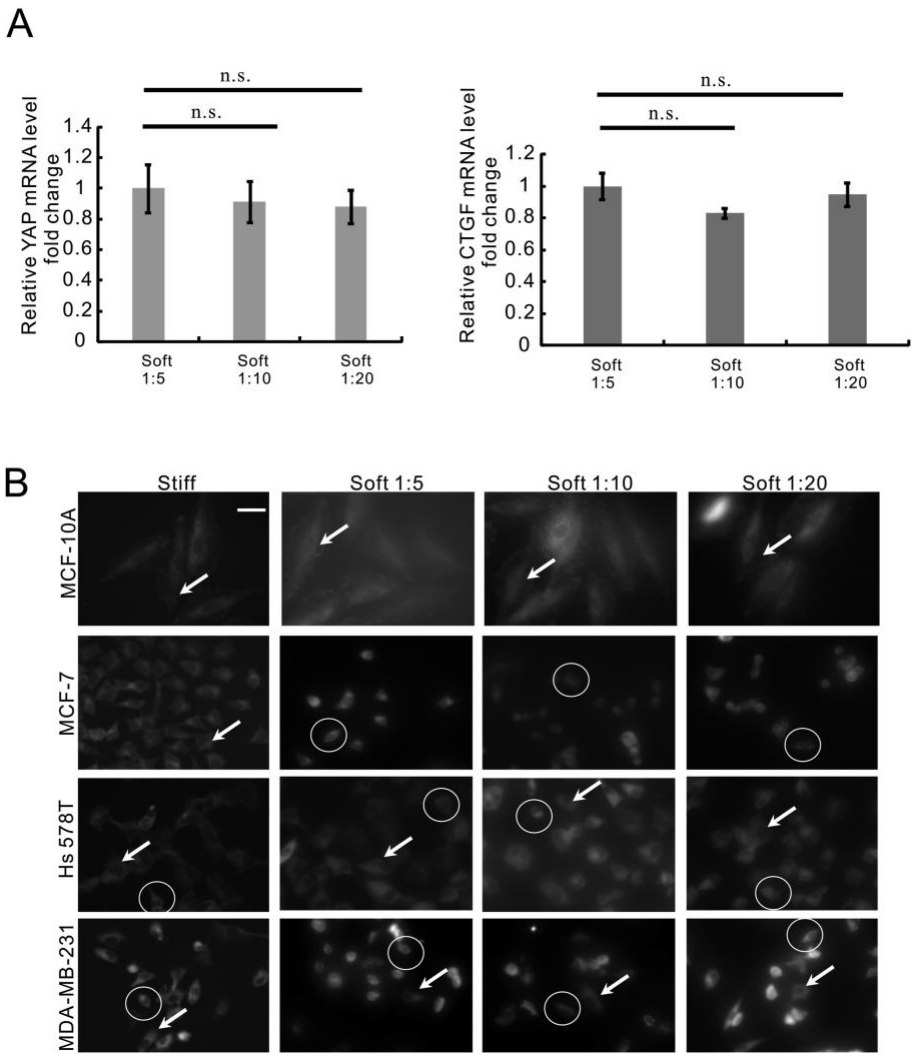

Figure 8: Focal adhesion dynamics in metastatic breast cancer cells were regulated by matrix stiffness. (A) qRT-PCR analysis of YAP (left panel) and CTGF (right panel) gene expression in MCF-7 and MDA-MB-231 cells that are cultured on stiff (plastic) or soft (PDMS) substrates (Soft 1:5, Soft 1:10, Soft 1:20). Data were represented as means ± SD (n = 3). n.s. not significant. (B) The paxillin staining in MCF-10A, MCF-7, Hs 578T and MDA-MB-231 cells that were cultured on stiff (plastic) or soft (PDMS) substrates (Soft 1:5, Soft 1:10, Soft 1:20). Field-of-views were selected randomly under each condition and photographed at a magnification of 40 ×. Scale bar, 10 μm. The representative cells with diffuse staining pattern of paxillin were highlighted using arrowheads and the representative cells with perinuclear staining pattern of paxillin were highlighted using circles[1].

2.5 Probing YAP O-GlcNacylation status in migratory TNBC

Previous evidence showed that YAP transcriptional activity can be regulated through O-GlcNacylation by inhibiting phosphorylation and driving nuclear entry [116]. As such, it is hypothesised that stiff surfaces which also show YAP nuclear localization may have glycosylated modification upon the transcription factor which aids in mediating its translocation to the nucleus. For this reason, an immunoprecipitation assay was performed to isolate O-GlcNac-YAP proteins. Two antibodies (Ab) were used to target O-GlcNac proteins including RL-2 and CTD110.6. After performing a global pulldown of all O-GlcNac proteins, immunoblotting for YAP was performed to isolate YAP from other glycosylated proteins. The results demonstrate the presence of light and heavy chains of the RL-2 antibody (Fig. 9A), and CTD110.6 (Fig. 9B). Also, reference YAP bands (75kDa) (Fig 9) from total cell lysate controls were faintly visible in MCF7 cell lysates and more prominently in MDA-MB-231 lysates (M231) (Fig. S4).

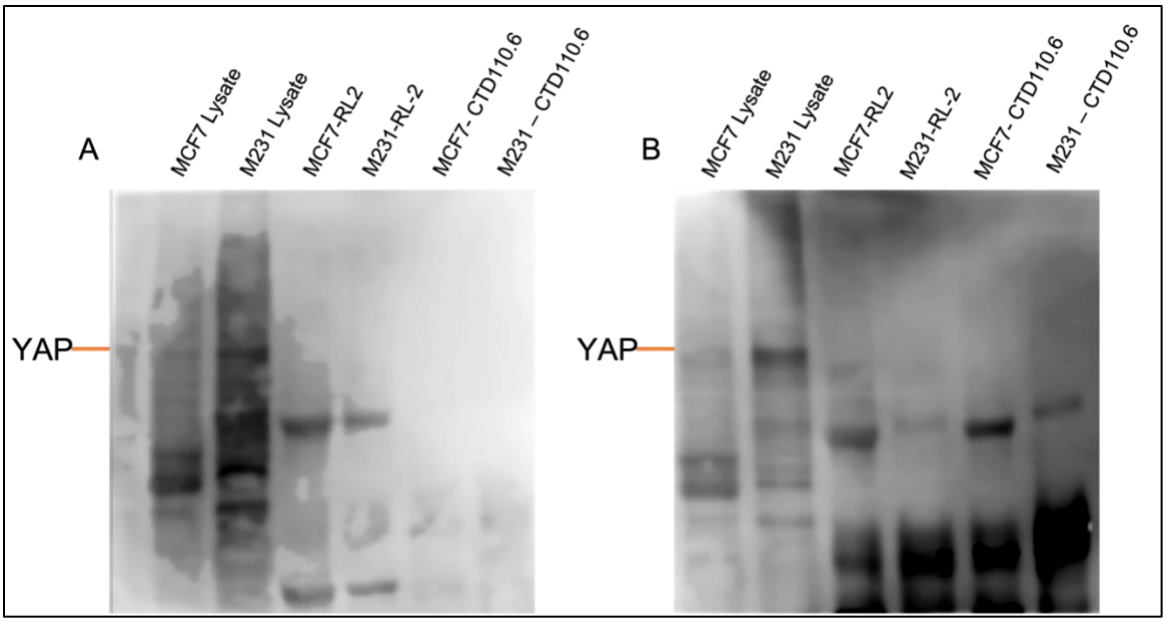

Figure 9: Comparing antibody efficiency in precipitating O-GlcNac-YAP (~75kDa) showing two replicate blots (A &B). 10μg of total cell lysate was loaded into the gel to identify references YAP bands (75kDa). (A) RL-2 treated lysates show light and heavy chain banding. (B) RL-2 treatment shows different light and heavy chain banding intensities. CTD110.6 treatment also shows different light and heavy chain banding intensities.

2.6 Troubleshooting O-GlcNac-YAP immunoprecipitation assay

Due to the lack of O-GlcNac-YAP banding (same position as YAP, ~75kDa) seen in Fig 9 a series of investigative assays were performed to better understand potential pitfalls in IP purification. Light and heavy chains of both anti-O-GlcNac antibodies were observed in western blots but at varying intensities. This suggests the conjugation efficiency between Sepharose beads and antibodies was inconsistent. As such, it was suspected that O-GlcNac-YAP was likely left unbound and washed away during processing steps. Thus, the wash buffer discard was examined via western blotting for the presence of YAP given that YAP and O-GlcNac-YAP are similar in structure and size. Figure 10 shows the presence of YAP in wash buffer discard for MDA-MB-231 cells

confirming poor capture efficiency. MCF7 cells showed no YAP banding but this was attributed to the inherently low levels of YAP in MCF7 cells [86].

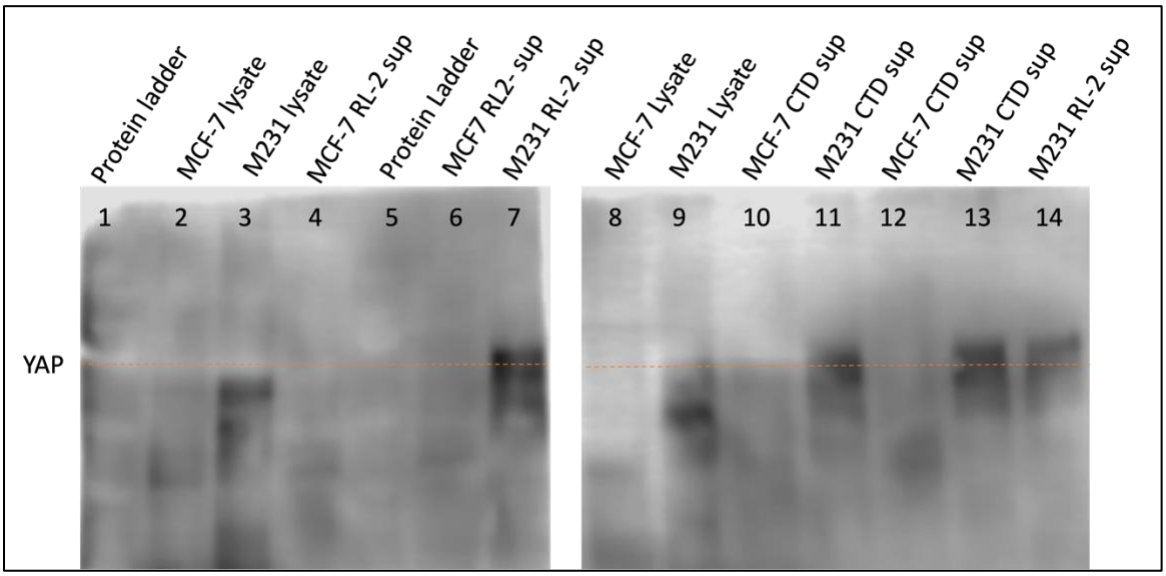

Figure 10: Wash buffer discard from previous IP experiments was collected and evaluated for the presence of YAP. Note that lane 14 and lane 5 are in opposite positions. YAP band is shown at 75kDa. 7μl MCF-7 and MDA-MB-231 (M231) IP discard was loaded into respective lanes 4-7 and 12-14. 10μg of respective cell lysate was loaded into well 2-3 and 8-9.

The next step in troubleshooting was to determine if bead-antibody conjugation efficiency was optimal. Thus, Sepharose beads were incubated with fluorescently tagged antibodies for two time periods, 2hrs at 4℃ (typical IP condition) and overnight at 4℃ (extended bead-antibody hybridization period). Fluorescent microscopy was performed to evaluate the hybridization efficiency. Results showed that overnight incubation of beads and antibodies have greater signal intensity and thus should serve as a preconditioning step in future IP experiments to aid in capturing detectable levels of O-GlcNac-YAP.

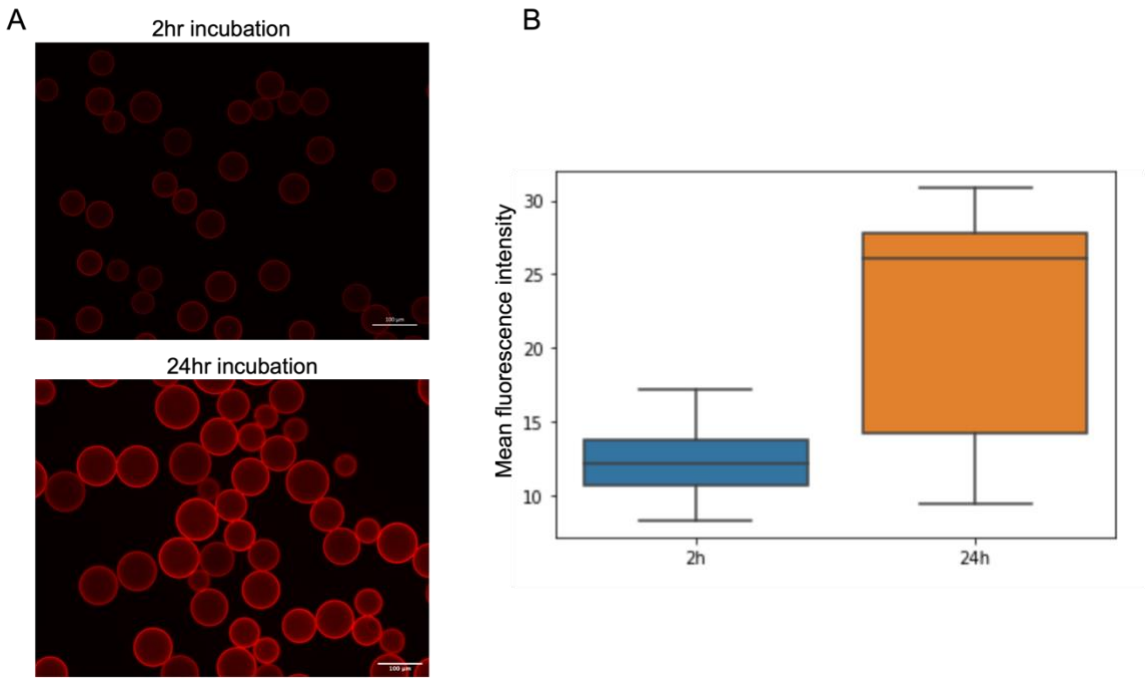

Figure 11: Comparison of bead-Ab incubation times and respective signal intensities. (A) Sepharose beads conjugated to fluorescent Ab for 2hr and 24hr incubation periods. Scale bar: 100μm at 10x magnification. n= 56. (B) Mean fluorescence intensity quantified via ImageJ for 2hr and 24hr incubation times.

2.7 Molecular dynamics simulation

With the future of mechanotransduction research in mind, a molecular dynamics analysis was conducted to establish a platform for drug screening that can be used to target mediators of mechanotransduction using novel or repurposed drugs. Molecular dynamics is a branch of *in silico* investigation that examines the binding interactions between proteins and their respective ligands. A read-out of binding affinity known as the root-mean-square deviation (RMSD), estimates the distance between proteins and their respective ligands [139]. RMSD values are inversely proportional to the distance between ligands and their target proteins [139]. This information can aid in predicting the overall stability of drug-target complexes [139]. TLR9 is a well characterized inflammatory

mediator and has different implications for predicting cancer prognosis [140]. Through Gene Ontology (GO), and Kyoto Encyclopedia of Genes and Genomics (KEGG) enrichment, TLR9 was shown to be a strong target of the drugs chloroquine (CQ), and hydroxychloroquine (HCQ) [141]. Simulation results show smaller mean RMSD value of TLR9-HCQ complex (2.339nm), compared to TLR9-CQ (3.069nm), and TLR9-WATER (3.226nm). This suggests the deviation of atoms between TLR9 and HCQ is less than that observed between TLR9-CQ.

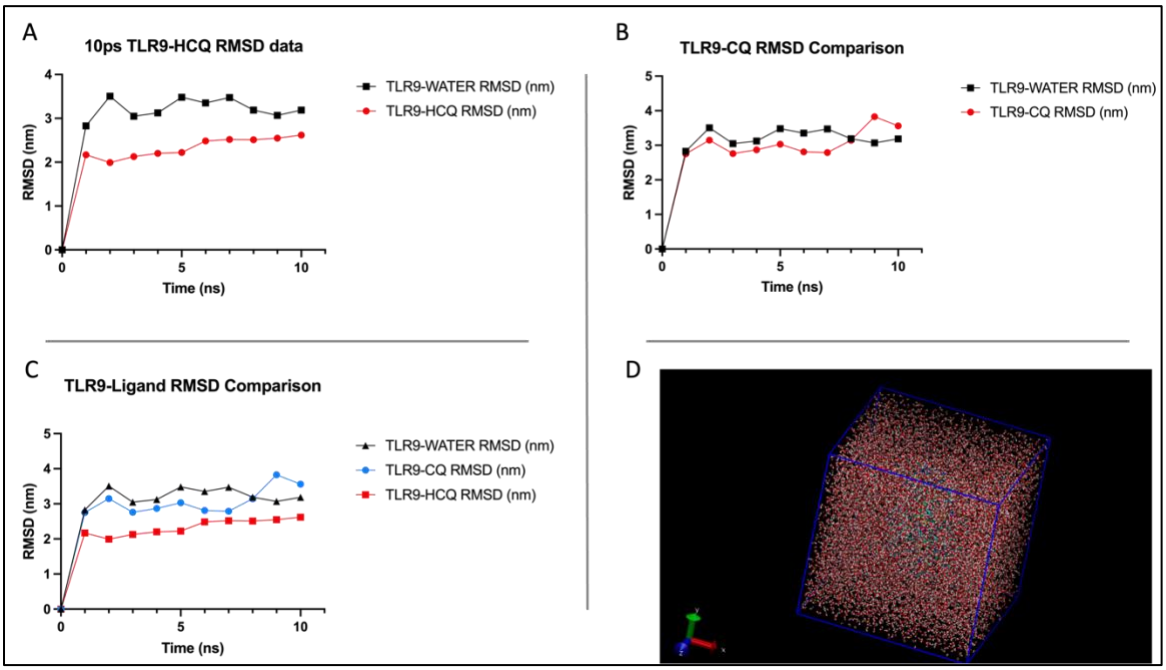

Figure 12: Molecular dynamics simulation demonstrates binding affinity between TLR9 and drug candidates' chloroquine (CQ) and hydroxychloroquine (HCQ). (A) Comparison of relative binding affinity (RMSD) between control test of TLR9 solvated in water and TLR9 bound to HCQ ($p<0.05$). (B) Comparison of relative binding affinity between control test of TLR9 solvated in water and TLR9 bound to CQ (n.s.). (C) Comparison of relative binding affinity between TLR9-WATER, TLR9-HCQ, and TLR9-CQ. (D) Boxed simulation void with TLR9-drug complex solvated in water molecules[2].

Discussion

Based on indentation testing, PDMS stiffnesses at different ratios were significantly different. This difference was also observed between substrates of different thicknesses except for 1:20 formulations. Typically, the mechanical properties of PDMS are considered isotropic [142], however, analysis of Young's modulus shows dimensionally dependency at thickness as low as 200μm [142]. This thickness dependence is attributed to shear stress experienced during fabrication, as it may reorder the orientation of polymer chain coils which create the support structure for the material [142]. Typically, elastomer and crosslinker need to be mixed well which causes shear stress. The mixing process however is essential to ensure uniform distribution of the crosslinker in the viscous elastomer gel. Also, the standard deviation for sample thickness increased when 2 g of PDMS were prepared. This is likely due to inconsistencies in mixing and possible surface tension which could cause the viscous polymer to adhere to the sidewalls of the 24 well plate.

The migration rate of breast cancer cells was shown to be YAP dependent however, the influence of stiffness on migration rate is still unclear. The PDMS stiffnesses presented in this study may not have covered a large enough range to elucidate a significant migratory response. Alternate research shows that brain and breast cancers proliferate more on stiff substrates but its effect on invasive or migratory phenotypes is only partially understood [68], [69], [136], [143], [144]. Further, to better visualize invasive fronts alternate techniques can be employed using culture stencils or electrical

impedance [145]. Additionally, fluorescently tagged reporter systems for YAP could allow for live intracellular tracking of YAP which may provide more comprehensive data on the relationship between YAP and substrate stiffness [146]. Two different patterns of paxillin staining were observed in TNBC (perinuclear and diffused). While the specific patterns do not seem to correlate with the invasive phenotype based on this data, the overall expression, and polarization of focal adhesions is a known characteristic of invasive morphologies [147].

To further understand the role of O-GlcNac modification on stiffness dependant YAP mechanotransduction, additional immunoprecipitation experiments need to be performed using extended incubation times for Sepharose bead-Ab complexing. Additionally, establishing more representative positive controls, such as cells expressing high levels of O-GlcNac-YAP will be essential in evaluating if antibody-antigen interaction is sufficient for O-GlcNac detection. GlcNac (an activator of O-GlcNacylation), and PuGNac and inhibitor of O-GlcNAcase (OGA), are examples of treatments that can be employed to artificially increase the expression of global O-GlcNacylation [148]. Additional methods such as fabrication of tagged proteins like O-GlcNac-YAP-Flag would allow the use of specific enzymes against the respective peptide tags to consistently precipitate O-GlcNac-YAP [149].

The molecular dynamics simulation conducted in this work serves as the basis for future work in investing drug targets of cancer biomarkers. As research on mechanotransduction progresses, new targets for therapy may emerge with the possibility of repurposing drugs for treatment. Given the complexity of cancer biology, molecular

dynamics and protein modelling help screen protein-protein interactions and elucidate the multifunctional role of bioactive compounds [150].

Conclusion

To summarize, stiff substrates appear to promote YAP mediated cell migration, particularly in TNBC cells. While the exact effect of focal adhesions in this context is unclear, supplemental literature suggests their activation induces cytoskeletal stress fiber formation and changes in cell shape [151]. Localization of YAP in the nucleus was observed on stiff substrates which may be linked to its glycosylation status, however, whether surface stiffness can modulate this modification is still unknown. Finally, molecular dynamics can be used as a framework for drug-protein and protein-protein interactions which can be applied to future targets related to mechanotransduction.

Chapter 3: Biomechanical properties of human brain tissue

Chapter motivation and overview

The next chapter of this thesis project explores the mechanical properties of human brain tissue under simple compression. Brain tissue is one of the most complex and compliant tissues in the body and its mechanics are correlated with brain function [152]. While computational models and imaging technologies are useful in gaining information otherwise unavailable through traditional diagnostic tools, realistic predictions require mechanical models that can provide actual numerical data [75]. Thus, these models must be able to capture the complex characteristics of ultrasoft and heterogeneous tissue. Due to its complexity, literature has produced contradictory evidence resulting in confusion and misdirection in characterizing brain biomechanics. The mechanical properties of the tissue such as the stiffness are thought to be related to several diseases including cancer [78], [106], [153]. Particularly, the connection between tissue mechanics and mechanobiology in the brain has been shown to play a role in cell apoptosis and tumor migration [154].

Given that cancerous brain tissue from humans is extremely difficult to gain access to, the mechanical properties of adjacent normal tissue were characterized to evaluate the possibility of a biomechanical precursor to cancer metastasis. As the nature of brain tissue is quite heterogenous, it was important to develop a system that could consistently measure the mechanical properties of ultra-soft materials. For this reason, a

feasibility study was initially conducted where different materials which progressively emulated brain tissue were tested under simple compression to evaluate the sensitivity and repeatability of the testing method. Initially, PDMS substrate was tested as it is known to have predictable elastic behaviour and thus was expected to produce relatively clean data using the Microtester system. The force resolution of this system is 10nN which is soft enough for quantifying brain tissue [75]. After testing PDMS, it was important to evaluate how the Microtester performed when compressing biological tissue. Thus, lamb brain was purchased from a local butcher shop and prepared for compression by sampling relatively cylindrical cores of tissue using a 3mm biopsy punch. Tissue testing revealed the viscoelastic property of biological materials which was previously not seen in PDMS testing. This highlighted another mechanical property that could be relevant in disease. Finally, human brain tissue was tested and data on stiffness as stress relaxation was collected representing two commonly examined material properties in biological tissue [155].

Introduction

3.1 Current understanding of brain biomechanics

The extreme compliance of the brain pushes the limits of traditional mechanical testing methods. Considerations regarding appropriate boundary conditions and high force sensitivity requirements make many mechanical models inappropriate for brain testing [75]. The brain's biphasic nature due to its high water content makes it difficult to control drainage conditions during biomechanical testing [156]. Thus, incompressible

fluid is trapped in the tissue or free to escape depending on the testing method applied [75]. Brain tissue is also highly fragile and can undergo permanent deformation after 20% compression or 18% tensile strain and measurements close to this threshold are likely to render meaningless results [75], [156]. The tissues stiffness is observed to be proportional to the strain rate applied highlighting the importance of experimenting with strain rates that are physiologically relevant [157]. This behaviour is attributed to the biphasic nature of the brain and is relevant in considering appropriate models for mechanical testing [75]. The highly compliant behaviour of the brain also results in different levels of stress relaxation even at low strain rates of 0.00761/s (2mm/min) producing hysteretic responses [76]. Brain tissue also softens upon preconditioning as cyclical loading of the tissue at progressively greater strains shows a gradual decrease in nominal stress [75]. This preconditioning effect is observed to fully recover after one hour of rest showing identical patterns of initial loading compared before and after recovery [158]. Further, regional mechanics appear to depend on a few factors including loading rate, tissue drainage conditions, size/area of mechanical probing, and even cellular density [75]. As such, in addition to regional trends, tissue properties may vary within a particular region of the brain depending on the type of mechanical testing method applied. For this reason, conclusions about brain biomechanics can, for the moment, only be compared between similar test conditions [75]. Importantly, the regional variability in cellular and extracellular structures is thought to conform with regional variations in mechanical properties and function [75]. Thus, studying the variation in regional stiffness may guide

our understanding of the interplay between tissue stiffness and mechanotransduction in health and disease.

3.2 Mechanical modelling

The primary components of the tissue under investigation in this work are elastic properties of solid skeleton consisting of cells, intracellular connections, and extracellular matrix. These structures are best investigated through unconfined compression (tested here), as fluid is free to escape and does not impact the stiffness measurement of tissue structures [75]. High loading rates are assumed to be inappropriate for examining the natural mechanics of the brain but may be appropriate for studying impact situations such as traumatic brain injury. For this reason, a quasi-static compression model is assumed to be the most appropriate as it circumvents the effect of fluid incompressibility in the brain (characteristic of high fluid content in the tissue) [75]. Keeping the highly compliant nature of the tissue in mind, compressing it well below its yield point (18-20%) is ideal to capture the tissue's elastic modulus (stiffness) [75]. One of the more complex phenomena of tissue mechanics is the viscoelastic response observed at constant strains. Maxwell bodies are typically used to model such behaviour in viscoelastic tissue and consist of a pair of sprints and dashpots connected in parallel [159]. This feature captures the exponential decay (dashpot dependence) in stress but has shortcomings in modelling the elastic component of stress relaxation [75]. As such, modifications can be made to fit a generalized model more accurately. For example, assuming an infinite viscosity effectively reduces a generalized Maxwell model (Figure 13A) to a Zener model (figure

13B) and enables better curve fitting for the method of brain tissue compression performed in this project [159]. Importantly this model can account for the initial elastic response in stress relaxation and capture the equilibrated stress (σ_e) of the tissue after the tissue has equilibrated at a constant strain (figure 13C). The different parameters of the Zener model capture elements of the overall viscoelastic response and can be compared across different brain regions to understand regional differences in stress relaxation [75].

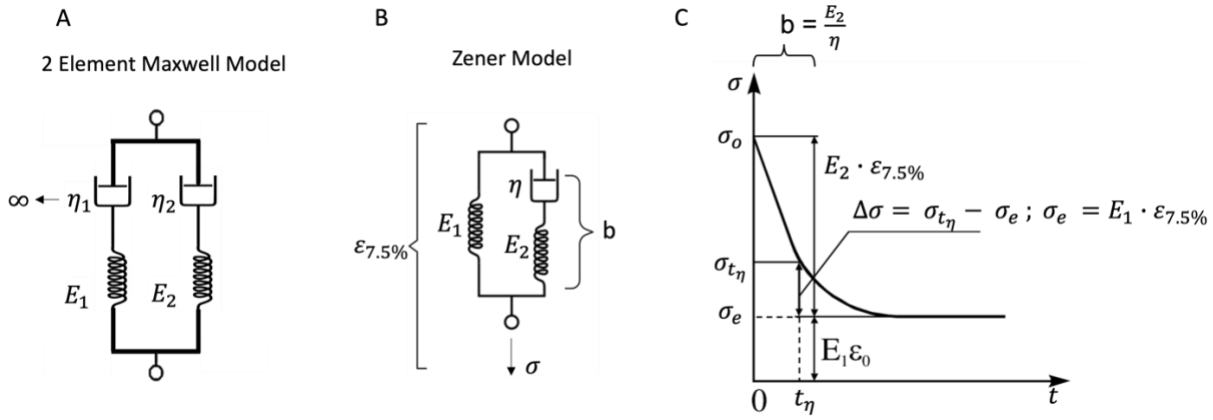

Figure 13: Biomechanical model for stress relaxation $\boldsymbol{\sigma(t) = \varepsilon_{7.5\%} * (\alpha e^{-bt}) + \sigma_e}$. (A) Standard 2 element Maxwell model used to characterize typical viscoelastic materials. This model was adapted to a Zener model which better characterizes brain tissue biomechanics by assuming infinite viscosity in the first dashpot ($\boldsymbol{\eta_1}$) thus reducing the model to (B) two springs and a single dashpot. (B) Zener model for representing stress relaxation where strain is held constant at 7.5% of sample height ($\boldsymbol{\varepsilon_{7.5\%}}$) and the decay term (b) in the model is shown to be a combination of spring and dashpot in series. (C) representation of where elements of the Zener model integrate during idealized stress relaxation behaviour. Strain in this instance corresponds to a compression of 7.5% of the sample height. Notice that the decay term b, is the time constant required to reach the equilibrated stress $\boldsymbol{\sigma_e}$.

Feasibility study

3.3 PDMS testing for system characterization

As brain tissue is extremely compliant it was important to evaluate the capabilities of the Microtester system using more predictable materials. Using the PDM as substrates

introduced in chapter 1, the micro tester was assessed in its ability to produce repeatable data using a quasi-static, and stepwise ramp method of compression. Figure 13 (A-D) shows typical data from quasi-static compression which produced three characteristic graphs. These were the force vs time, displacement vs time, and force vs displacement graphs. In the quasi-static method, the substrate was compressed by 40% to observe the upper bounds in force resolution quantified at $3000\mu N$. In the subsequent stepwise compression (Figure 14 E-H) the PDMS substrate behaved predictably with no observable stress relaxation (Figure 14 F) and minimal hysteretic effect (figure 14 H).

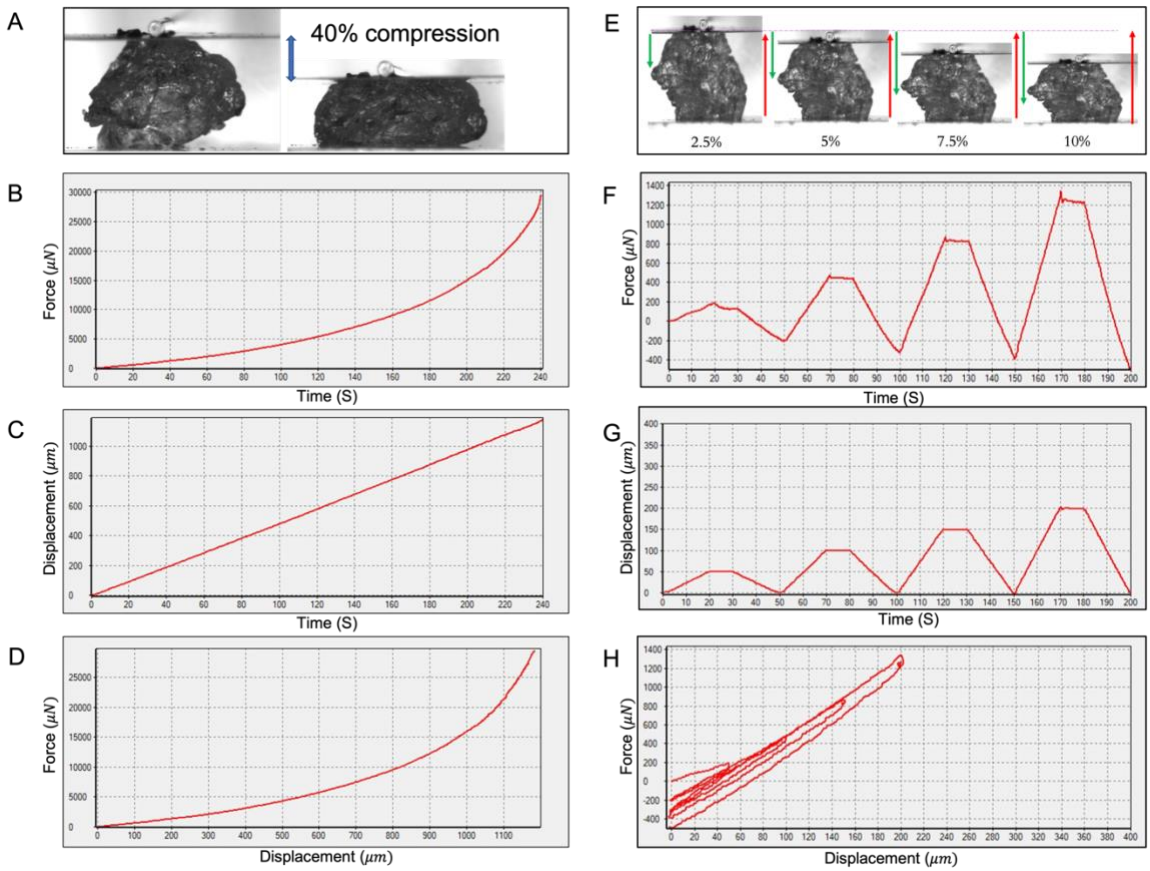

Figure 14: Feasibility testing of Microtester system using PDMS to validate signal quality and test methodology. A-D pertains to quasi-static testing set-up while E-F pertains to stepwise compression testing. (A) Illustrating gradual 40% compression in quasi-static testing model with a slow strain rate of $0.002s^{-1}$. (B) Force ($\boldsymbol{\mu N}$) vs time (s) graph. (C) Displacement ($\boldsymbol{\mu m}$) vs time (s)

graphs. (D) Force ($\boldsymbol{\mu N}$) vs displacement ($\boldsymbol{\mu m}$) graph. (E) Illustration of cyclical loading in stepwise compression at different percentages of sample height. (F) Force ($\boldsymbol{\mu N}$) vs time (s) graph. (G) Displacement ($\boldsymbol{\mu m}$) vs time (s) graphs. (H) Force ($\boldsymbol{\mu N}$) vs displacement ($\boldsymbol{\mu m}$) graph displaying hysteresis phenomenon observed due to material recovery.

3.4 Lamb brain testing for assessing tissue behaviour in compression

As the data from PDMS testing was relatively clean with minimal noise the progression was made to lamb brain to gain insight into the mechanical effects of testing actual tissue. Importantly sample geometry is critical to accurately measure stress (force/area). Using the Squisher Joy software crosshair style markers were placed on the edges of the sample and diameter measurements were taken at 3 different locations of the tissue (top, middle, and bottom) to get the height and average diameter for the specimen (A). In this trial, stepwise compression was performed to observe the expected stress relaxation behaviour of the tissue (B). At the second cyclic loading cycle (5%) stress relaxation behaviour is notably observed as force decreases exponentially while the sample is held at a constant displacement as indicated by figure 14C. As higher strains are experienced, the stress relaxation behaviour increases characterized by a higher rate of decay. Similarly, the respective hysteretic effect is captured in figure 14D.

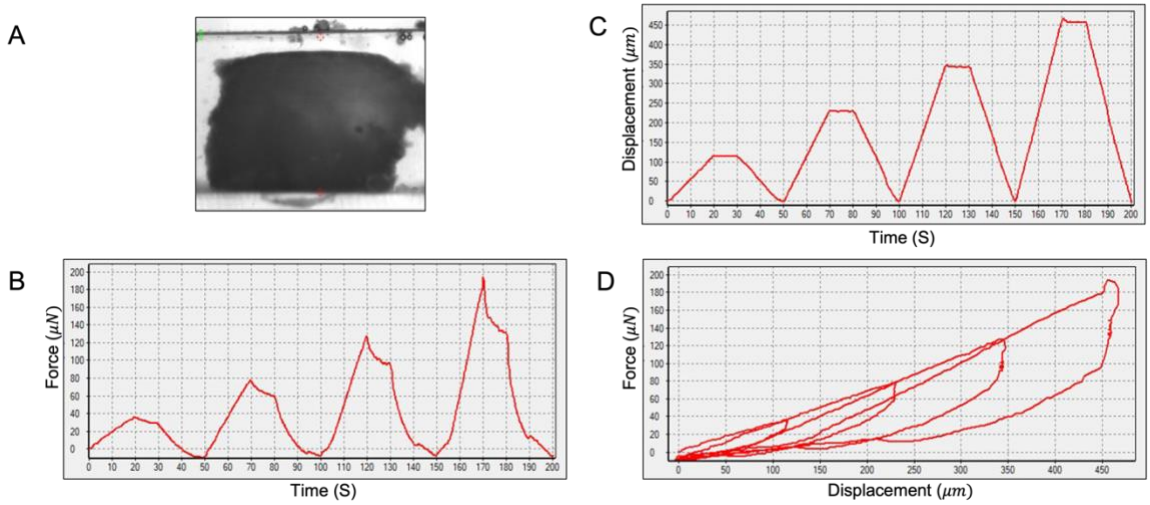

Figure 15: Assessing lamb brain tissue properties in cyclical loading at percent strains of 2.5%, 5%, 7.5%, and 10%. (A) Image of lamb brain under Microtester before compression testing showing relatively symmetrical geometry. (B) Force ($\boldsymbol{\mu N}$) vs time (s) curve showing stress relaxation behaviour of tissue distinguishable at second loading peak corresponding to 5% strain. (C) Displacement ($\boldsymbol{\mu m}$) vs time (s) graph showing relatively constant displacement of tissue over progressive loading cycles. (D) Force ($\boldsymbol{\mu N}$) vs displacement ($\boldsymbol{\mu m}$) graph displaying hysteresis due to tissue recovery.

Results

3.5 Human brain tissue is heterogeneous in stiffness

As the data produced from lamb brain specimens was relatively clean and sample preparation was optimized for the Microtester system, a progression was made to human brain specimens. Tissues were subjected to 10% compression over a 10-minute interval which translates to a very low strain rate of $1.6 \times 10^{-7} s^{-1}$ representative of quasi-static models. Such low strain rates negate the incompressibility of fluid in the tissue and aid in measuring structural components like ECM and cell bodies. Further tissue was kept in a fluid bath of PBS to minimize degradation of the tissue. Regions such as the white matter showed average stiffnesses of ~ 1300Pa in patient 1 and ~300Pa in patient 2. Grey-white

junctions showed less variability in stiffness between patients (~600Pa for Patient 1 and ~900Pa) for Patient 2). The Thalamus and Basal Ganglia were other variable regions of the brain in terms of their stiffness likely due to the extremely high intraregional structural heterogeneity [76]. Most posterior regions such as the Caudate head, Corona Radiata, Pons, and Cerebellum showed stiffnesses <500Pa.

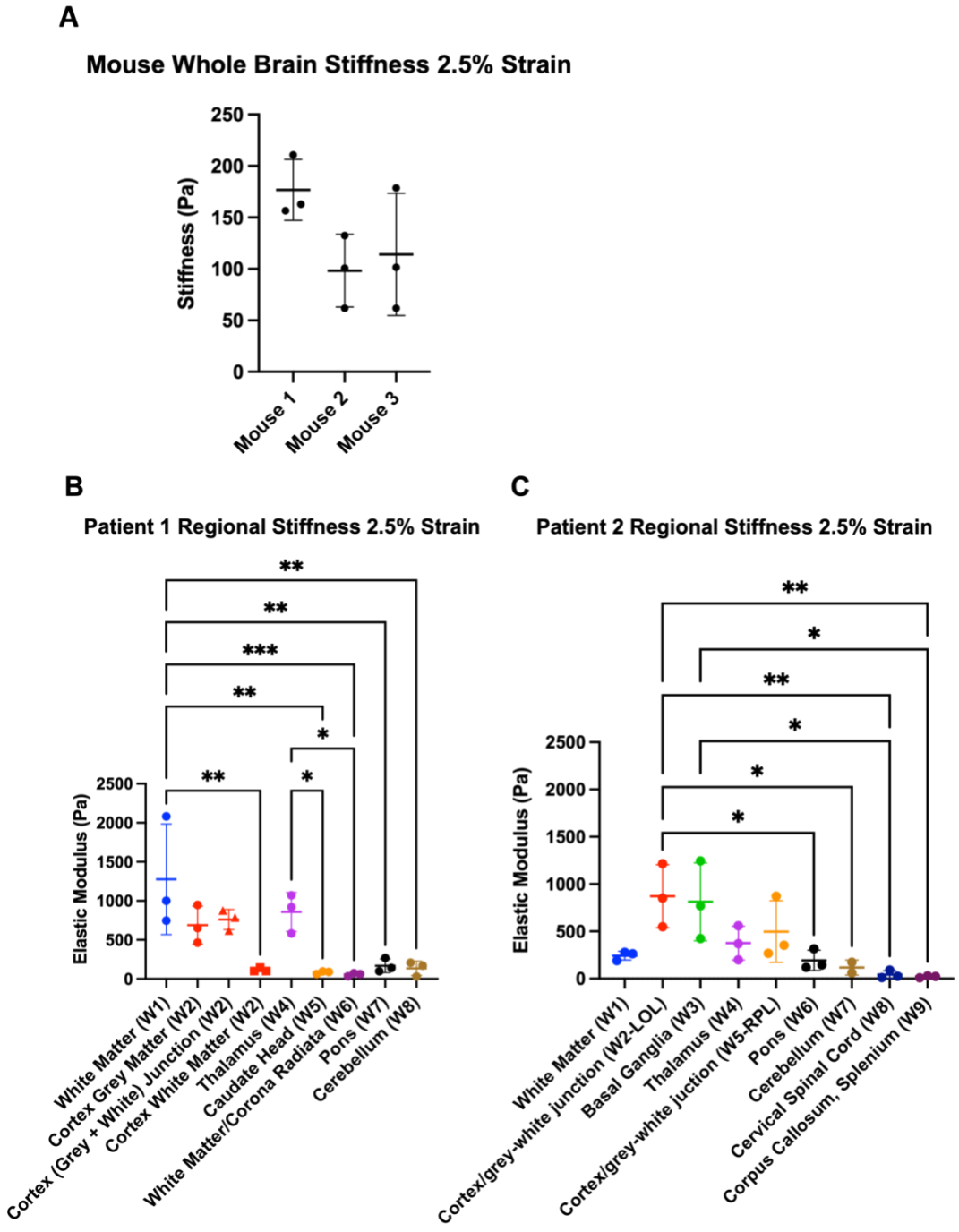

Figure 16: Compression testing of mouse brain (A) and different human brain regions (B). Elastic Modulus reported based on quasi-static compression method. Colour coded data points corresponds to regions of similar tissue composition. *p<0.05, **p≤0.01, ***p≤ **0. 001**. Basal ganglia for patient 1 (W3) was classified through outlier identification in GraphPad prism. LOL: left occipital lobe. RPL: right parietal lobe.

3.6 Anterior regions of the brain are stiffer than posterior

In sectioning the brain, 10 coronal cuts were made to create the cross-sections seen in Figure 17. In general, anterior regions of the brain were observed to be significantly stiffer than posterior regions. Deeper structures such as the Caudate head were also relatively soft compared to regions of the cortex including cortical white matter. The data shown here represents patient 1, however similar regional trends are seen for patient 2 as illustrated in Figure 16. Exceptions to these differences appear to be present when examining the basal ganglia (BG) of patient 2 which is a deeper structure resembling stiffness values of the grey-white junction of the cortex in the left occipital lobe). Additionally, the white matter (W1) of patient two appears to be quite softer with reduced variability than that of patient one. The Pons, Cerebellum, Corpus Callosum, and Cervical Spinal Cord are all significantly softer than regions of the grey-white matter from the cortex of patient two ($p<0.05$).

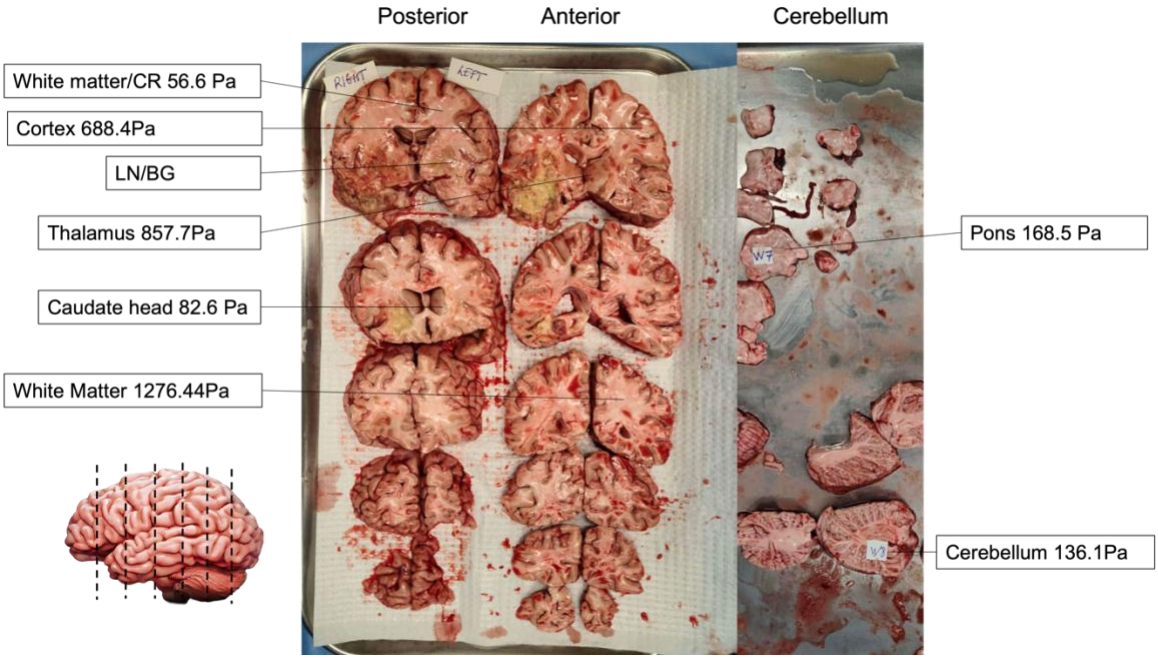

Figure 17: Anatomical arrangement of the human brain with coronal cross-sections showing the location of different regions and their respective elastic modulus. CR = corona radiata, LN = Lentiform Nuclei, BG = Basal Ganglia. LN/BG section was classified as outlier data thus mean stiffness could not be reliably calculated.

3.7 Comparison of viscoelastic model parameters

In the interest of modelling the tissue's viscoelastic response, stress relaxation data from stepwise ramp compressions at 7.5% strain were isolated and curve fitted using the curve fitting tool in Matlab. The model solves for three parameters in the equation which quantifies the observed stress relaxation behaviour (1) $\sigma(t) = \varepsilon_{7.5\%} * (\alpha e^{-bt}) + \sigma_e$. Notice that the ratio $\frac{\sigma_e}{\varepsilon_{7.5\%}}$ provides an elastic modulus at the point of stress equilibration at 7.5% compression. This can be compared across different regions in Figure 18 C & F. The coefficient of the spring parameter α is quite variable in patient 1 but shows significant ($p<0.05$, Fig. S7) gradual decline in patient 2 (Fig.18: A &D). The decay term (b), which models the decline in stress is relatively consistent across both

patients and shows no significant differences across brain regions (Figure 18: B & E). In comparing the equilibrated stress σ_e (Figure 18 C & F), no significant differences are observed in Patient 1 however, patient two shows region-specific decline trending towards the posterior regions (Fig S8). This may indicate a greater stress relaxation response in posterior regions of patient two and highlights the reality of mechanistic variation across different patients.

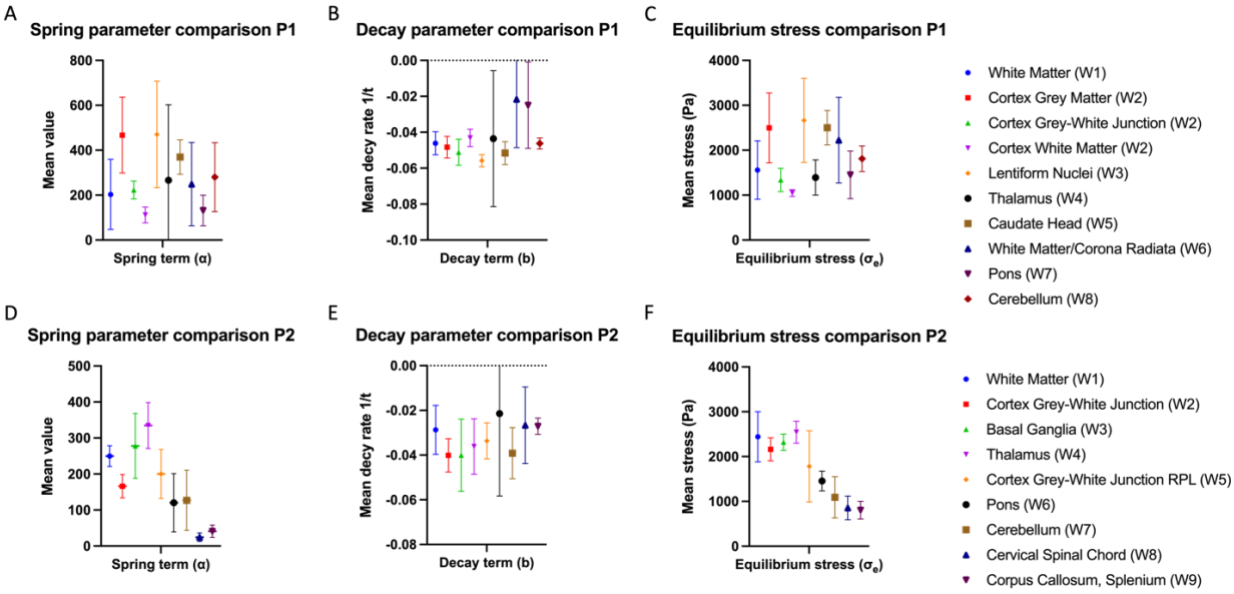

Figure 18: Comparison of the viscoelastic parameters of different brain regions. P1 = Patient 1 and P2 = Patient 2.

3.8 Mouse brain is closer in stiffness to posterior regions of the human brain than anterior regions

As a comparison to the human brain, mouse brains were also tested to examine similarities in stiffness between typical animal models and actual human tissue. Three mouse brains were compressed using the quasi-static compression method on samples

taken from the cerebrum. Regional sectioning was not possible due to the small size of the mouse brain. Based on the data in figure 16 mouse brain tissue resembles the stiffness of the softer, posterior regions of the human brain. Tissue from the Caudate head, Corona Radiata, Pons, and Cerebellum in Patient 1 was comparable to stiffnesses seen in mouse brain. Similarly, regions such as the Pons, Cerebellum, corpus callosum, and cervical spinal cord from patient two reassembled mouse brain stiffness.

Discussion

One of the biggest changes with mechanical testing of brain tissue is the sample preparation [155]. As the tissue is amorphous and highly hydrated obtaining a planar surface to contact the platen during compression is quite difficult without precise tools or standardized sectioning methods. Knowing that the tissue recovers from preconditioning, the samples were minutely compressed to obtain proper contact between the platen and specimen. Further, to prevent tissue degradation because of osmotic loss the specimens needed to be submerged in saline solution hence the use of a fluid bath filled with PBS (Fig S9). Another challenge is maintaining consistent geometry of the tissue during compression. When the tissue is compressed, the cross-sectional area contacting the platen expands radially (Figure 14A), and thus the stress experienced by the tissue changes given that stress is a ratio of force per cross-section area ($\sigma = \frac{force}{area}$). The model used here lacks a method to account for this change in stress and assumes the area of expansion is negligible. Measuring the change in diameter at multiple time points during quasi-static compression might be one possible solution to account for the change in

tissue geometry and subsequent stress. Another method to circumvent this issue would be to perform indentation testing with an indenter probe of known geometry [155]. While this places a limit on indentation depth, sample geometry is less of a concern [75]. Finite modelling may be a required addition to improving this method of testing to help access the inhomogeneous deformation experienced in compression [75].

Modelling viscoelastic behaviour is another challenge as the relaxation of the tissue requires very high level of sensitivity of force measurement. For this reason, not all curves fitted to the Zener model present strong goodness of fit ($r^2 \geq 0.9$) (Table S2 & S3) due to observed noise in the stress relaxation measurements. In addition to correcting sample geometry, this issue might be addressed by using a smaller gauge cantilever to increase force sensitivity. However, this may simultaneously increase noise in the measurements hence selecting the correct cantilever requires certain trade-offs to obtain precise forces readings.

The results obtained here show the highly heterogeneous nature of brain tissue stiffness and open the door for further investigations into the impacts of numerous other factors on tissue mechanical properties. Given the high variation in stiffness seen between patients, questions regarding age, and the effect of chemotherapy on healthy brain mechanics need to be probed to further understand these results. Recent data suggest that cells become 55-75% less stiff when treated with chemotherapeutic agents which may partially contribute to the variability of these results [160]. Additionally, the cellular and extracellular composition of the brain differs depending on region and subsequent function [161]. When we learn new tasks, the neurons responsible for the associated skill

will form further connections and create new synapses [75]. Thus, it is hypothesized that brain plasticity which initiates changes in tissues microstructure affects the mechanical response [75]. ECM composition is connected to this line of questioning given that a positive correlation exists between myelination and stiffness [162]. Whether this correlation can also be observed in compression testing is currently not understood and might be another area for future work.

Conclusion

The work done in this chapter highlights the differences in elastic modulus between different brain regions across two different patients. Significant differences in stiffness were observed in 5 different pairwise comparisons of brain regions ($p<0.05$). General trends such as progressive softness in the tissue towards the posterior regions of the brain were also observed. Also, mouse brains were shown to only resemble posterior regions of the human brain calling into question the validity of this model for biomechanically relevant research. Finally, high variability was observed in the viscoelastic response of tissue from both patients. However, like regional trends in stiffness, there appear to be patterns of stress relaxation in Patient 1 showing decreasing equilibrated stress trending towards posterior regions of the brain.

Chapter 4: Probing mechanotransduction biomarkers in brain tissue

Chapter motivation and overview

The final chapter of this thesis focuses on understanding the connection between the stiffness heterogeneity in the brain and the related Piezo1 expression. In the larger scope of this research, this work may help to establish a connection between stiffness modulation, Piezo1 activation, and downstream YAP or β-catenin expression. Piezo1 is activated through modulation of surface stiffness [94], [163] just like YAP [86], [112], [164] and β-catenin [165]. Given that Piezo1 is upstream of YAP, there is reason to speculate that Piezo1 expression and YAP activity may be connected [95], [166]. This has implications in cancer metastasis, specifically in breast and brain cancers [64], [167]. The commonalities in Piezo1 expression between primary breast and brain cancers could highlight certain analogous pathways which are perturbed in breast cancers. These changes could aid metastatic breast cancers in colonizing the vastly different mechanical environment of the brain. As such, understanding the stiffness-Piezo1-YAP connection may further our understanding of how tumors adapt to their microenvironment and elucidate potential biomarkers for therapeutic targeting.

Due to the complexity of probing stiffness dependent cellular pathways, the preliminary work carried out here examines whether Piezo1 expression correlates with tissue stiffness as quantified in chapter 3. As Piezo1 expression is correlated with stiffness, it was used as a readout to measure cellular responses to the differences in

stiffness heterogeneity at the cellular level. In non-cancerous brain tissue, this serves to establish basal levels of Piezo1 expression which can be compared to diseased conditions such as cancer and other neurological diseases in future work.

Two regions of the brain, white matter, and grey-white matter junctions were probed for Piezo1 expression through immunofluorescent (IF) staining. To accurately capture the signal of DAPI (nuclear stain) and Piezo1 a segmentation workflow was automated by developing a macro script in ImageJ. When comparing IF stains, a reference H&E image was used to observe cellular morphology within the brain tissue. Next, downstream effector YAP was examined through immunoblotting to observe whether basal levels of Piezo1 induce expression of YAP in non-diseased tissue. In conjunction, β-catenin abundance was examined as it is a key regulator of the Wnt pathway which is known to have overlapping effects with YAP in the Hippo pathway [130], [131].

Introduction

4.1 Piezo1 expression in the brain

During development, brain cells experience force induced by cell motility, cell-cell contact, and ECM stiffness which dictate neuronal stem cell lineages and regional growth patterns [168]. Piezo1 has been shown to dictate neuronal stem cell lineage, and axonal growth through mechanotransduction [169], [170]. Specifically, Piezo1 activation elicits transient Ca^{2+} passage showing stiffness dependency which favours nuclear localization of YAP and influences neuronal vs glial differentiation [170]. As such,

aberrant Piezo1 activity might serve as a prognostic marker in diseases that take advantage of perturbed stiffness and cellular plasticity such as cancer [167]. In terms of innate expression in the brain, Piezo1 mRNA is expressed mainly in neurons of healthy human brains and absent from astrocytes [171]. In diseased conditions such as Alzheimer's, Piezo1 mRNA expression is high in astrocytes but relatively low in neurons suggesting altered mechanotransduction [171]. Whether similar expression profiles are seen across all regions of the brain and in different diseases remains unclear, however the heterogeneous nature of the brain suggests significant complexity in Piezo1 related mechanotransduction. Thus, breaking down this complex area of work by studying basal levels of Piezo1 in different regions of non-diseased brain serves as a foundation for understanding perturbed mechanotransduction in brain diseases.

4.2 Piezo1 interactions with YAP and β-catenin

On soft substrates, calcium influx driven by Piezo1 is relatively low but scales with increasing stiffness [170]. Similarly, nuclear localization of YAP is minimal on soft substrates but scales proportionally with substrate stiffness [86]. In examining the interaction of these seemingly independent events, Piezo1 knock down experiments showed nuclear exclusion of YAP, on stiff substrates [170]. Thus, Piezo1 activity is thought to directly influence YAP nucleo-cytoplasmic shuttling likely initiated through tractional forces [170]. The localization of YAP is known to influence cancer cell motility and metastasis and is exacerbated on stiff substrates [86]. Similar phenomena are observed in other types of cancer such as breast, gastric, colorectal, pancreatic, and

prostate cancer [64]. Specifics on how Piezo1 upregulation modulates the biochemical checkpoints of YAP homeostasis however have yet to be elucidated. In addition, Piezo1 is shown to interact with β-catenin-cadherin complexes showing a biochemical and functionally tethered mechanism for mechanogating [122]. Disrupting β-catenin and its cytoskeletal binding partners leads to Piezo1 dysfunction highlighting its interaction with proteins that modulate intracellular tension [122]. Given that cytoskeletal tension is correlated with stiff substrates and is known to regulate cell proliferation and metastasis, understanding locations that have intrinsically high levels of cellular tension could identify preferential metastatic sites [172]. For this reason, examining the regional heterogeneity in Piezo1 expression within the brain could identify a possible pre-metastatic niche based on tissue biomechanics.

Results

4.3 Segmentation analysis for capturing immunofluorescence

The regional expression of Piezo1 was observed by performing immunofluorescent staining on the white matter and grey-white matter junctions of the cortex in patient 1. Before quantifying the relative expression of Piezo1 a segmentation workflow was developed to automate signal quantification in IF images (Figure 19A). Using a macro script in ImageJ the fluorescent signals of DAPI (nuclei) and Texas Red (Piezo1) were isolated by applying thresholds and a series of masks for each channel. Using the Watershed and Kuwahara filter, joined nuclei were separated, and membranous edges were preserved respectively. The segmentation feature was then applied to

numerically isolate the respective fluorescent areas (Fig. 19B) and intensity measurements were taken from the original image. Approximately 90% of the signal for DAPI and Piezo1 were captured by defining a particle exclusion size of 200 pixels or greater.

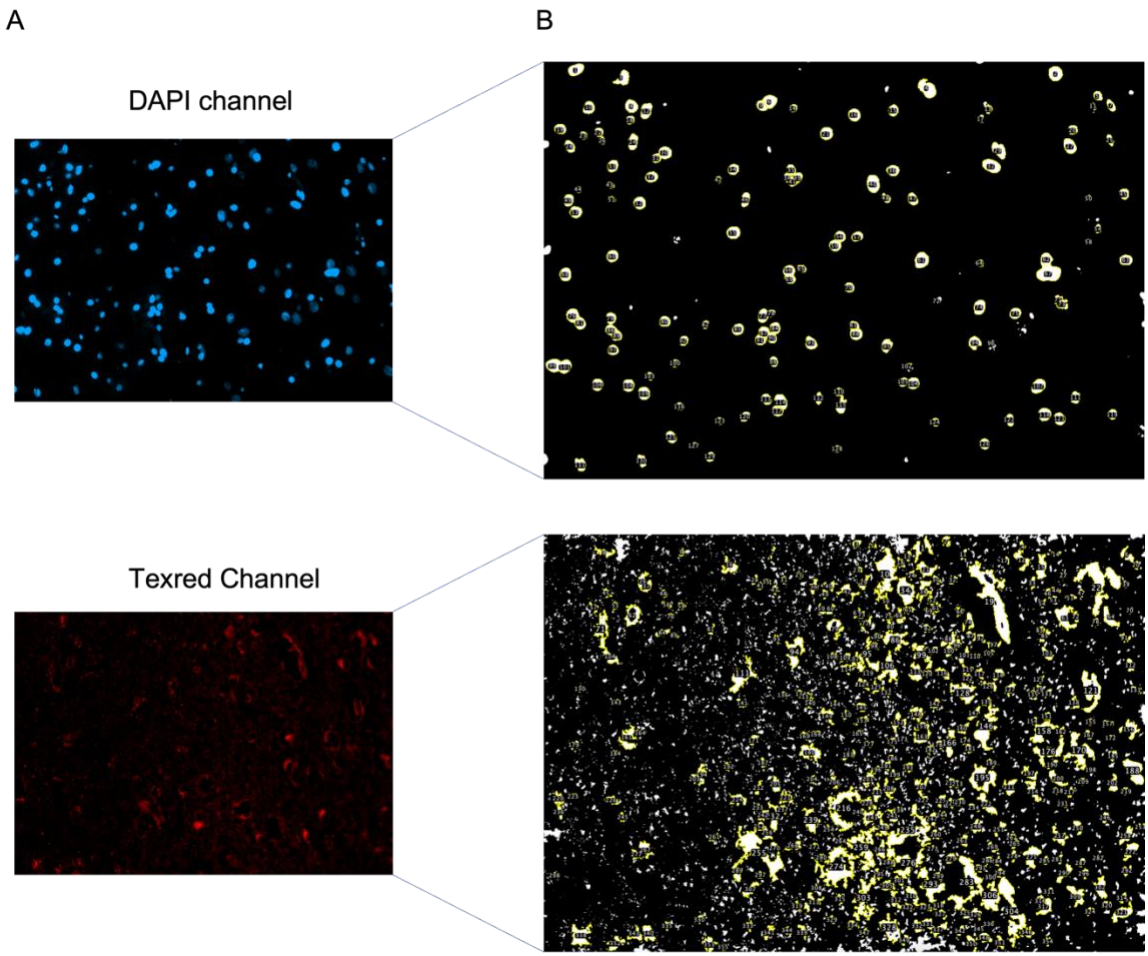

Figure 19: Applying segmentation workflow to automate immunofluorescence signal isolation. After creating a masking layer on initial fluorescent images (A), specific signals based on particle size can be isolated using the threshold feature in Fiji. The segmentation algorithm is then applied (B) to numerically isolate fluorescent signals and measure their mean intensity in the original image using the segmented masking layer in B. Particle size $\geq$ 200 pixels.

4.4 Region specific expression of Piezo1

The region-specific characterization of Piezo1 shows that white matter from Patient 1 has significantly lower expression compared to other regions from the same patient and in comparison to Patient 2 (Fig 20A, B). Tissue architecture for each section of each region was also characterized using H&E staining. The grey-white matter junction is separated by a white line in H&E images (Fig 20A). Nuclear size and arrangement were indicative of the interface of grey and white matter. Cells to the right of the white lines show circular nuclei with small white perimeters indicative of oligodendroglia in white matter (Fig. 20A). Conversely, triangular, and pyramidal cell morphologies (left of white lines, Fig. 20A) are indicative of neurons primarily found in grey matter. Many pyramidal neurons have small round nuclei associated with them known as satellite cells which are oligodendroglia cells in grey matter (left of white line Fig. 20A). Piezo1 staining seems to border the nuclei of cells which is characteristic of its membranous staining pattern. The total area of Piezo1 expression was significantly higher in the grey matter of patient 2 compared to the grey and white matter of patient 1. Mouse retina was used as the positive control due to its inherently high expression of Piezo1.

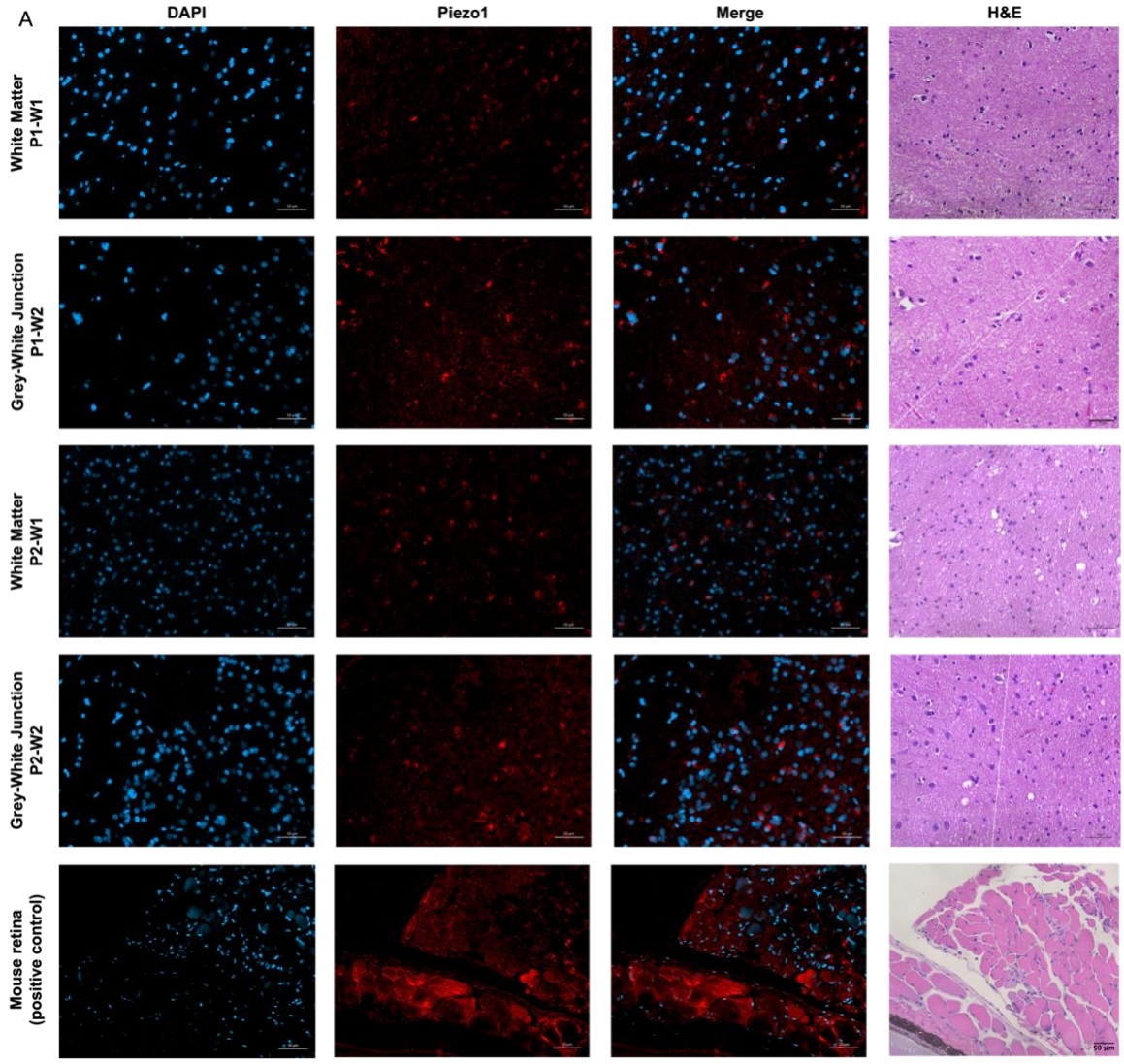
A
DAPI
Piezo1
Merge
H&E
White Matter P1-W1
Grey-White Junction P1-W2
White Matter P2-W1
Grey-White Junction P2-W2
Mouse retina (positive control)
50 µm

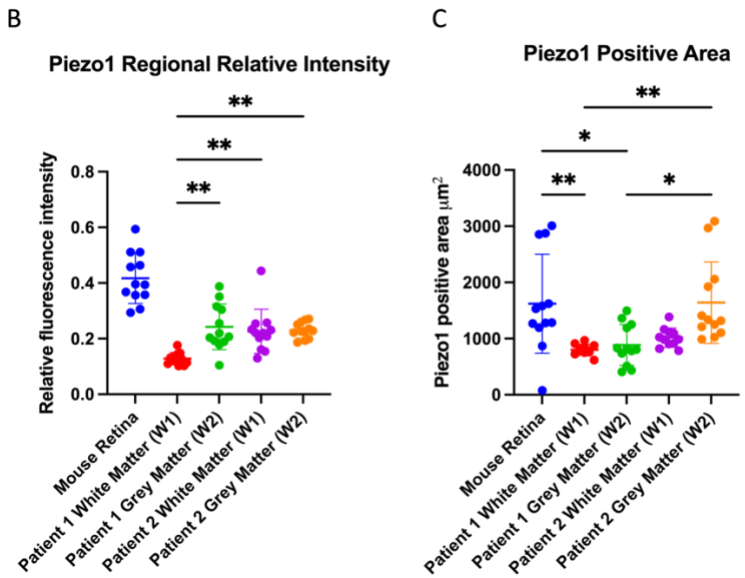

Figure 20: Regional characterization of Piezo1 expression. (B) Piezo1 expression normalized against DAPI showing the relative mean fluorescence intensity per cell across multiple regions of interest (n=12). (C) Mean area of positive Piezo1 expression per region across multiple regions of interest (n=12). *p < 0.05, **p<0.01. Scale bar = 50μm. Mouse retina was used as a Piezo1 positive control.

4.5 Screening regulators of Hippo and Wnt pathway in brain regions

Immunoblotting was performed on several key proteins to validate Piezo1 expression observed through IF staining and to identify active downstream pathways. In an initial screening, the abundance of Piezo1, YAP, pYAP, and β-catenin was evaluated with β-actin serving as the internal loading control (Fig. 21A). Results demonstrated a relatively low abundance of YAP and pYAP (Fig. 21A). In contrast, at higher quantities of loaded protein (20μg), discernable banding was observed for Piezo1 in both white matter and at the grey-white junction (Fig. 21A). β-catenin intensity was greatest in white matter at 10 μg for this initial screening which was the highest intensity across all other

regions (Fig. 21 A) Thus, for subsequent blots, the proteins of focus were Piezo1, and β-catenin using 20μg as the input quantity. The subsequent repeat blots (Fig. 21 B, C) showed similar expression of Piezo1 in both regions as quantified through band intensity (Fig. 21D). In contrast, the expression of β-catenin was quite variable with no significant difference in expression across regions (Fig. 21D).

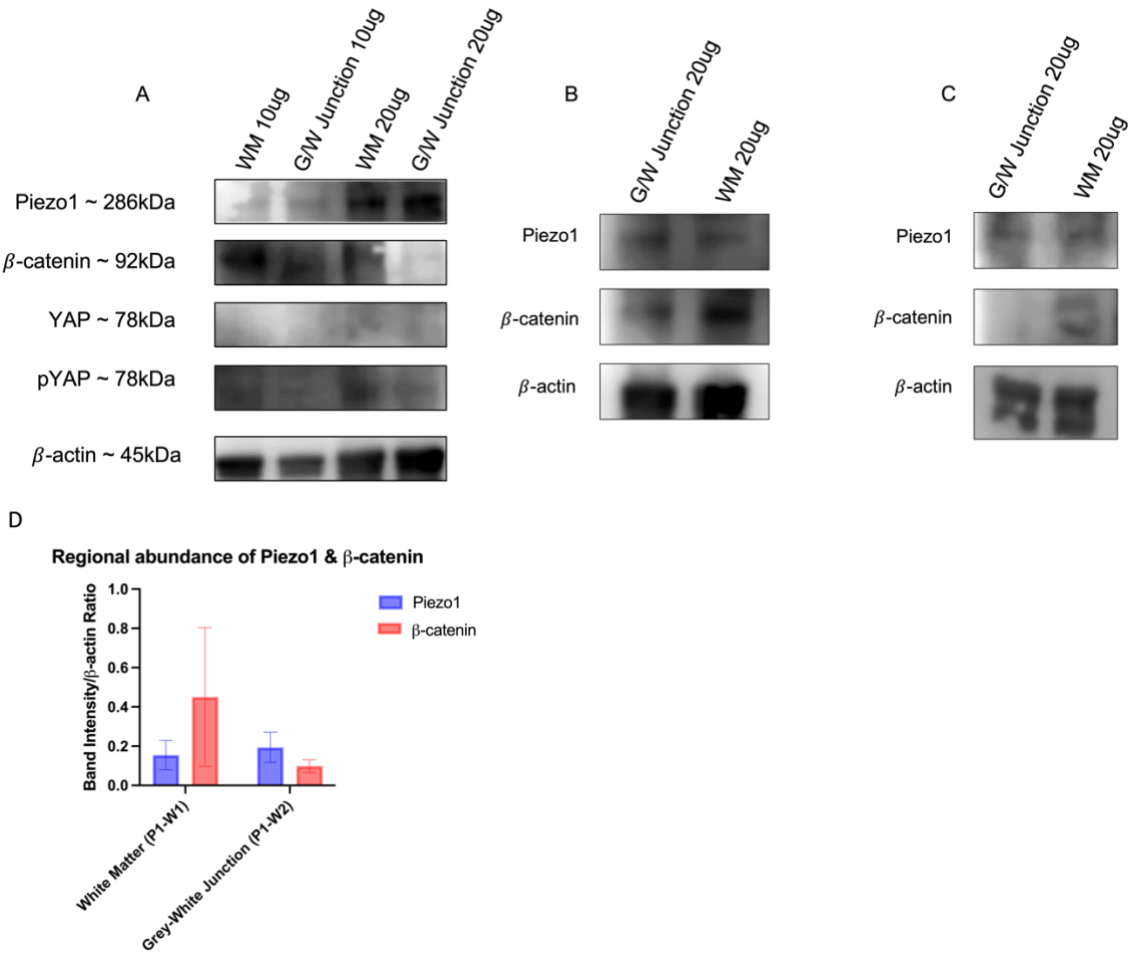

Figure 21: Screening Hippo and Wnt regulators through immunoblotting analysis. WM (White Matter from Cortex), G/W Junction (Grey-White Matter Junction from Cortex). Samples acquired only from Patient 1. (A) Initial screening of key proteins of Hippo and Wnt pathway using YAP and β-catenin as respective markers. (B) Probing Piezo1 and β-catenin expression using only 20μg of protein lysate. (C) Replicate blot as produced in B. Band intensity calculated via a ratio of target protein band divided by the associated β-actin band.

Discussion

This chapter examines the basal levels of Piezo1 expression in brain tissue of two different regions, including white matter and grey-white matter junctions. No significant differences were observed in Piezo1 expression between the regions. While mouse tissue served as a positive control of Piezo1 expression, effective negative controls should be established in future studies. The use of nonspecific blockers such as GsMTx-4 could serve as negative controls by reducing Piezo1 in cells for IF staining [102]. Although the expression of Piezo1 between grey and white matter was similar, additional testing should be performed on softer regions of the brain such as the Pons or Cerebellum. Theoretically, soft tissues induce less mechanical stress via stress fibers and therefore have less Piezo1 expression [87], [169], [173]. Further, these preliminary observations do not examine the expression of Piezo1 in the various other regions mechanically examined in Chapter 3 due to time and resource limitations. Subcortical white matter such as the Corona Radiata, and areas with greater mechanical heterogeneity like the Thalamus might show unique Piezo1 expression levels. In rat brains with Alzheimer's, relatively higher levels of Piezo1 were observed in the Choroid Plexus [171]. Comparatively, the white matter tracts in the Thalamus and Striatum expressed more Piezo1 than grey matter areas [171]. Whether this differential expression is analogous in human brains however remains unclear.

Optimizations in immunoblotting analysis could include gentle tissue homogenization achieved through manual grinding rather than high speed blending. This might aid in further preserving the various proteins in the tissue samples and prevent degradation due to shearing and excessive frothing. Also, the choice of primary and

secondary antibodies might need to be optimized and thus subsequent incubation conditions must be re-evaluated to achieve consistent protein banding.

Membrane deformation via substrate stiffness is known to regulate Piezo1 activity of brain cells [170]. Whether breast cancer cells can modulate their own Piezo channel expression to colonize ultrasoft tissue such as the brain remain unknown. Given that triple-negative breast cancers are less perturbed by soft stiffnesses, they may have adapted mechanotransduction features including aberrant Piezo1 channel expression that aid in colonizing soft substrates [136]. Piezo1 however, is correlated with proliferation and migration of breast cancer cells [174]. Inhibiting Piezo1 restricts migration by reducing the formation of invadopodia and the expression of metalloproteinases (MMPs) [174]. Overall, the connection between Piezo1 and downstream mechanosensors like YAP and β-catenin remains unclear. For this reason, studying their regional variability in the brain may provide clues into tissue biomechanics and the development of pre-metastatic niches that favour cancer colonization.

Conclusion

In this chapter, the expression of Piezo1 was quantified using cell segmentation analysis to capture the fluorescent intensity of Piezo1 in the white and grey matter of human brain tissue. Results demonstrated that white matter from Patient 1 had less Piezo1 expression compared to grey matter from the same patient and grey and white matter from Patient 2. The area of Piezo1 expression was most widespread in Patient 2 grey matter compared to the Piezo1 distribution in Patient 1. Immunoblotting showed no

significant differences in Piezo1 expression and subsequent mechanotransduction regulators including YAP and β-catenin. Future work to characterize the expression of these mechanosensors in softer regions of the brain should be performed to obtain a complete picture of the regional Piezo1 heterogeneity.

Chapter 5

Summary

This thesis was inspired by gaps in research surrounding brain biomechanics and cellular mechanotransduction relating to breast cancer metastasis. Given the complex and dynamic behaviour of cancer in the body, there is no single avenue to finding treatments. Thus, investigating cancer from unique perspectives such as the biomechanical interplay between surface stiffness and mechanotransduction may shed light on preventative measures and potential therapeutic targets. Therefore, this work investigated the effects of stiffness on key mechanotransduction regulator YAP in breast cancer cells. As breast-to-brain metastasis is extremely lethal, characterization of stiffness heterogeneity within human brain tissue was performed to identify possible pre-metastatic niches based on the tissue's biomechanics. Finally, Piezo1 which is a stiffness dependent biomarker upstream of YAP was probed for its region-specific expression to determine if cells within the brain can detect variations in tissue stiffness. This serves as foundational work for possible cancer therapies that could target mechanotransduction proteins.

In chapter two, the stiffness dependency of cancer migration was investigated. Initially, an appropriate range of surface stiffnesses were required thus various formulations of PDMS substrate were prepared to examine the effect of formulation composition on substrate stiffness. Overall, the stiffness inversely correlated to quantities of crosslinker added to the elastomer base. Using this information, the migratory capabilities of cancer cells were evaluated on stiff and soft substrates. TNBC showed

greater migratory capability on stiff substrates compared to cultures on soft substrates. YAP nuclear localization is thought to modulate migratory phenotypes of cancer cells however its response to surface stiffness in breast cancer is not fully understood [87], [113]. The colocalization assay performed in this chapter showed increased nuclear entry of YAP on stiff substrates in TNBC and is correlated with a greater migratory phenotype. While focal adhesion dynamics were not fully understood through paxillin staining in this work, there is evidence to suggest the density of these complexes is proportional to surface stiffness [108], [175], [176]. This might indicate that cancer cells adhere to stiff substrates more readily which is critical for their growth and migration [177].

O-GlcNac modifications of YAP are also shown to induce its nuclear localization [137], [138], [148]. The interplay between this post-translational modification and substrate stiffness was another area of investigation in this chapter. Immunoprecipitation and subsequent immunoblotting were used to capture O-GlcNac-YAP in TNBC. Through troubleshooting, the incubation time to create bead-Ab complexes was found to be suboptimal for immunoprecipitation. Overnight incubation improved the relative abundance of hybridized capture antibodies on the Sepharose beads which is an encouraging improvement on the current method. Knowing this, future experiments can be conducted using these enhanced IP pre-processing steps to hopefully capture detectable levels of O-GlcNac-YAP. Investigating whether YAP-O-GlcNac status changes in cancer cells cultured on stiff-soft substrate gradients could provide evidence linking mechanical cues, biochemical signalling, and YAP activation. Overall, the

findings in this chapter suggest that stiff matrices promote the migration of TNBC through YAP mediated signalling.

In chapter 3, the stiffness heterogeneity of brain tissue which is a lethal metastatic site for breast cancer was mechanically characterized. As cancer metastasis is thought to be a non-random process governed partially by mechanical cues [7], [12], examining the local variations in tissue stiffness may provide insight into sub-locations that are better suited for cancer colonization. Overall, human brain tissue was shown to be mechanically heterogeneous as five to six pairwise comparisons between different regions showed significant variations in stiffness. Further, anterior regions of the brain were generally observed to be stiffer compared to posterior regions. Some of the stiffer regions include the gray to white matter junctions in the cortex and the white matter of the cortex. Conversely, regions such as the Pons, Cerebellum, Corona Radiata, Cervical Spinal Cord, and Corpus Callosum were significantly softer. As a comparison, mouse brain was also tested showing comparable stiffness to posterior regions of the human brain. The viscoelastic properties were considerably more variable than elastic modulus data. Using a Zener model, the equilibrium stress after tissue relaxation was shown to be significantly different in multiple regions of Patient 2 but not Patient 1. Additionally, the spring parameter associated with viscoelastic decay was different in multiple regions from Patient 2. The quasi-static and stepwise compression methods used here appear to produce consistent results based on the relatively clean data observed in Figures 14, 15, and S6. Importantly, mechanical properties of highly amorphous tissues such as the brain hold true for a given testing method, and thus absolute values for stiffness and

viscoelasticity are dependent on the testing method applied. Consistency in sample preparation and repeatability in mechanical testing is the primary driver for reliable characterization of brain specimens [75].

Chapter 4 expands on information acquired from the previous chapters to examine the combined effect of tissue stiffness and associated mechanotransduction pathways. Numerous biomarkers exist that allow cells to modulate their intracellular trafficking in response to external mechanical cues [85], [122], [174], [175]. Piezo1 is an example of such a biomarker that becomes activated on stiff substrates and is connected to YAP and B-catenin which are key transcription factors in the Hippo and Wnt pathways [95], [106], [122]. For this reason, Piezo1 expression was used as a readout of tissue stiffness across the different brain regions examining the notion of whether cells can detect the stiffness heterogeneity observed through mechanical characterization. Results showed that Piezo1 fluorescent intensity in the white matter of Patient 1 was significantly less than other regions including those of Patient 2. Additionally, the total area of Piezo1 expression was marginally greater in the grey matter of Patient 2 showing significant differences when compared to both regions of Patient 1. When screening for YAP and β-catenin abundance no significant differences were observed between the tissue regions. However, immunoblotting analysis showed that Piezo1 is detectable using 20μg of protein input and thus further analysis using optimized tissue homogenization and immunoblotting conditions may enhance the signal in future experiments. Future study in this chapter necessitates investigation of tissues derived from softer regions of the brain such as the

Pons, and Cerebellum. Understanding how Piezo1 expression changes based on stiffness remains incompletely understood. Thus, investigating its regional expression in the brain may provide clues on microenvironments that biomechanically favour cancer metastasis.

Although the *in vitro* model and mechanical testing work conducted in this project produce valuable data for investigating the interplay between stiffness heterogeneity and mechanotransduction, there are limitations to the various systems. As observed in chapter 2, stiffness does play a role in cancer migration however the effect of ECM proteins is not characterized here. *In vivo,* the various tissue surfaces are composed of complex ECM networks that need to be incorporated to obtain better mimic cancer behaviour *in vitro.* Additionally, while 2D models are commonly used in biological research, cells grow in the 3D microenvironments within the body. The growth patterns and effectiveness of therapeutics are shown to be altered in 3D culture systems which further recapitulate the cellular response *in vivo* [178]. In examining the effect of YAP-O-GlcNacylation, establishing refined control conditions is necessary to assess the reproducibility of immunoprecipitation assays. Treating breast cancer cells with PuGNac of GlcNac are examples of methods used to artificially increase global O-GlcNacylation which could serve as a positive control in future immunoprecipitation assays [148]. Another avenue in examining O-GlcNacylation-YAP interaction is by preventing YAP phosphorylation through mutant cell lines. Recall that the result of YAP-O-GlcNacylation promotes YAP nuclear entry by blocking its phosphorylation from LATS1/2 [137]. An analogous response might be observed by creating mutant cell lines that lack the peptide sequence

required for phosphorylation. This can be achieved by introducing point mutations in genes that encode YAP phosphorylation residues such as serine 127 (S127) or serine 109 (S109) [179]. Examining the growth patterns of such mutant cell lines on a stiffness gradient could help elucidate the interplay between YAP post-translational modifications and YAP mechanotransduction.

The current method used to quantify brain tissue stiffness requires precise sample preparation and is sensitive to variations in sample geometry. The use of indentation testing could circumvent this problem as small indenter diameters could probe larger sections of different topography without the need to cut smaller sections of tissue [158]. Additionally optimizing the mechanical model to improve viscoelastic curve fitting may be beneficial if more accurate predictions of materials properties can be achieved [75].

Piezo1 expression was incompletely examined across the different brain regions and thus staining the remaining regions apart from grey and white matter could provide greater insight into the regional differences in brain cell mechanosensing. Applying a counter membranous stain in future experiments could validate the expected staining patterns of Piezo1 particularly since different cells have variable levels of Piezo1 expression. To this end, investigating the cellular variability in Piezo1 expression depending on cell type is another unique research question given that brain tissue is composed of several different cell types.

In conclusion, this research demonstrated the interdisciplinary nature of mechanotransduction from a biomechanical perspective. In application, this may help determine if tissue biomechanics and their associated mechanotransduction biomarkers

can predict a pre-metastatic niche that is conducive to secondary metastases. The interplay between YAP mechanotransduction, tissue stiffness, and Piezo1 activity is still unknown. As the biomechanical perspective in cancer research is relatively novel, this area of work has the potential to elucidate new biomarkers for breast cancer therapy that may change the way we understand this complex disease.

Bibliography

[1] A. I. Riggio, K. E. Varley, and A. L. Welm, "The lingering mysteries of metastatic recurrence in breast cancer," *British Journal of Cancer*, vol. 124, no. 1, pp. 13–26, Jan. 2021, doi: 10.1038/s41416-020-01161-4.

[2] D. X. Nguyen, P. D. Bos, and J. Massagué, "Metastasis: from dissemination to organ-specific colonization," *Nature Reviews Cancer*, vol. 9, no. 4, pp. 274–284, Apr. 2009, doi: 10.1038/nrc2622.

[3] S. Dawood, X. Lei, J. K. Litton, T. A. Buchholz, G. N. Hortobagyi, and A. M. Gonzalez-Angulo, "Incidence of brain metastases as a first site of recurrence among women with triple receptor–negative breast cancer," *Cancer*, vol. 118, no. 19, pp. 4652–4659, Oct. 2012, doi: https://doi.org/10.1002/cncr.27434.

[4] N. Harbeck *et al.*, "Breast cancer," *Nature Reviews Disease Primers*, vol. 5, no. 1, p. 66, Dec. 2019, doi: 10.1038/s41572-019-0111-2.

[5] X. Lu and Y. Kang, "Organotropism of Breast Cancer Metastasis," *Journal of Mammary Gland Biology and Neoplasia*, vol. 12, no. 2–3, pp. 153–162, Aug. 2007, doi: 10.1007/s10911-007-9047-3.

[6] P. S. Steeg, "Tumor metastasis: mechanistic insights and clinical challenges," *Nature Medicine*, vol. 12, no. 8, pp. 895–904, Aug. 2006, doi: 10.1038/nm1469.

[7] R. R. Langley and I. J. Fidler, "The seed and soil hypothesis revisited--the role of tumor-stroma interactions in metastasis to different organs," *Int J Cancer*, vol. 128, no. 11, pp. 2527–2535, Jun. 2011, doi: 10.1002/ijc.26031.

[8] N. N. Pavlova and C. B. Thompson, "The Emerging Hallmarks of Cancer Metabolism," *Cell Metabolism*, vol. 23, no. 1, pp. 27–47, Jan. 2016, doi: 10.1016/j.cmet.2015.12.006.

[9] D. Hanahan and R. A. Weinberg, "Hallmarks of Cancer: The Next Generation," *Cell*, vol. 144, no. 5, pp. 646–674, Mar. 2011, doi: 10.1016/j.cell.2011.02.013.

[10] D. Zhang *et al.*, "CHG: A Systematically Integrated Database of Cancer Hallmark Genes," *Frontiers in Genetics*, vol. 11, Feb. 2020, doi: 10.3389/fgene.2020.00029.

[11] N. Zaman *et al.*, "Signaling Network Assessment of Mutations and Copy Number Variations Predict Breast Cancer Subtype-Specific Drug Targets," *Cell Reports*, vol. 5, no. 1, pp. 216–223, Oct. 2013, doi: 10.1016/j.celrep.2013.08.028.

[12] B. Psaila and D. Lyden, "The metastatic niche: adapting the foreign soil," *Nature Reviews Cancer*, vol. 9, no. 4, pp. 285–293, Apr. 2009, doi: 10.1038/nrc2621.

[13] S. A. Chikarmane, S. H. Tirumani, S. A. Howard, J. P. Jagannathan, and P. J. DiPiro, "Metastatic patterns of breast cancer subtypes: What radiologists should know in the era of personalized cancer medicine," *Clinical Radiology*, vol. 70, no. 1, pp. 1–10, Jan. 2015, doi: 10.1016/j.crad.2014.08.015.

[14] A. F. Chambers, A. C. Groom, and I. C. MacDonald, "Dissemination and growth of cancer cells in metastatic sites," *Nature Reviews Cancer*, vol. 2, no. 8, pp. 563–572, Aug. 2002, doi: 10.1038/nrc865.

[15] F. van Zijl, G. Krupitza, and W. Mikulits, “Initial steps of metastasis: Cell invasion and endothelial transmigration,” *Mutation Research/Reviews in Mutation Research*, vol. 728, no. 1–2, pp. 23–34, Jul. 2011, doi: 10.1016/j.mrrev.2011.05.002.
[16] A. Haeger, K. Wolf, M. M. Zegers, and P. Friedl, “Collective cell migration: guidance principles and hierarchies,” *Trends in Cell Biology*, vol. 25, no. 9, pp. 556–566, Sep. 2015, doi: 10.1016/j.tcb.2015.06.003.
[17] K. Wolf *et al.*, “Physical limits of cell migration: Control by ECM space and nuclear deformation and tuning by proteolysis and traction force,” *Journal of Cell Biology*, vol. 201, no. 7, pp. 1069–1084, Jun. 2013, doi: 10.1083/jcb.201210152.
[18] P. Friedl and S. Alexander, “Cancer Invasion and the Microenvironment: Plasticity and Reciprocity,” *Cell*, vol. 147, no. 5, pp. 992–1009, Nov. 2011, doi: 10.1016/j.cell.2011.11.016.
[19] S. P. H. Chiang, R. M. Cabrera, and J. E. Segall, “Tumor cell intravasation,” *American Journal of Physiology-Cell Physiology*, vol. 311, no. 1, pp. C1–C14, Jul. 2016, doi: 10.1152/ajpcell.00238.2015.
[20] O. J. Scully, B.-H. Bay, G. Yip, and Y. Yu, “Breast Cancer Metastasis,” *Cancer Genomics - Proteomics*, vol. 9, no. 5, p. 311, Sep. 2012, [Online]. Available: http://cgp.iiarjournals.org/content/9/5/311.abstract
[21] A. Bonnomet *et al.*, “Epithelial-to-Mesenchymal Transitions and Circulating Tumor Cells,” *Journal of Mammary Gland Biology and Neoplasia*, vol. 15, no. 2, pp. 261–273, Jun. 2010, doi: 10.1007/s10911-010-9174-0.
[22] Y. Xin, K. Li, M. Yang, and Y. Tan, “Fluid Shear Stress Induces EMT of Circulating Tumor Cells via JNK Signaling in Favor of Their Survival during Hematogenous Dissemination,” *International Journal of Molecular Sciences*, vol. 21, no. 21, p. 8115, Oct. 2020, doi: 10.3390/ijms21218115.
[23] D. S. Micalizzi, S. Maheswaran, and D. A. Haber, “A conduit to metastasis: circulating tumor cell biology,” *Genes & Development*, vol. 31, no. 18, pp. 1827–1840, Sep. 2017, doi: 10.1101/gad.305805.117.
[24] N. P. A. D. Gunasinghe, A. Wells, E. W. Thompson, and H. J. Hugo, “Mesenchymal–epithelial transition (MET) as a mechanism for metastatic colonisation in breast cancer,” *Cancer and Metastasis Reviews*, vol. 31, no. 3–4, pp. 469–478, Dec. 2012, doi: 10.1007/s10555-012-9377-5.
[25] A. Irmisch and J. Huelsken, “Metastasis: New insights into organ-specific extravasation and metastatic niches,” *Experimental Cell Research*, vol. 319, no. 11, pp. 1604–1610, Jul. 2013, doi: 10.1016/j.yexcr.2013.02.012.
[26] R. Schmadeka, B. E. Harmon, and M. Singh, “Triple-Negative Breast Carcinoma,” *American Journal of Clinical Pathology*, vol. 141, no. 4, pp. 462–477, Apr. 2014, doi: 10.1309/AJCPQN8GZ8SILKGN.
[27] K.-L. Lee, G. Chen, T.-Y. Chen, Y.-C. Kuo, and Y.-K. Su, “Effects of Cancer Stem Cells in Triple-Negative Breast Cancer and Brain Metastasis: Challenges and Solutions,” *Cancers (Basel)*, vol. 12, no. 8, p. 2122, Jul. 2020, doi: 10.3390/cancers12082122.

[28] J. Qiu *et al.*, “Comparison of Clinicopathological Features and Prognosis in Triple-Negative and Non-Triple Negative Breast Cancer,” *J Cancer*, vol. 7, no. 2, pp. 167–173, 2016, doi: 10.7150/jca.10944.
[29] Y. Bareche *et al.*, “Unravelling triple-negative breast cancer molecular heterogeneity using an integrative multiomic analysis,” *Annals of Oncology*, vol. 29, no. 4, pp. 895–902, Apr. 2018, doi: 10.1093/annonc/mdy024.
[30] M. D. Burstein *et al.*, “Comprehensive Genomic Analysis Identifies Novel Subtypes and Targets of Triple-Negative Breast Cancer,” *Clinical Cancer Research*, vol. 21, no. 7, pp. 1688–1698, Apr. 2015, doi: 10.1158/1078-0432.CCR-14-0432.
[31] G. Prado-Vázquez *et al.*, “A novel approach to triple-negative breast cancer molecular classification reveals a luminal immune-positive subgroup with good prognoses,” *Scientific Reports*, vol. 9, no. 1, p. 1538, Dec. 2019, doi: 10.1038/s41598-018-38364-y.
[32] K. R. Bauer, M. Brown, R. D. Cress, C. A. Parise, and V. Caggiano, “Descriptive analysis of estrogen receptor (ER)-negative, progesterone receptor (PR)-negative, and HER2-negative invasive breast cancer, the so-called triple-negative phenotype,” *Cancer*, vol. 109, no. 9, pp. 1721–1728, May 2007, doi: 10.1002/cncr.22618.
[33] E. Koedoot *et al.*, “Uncovering the signaling landscape controlling breast cancer cell migration identifies novel metastasis driver genes,” *Nature Communications*, vol. 10, no. 1, p. 2983, Dec. 2019, doi: 10.1038/s41467-019-11020-3.
[34] D. P. Kodack, V. Askoxylakis, G. B. Ferraro, D. Fukumura, and R. K. Jain, “Emerging Strategies for Treating Brain Metastases from Breast Cancer,” *Cancer Cell*, vol. 27, no. 2, pp. 163–175, Feb. 2015, doi: 10.1016/j.ccell.2015.01.001.
[35] K.-L. Lee, Y.-C. Kuo, Y.-S. Ho, and Y.-H. Huang, “Triple-Negative Breast Cancer: Current Understanding and Future Therapeutic Breakthrough Targeting Cancer Stemness,” *Cancers (Basel)*, vol. 11, no. 9, p. 1334, Sep. 2019, doi: 10.3390/cancers11091334.
[36] B. Salhia *et al.*, “Integrated Genomic and Epigenomic Analysis of Breast Cancer Brain Metastasis,” *PLoS ONE*, vol. 9, no. 1, p. e85448, Jan. 2014, doi: 10.1371/journal.pone.0085448.
[37] P. D. Bos *et al.*, “Genes that mediate breast cancer metastasis to the brain,” *Nature*, vol. 459, no. 7249, pp. 1005–1009, Jun. 2009, doi: 10.1038/nature08021.
[38] R. Carvalho, J. Paredes, and A. S. Ribeiro, “Impact of breast cancer cells´ secretome on the brain metastatic niche remodeling,” *Seminars in Cancer Biology*, vol. 60, pp. 294–301, Feb. 2020, doi: 10.1016/j.semcancer.2019.10.011.
[39] L. Jadin *et al.*, “Hyaluronan expression in primary and secondary brain tumors.,” *Ann Transl Med*, vol. 3, no. 6, p. 80, Apr. 2015, doi: 10.3978/j.issn.2305-5839.2015.04.07.
[40] B. P. Toole, “Hyaluronan: from extracellular glue to pericellular cue,” *Nature Reviews Cancer*, vol. 4, no. 7, pp. 528–539, 2004, doi: 10.1038/nrc1391.

[41] A. Kostic, C. D. Lynch, and M. P. Sheetz, “Differential Matrix Rigidity Response in Breast Cancer Cell Lines Correlates with the Tissue Tropism,” *PLoS ONE*, vol. 4, no. 7, p. e6361, Jul. 2009, doi: 10.1371/journal.pone.0006361.
[42] L. Barney, L. Jansen, S. Polio, S. Galarza, M. Lynch, and S. Peyton, “The predictive link between matrix and metastasis,” *Current Opinion in Chemical Engineering*, vol. 11, pp. 85–93, Feb. 2016, doi: 10.1016/j.coche.2016.01.001.
[43] R. J. Weil, D. C. Palmieri, J. L. Bronder, A. M. Stark, and P. S. Steeg, “Breast Cancer Metastasis to the Central Nervous System,” *The American Journal of Pathology*, vol. 167, no. 4, pp. 913–920, Oct. 2005, doi: 10.1016/S0002-9440(10)61180-7.
[44] F. Colin, V. Gensbittel, and J. G. Goetz, “Biomechanics: a driving force behind metastatic progression,” *Comptes Rendus. Biologies*, vol. 344, no. 3, pp. 249–262, Nov. 2021, doi: 10.5802/crbiol.62.
[45] A. Elosegui-Artola *et al.*, “Force Triggers YAP Nuclear Entry by Regulating Transport across Nuclear Pores,” *Cell*, vol. 171, no. 6, pp. 1397-1410.e14, 2017, doi: https://doi.org/10.1016/j.cell.2017.10.008.
[46] T. Moroishi, C. G. Hansen, and K.-L. Guan, “The emerging roles of YAP and TAZ in cancer,” *Nature Reviews Cancer*, vol. 15, no. 2, pp. 73–79, Feb. 2015, doi: 10.1038/nrc3876.
[47] M. E. Fernández-Sánchez *et al.*, “Mechanical induction of the tumorigenic β-catenin pathway by tumour growth pressure,” *Nature*, vol. 523, no. 7558, pp. 92–95, Jul. 2015, doi: 10.1038/nature14329.
[48] N. Xiong *et al.*, “Involvement of caveolin-1 in low shear stress-induced breast cancer cell motility and adhesion: Roles of FAK/Src and ROCK/p-MLC pathways,” *Biochimica et Biophysica Acta (BBA) - Molecular Cell Research*, vol. 1864, no. 1, pp. 12–22, Jan. 2017, doi: 10.1016/j.bbamcr.2016.10.013.
[49] T. Stylianopoulos *et al.*, “Causes, consequences, and remedies for growth-induced solid stress in murine and human tumors,” *Proceedings of the National Academy of Sciences*, vol. 109, no. 38, pp. 15101–15108, Sep. 2012, doi: 10.1073/pnas.1213353109.
[50] D.-H. Kim *et al.*, “Biomechanical interplay between anisotropic re-organization of cells and the surrounding matrix underlies transition to invasive cancer spread,” *Scientific Reports*, vol. 8, no. 1, p. 14210, Dec. 2018, doi: 10.1038/s41598-018-32010-3.
[51] D. T. Butcher, T. Alliston, and V. M. Weaver, “A tense situation: forcing tumour progression,” *Nature Reviews Cancer*, vol. 9, no. 2, pp. 108–122, Feb. 2009, doi: 10.1038/nrc2544.
[52] B. A. Aguado, G. G. Bushnell, S. S. Rao, J. S. Jeruss, and L. D. Shea, “Engineering the pre-metastatic niche,” *Nature Biomedical Engineering*, vol. 1, no. 6, p. 0077, Jun. 2017, doi: 10.1038/s41551-017-0077.
[53] Q. Huang *et al.*, “Fluid shear stress and tumor metastasis,” *Am J Cancer Res*, vol. 8, no. 5, pp. 763–777, May 2018, [Online]. Available: https://pubmed.ncbi.nlm.nih.gov/29888101

[54] A. Spencer *et al.*, “Biomechanical regulation of breast cancer metastasis and progression,” *Scientific Reports*, vol. 11, no. 1, p. 9838, Dec. 2021, doi: 10.1038/s41598-021-89288-z.
[55] H. Y. Choi *et al.*, “Hydrodynamic shear stress promotes epithelial-mesenchymal transition by downregulating ERK and GSK3β activities,” *Breast Cancer Research*, vol. 21, no. 1, p. 6, Dec. 2019, doi: 10.1186/s13058-018-1071-2.
[56] H. J. Lee, A. Ewere, M. F. Diaz, and P. L. Wenzel, “TAZ responds to fluid shear stress to regulate the cell cycle,” *Cell Cycle*, vol. 17, no. 2, pp. 147–153, Jan. 2018, doi: 10.1080/15384101.2017.1404209.
[57] H. J. Lee *et al.*, “Fluid shear stress activates YAP1 to promote cancer cell motility,” *Nat Commun*, vol. 8, p. 14122, Jan. 2017, doi: 10.1038/ncomms14122.
[58] J. Jin, K. Tang, Y. Xin, T. Zhang, and Y. Tan, “Hemodynamic shear flow regulates biophysical characteristics and functions of circulating breast tumor cells reminiscent of brain metastasis,” *Soft Matter*, vol. 14, no. 47, pp. 9528–9533, 2018, doi: 10.1039/c8sm01781f.
[59] J. M. Tse *et al.*, “Mechanical compression drives cancer cells toward invasive phenotype,” *Proceedings of the National Academy of Sciences*, vol. 109, no. 3, pp. 911–916, Jan. 2012, doi: 10.1073/pnas.1118910109.
[60] M. Kalli *et al.*, “Mechanical Compression Regulates Brain Cancer Cell Migration Through MEK1/Erk1 Pathway Activation and GDF15 Expression,” *Frontiers in Oncology*, vol. 9, Sep. 2019, doi: 10.3389/fonc.2019.00992.
[61] J. M. Northcott, I. S. Dean, J. K. Mouw, and V. M. Weaver, “Feeling Stress: The Mechanics of Cancer Progression and Aggression,” *Frontiers in Cell and Developmental Biology*, vol. 6, Feb. 2018, doi: 10.3389/fcell.2018.00017.
[62] G. L. Nicolson, “Cell Membrane Fluid–Mosaic Structure and Cancer Metastasis,” *Cancer Research*, vol. 75, no. 7, pp. 1169–1176, Apr. 2015, doi: 10.1158/0008-5472.CAN-14-3216.
[63] S. A. Gudipaty *et al.*, “Mechanical stretch triggers rapid epithelial cell division through Piezo1,” *Nature*, vol. 543, no. 7643, pp. 118–121, Mar. 2017, doi: 10.1038/nature21407.
[64] J. A. Dombroski, J. M. Hope, N. S. Sarna, and M. R. King, “Channeling the Force: Piezo1 Mechanotransduction in Cancer Metastasis,” *Cells*, vol. 10, no. 11, p. 2815, Oct. 2021, doi: 10.3390/cells10112815.
[65] M. E. Fernández-Sánchez *et al.*, “Mechanical induction of the tumorigenic β-catenin pathway by tumour growth pressure,” *Nature*, vol. 523, no. 7558, pp. 92–95, Jul. 2015, doi: 10.1038/nature14329.
[66] H. T. Nia *et al.*, “Solid stress and elastic energy as measures of tumour mechanopathology,” *Nature Biomedical Engineering*, vol. 1, no. 1, p. 0004, Jan. 2017, doi: 10.1038/s41551-016-0004.
[67] S. Huang and D. E. Ingber, “Cell tension, matrix mechanics, and cancer development,” *Cancer Cell*, vol. 8, no. 3, pp. 175–176, Sep. 2005, doi: 10.1016/j.ccr.2005.08.009.

[68] I. Acerbi *et al.*, “Human breast cancer invasion and aggression correlates with ECM stiffening and immune cell infiltration,” *Integrative Biology*, vol. 7, no. 10, pp. 1120–1134, Oct. 2015, doi: 10.1039/c5ib00040h.
[69] B. Ananthanarayanan, Y. Kim, and S. Kumar, “Elucidating the mechanobiology of malignant brain tumors using a brain matrix-mimetic hyaluronic acid hydrogel platform,” *Biomaterials*, vol. 32, no. 31, pp. 7913–7923, 2011, doi: 10.1016/j.biomaterials.2011.07.005.
[70] A. J. Berger *et al.*, “Scaffold stiffness influences breast cancer cell invasion via EGFR-linked Mena upregulation and matrix remodeling,” *Matrix Biology*, vol. 85–86, pp. 80–93, Jan. 2020, doi: 10.1016/j.matbio.2019.07.006.
[71] C. M. Kraning-Rush, J. P. Califano, and C. A. Reinhart-King, “Cellular Traction Stresses Increase with Increasing Metastatic Potential,” *PLoS ONE*, vol. 7, no. 2, p. e32572, Feb. 2012, doi: 10.1371/journal.pone.0032572.
[72] C. T. Mierke, “The matrix environmental and cell mechanical properties regulate cell migration and contribute to the invasive phenotype of cancer cells,” *Reports on Progress in Physics*, vol. 82, no. 6, p. 064602, Jun. 2019, doi: 10.1088/1361-6633/ab1628.
[73] M. W. Conklin *et al.*, “Aligned collagen is a prognostic signature for survival in human breast carcinoma,” *American Journal of Pathology*, vol. 178, no. 3, pp. 1221–1232, 2011, doi: 10.1016/j.ajpath.2010.11.076.
[74] K. R. Levental *et al.*, “Matrix Crosslinking Forces Tumor Progression by Enhancing Integrin Signaling,” *Cell*, vol. 139, no. 5, pp. 891–906, 2009, doi: https://doi.org/10.1016/j.cell.2009.10.027.
[75] S. Budday, T. C. Ovaert, G. A. Holzapfel, P. Steinmann, and E. Kuhl, *Fifty Shades of Brain: A Review on the Mechanical Testing and Modeling of Brain Tissue*, vol. 27, no. 4. Springer Netherlands, 2019. doi: 10.1007/s11831-019-09352-w.
[76] S. Budday *et al.*, “Mechanical characterization of human brain tissue,” *Acta Biomaterialia*, vol. 48, pp. 319–340, 2017, doi: 10.1016/j.actbio.2016.10.036.
[77] M. M. Knüpfer, H. Poppenborg, M. Hotfilder, K. Kühnel, J.E.A. Wolff, and M. Domula, “CD44 expression and hyaluronic acid binding of malignant glioma cells,” *Clinical & Experimental Metastasis*, vol. 17, no. 1, pp. 81–86, 1999, doi: 10.1023/A:1026425519497.
[78] Y. A. Miroshnikova *et al.*, “Tissue mechanics promote IDH1-dependent HIF1α–tenascin C feedback to regulate glioblastoma aggression,” vol. 18, no. 12, pp. 1336–1345, 2017, doi: 10.1038/ncb3429.Tissue.
[79] A. A. Narkhede, J. H. Crenshaw, R. M. Manning, and S. S. Rao, “The influence of matrix stiffness on the behavior of brain metastatic breast cancer cells in a biomimetic hyaluronic acid hydrogel platform,” *Journal of Biomedical Materials Research Part A*, vol. 106, no. 7, pp. 1832–1841, Jul. 2018, doi: 10.1002/jbm.a.36379.
[80] J. D. Hebert *et al.*, “Proteomic profiling of the ECM of xenograft breast cancer metastases in different organs reveals distinct metastatic niches,” *Cancer Research*, vol. 80, no. 7, pp. 1475–1485, 2020, doi: 10.1158/0008-5472.CAN-19-2961.

[81] N. F. Boyd *et al.*, “Evidence That Breast Tissue Stiffness Is Associated with Risk of Breast Cancer,” *PLoS ONE*, vol. 9, no. 7, p. e100937, Jul. 2014, doi: 10.1371/journal.pone.0100937.
[82] J. Fenner, A. C. Stacer, F. Winterroth, T. D. Johnson, K. E. Luker, and G. D. Luker, “Macroscopic Stiffness of Breast Tumors Predicts Metastasis,” *Scientific Reports*, vol. 4, no. 1, p. 5512, May 2015, doi: 10.1038/srep05512.
[83] Y. Tran *et al.*, “Novel regions of allelic deletion on chromosome 18p in tumors of the lung, brain and breast,” *Oncogene*, vol. 17, no. 26, pp. 3499–3505, Dec. 1998, doi: 10.1038/sj.onc.1202258.
[84] V. Koka *et al.*, “Role of Her-2/neu Overexpression and Clinical Determinants of Early Mortality in Glioblastoma Multiforme,” *American Journal of Clinical Oncology*, vol. 26, no. 4, pp. 332–335, Aug. 2003, doi: 10.1097/01.COC.0000020922.66984.E7.
[85] F. Martino, A. R. Perestrelo, V. Vinarský, S. Pagliari, and G. Forte, “Cellular Mechanotransduction: From Tension to Function,” *Frontiers in Physiology*, vol. 9, Jul. 2018, doi: 10.3389/fphys.2018.00824.
[86] W. Chen *et al.*, “The migration of metastatic breast cancer cells is regulated by matrix stiffness via YAP signalling,” *Heliyon*, vol. 7, no. 2, p. e06252, 2021, doi: https://doi.org/10.1016/j.heliyon.2021.e06252.
[87] M. Aragona *et al.*, “A mechanical checkpoint controls multicellular growth through YAP/TAZ regulation by actin-processing factors,” *Cell*, vol. 154, no. 5, pp. 1047–1059, 2013, doi: 10.1016/j.cell.2013.07.042.
[88] A. Elosegui-Artola *et al.*, “Force Triggers YAP Nuclear Entry by Regulating Transport across Nuclear Pores,” *Cell*, vol. 171, no. 6, pp. 1397-1410.e14, Nov. 2017, doi: 10.1016/j.cell.2017.10.008.
[89] M. E. Fernández-Sánchez *et al.*, “Mechanical induction of the tumorigenic β-catenin pathway by tumour growth pressure,” *Nature*, vol. 523, no. 7558, pp. 92–95, Jul. 2015, doi: 10.1038/nature14329.
[90] B. W. Benham-Pyle, B. L. Pruitt, and W. J. Nelson, “Mechanical strain induces E-cadherin–dependent Yap1 and β-catenin activation to drive cell cycle entry,” *Science (1979)*, vol. 348, no. 6238, pp. 1024–1027, May 2015, doi: 10.1126/science.aaa4559.
[91] F. Zanconato, M. Cordenonsi, and S. Piccolo, “YAP and TAZ: a signalling hub of the tumour microenvironment,” *Nature Reviews Cancer*, vol. 19, no. 8, pp. 454–464, 2019, doi: 10.1038/s41568-019-0168-y.
[92] J. Rosenbluh *et al.*, “β-Catenin-Driven Cancers Require a YAP1 Transcriptional Complex for Survival and Tumorigenesis,” *Cell*, vol. 151, no. 7, pp. 1457–1473, Dec. 2012, doi: 10.1016/j.cell.2012.11.026.
[93] N. Prevarskaya, H. Ouadid-Ahidouch, R. Skryma, and Y. Shuba, “Remodelling of Ca^{2+} transport in cancer: how it contributes to cancer hallmarks?,” *Philosophical Transactions of the Royal Society B: Biological Sciences*, vol. 369, no. 1638, p. 20130097, Mar. 2014, doi: 10.1098/rstb.2013.0097.

[94] B. Coste *et al.*, “Piezo1 and Piezo2 Are Essential Components of Distinct Mechanically Activated Cation Channels,” *Science (1979)*, vol. 330, no. 6000, pp. 55–60, Oct. 2010, doi: 10.1126/science.1193270.
[95] Q. Zhao *et al.*, “Structure and mechanogating mechanism of the Piezo1 channel,” *Nature*, vol. 554, no. 7693, pp. 487–492, Feb. 2018, doi: 10.1038/nature25743.
[96] X.-Z. Fang *et al.*, “Structure, kinetic properties and biological function of mechanosensitive Piezo channels,” *Cell & Bioscience*, vol. 11, no. 1, p. 13, Dec. 2021, doi: 10.1186/s13578-020-00522-z.
[97] K. Saotome, S. E. Murthy, J. M. Kefauver, T. Whitwam, A. Patapoutian, and A. B. Ward, “Structure of the mechanically activated ion channel Piezo1,” *Nature*, vol. 554, no. 7693, pp. 481–486, Feb. 2018, doi: 10.1038/nature25453.
[98] N. Prevarskaya, R. Skryma, and Y. Shuba, “Calcium in tumour metastasis: new roles for known actors,” *Nature Reviews Cancer*, vol. 11, no. 8, pp. 609–618, Aug. 2011, doi: 10.1038/nrc3105.
[99] P. A. Gottlieb, “A Tour de Force,” 2017, pp. 1–36. doi: 10.1016/bs.ctm.2016.11.007.
[100] Z. Pethő, K. Najder, E. Bulk, and A. Schwab, “Mechanosensitive ion channels push cancer progression,” *Cell Calcium*, vol. 80, pp. 79–90, Jun. 2019, doi: 10.1016/j.ceca.2019.03.007.
[101] N. Prevarskaya, R. Skryma, and Y. Shuba, “Ion Channels in Cancer: Are Cancer Hallmarks Oncochannelopathies?,” *Physiological Reviews*, vol. 98, no. 2, pp. 559–621, Apr. 2018, doi: 10.1152/physrev.00044.2016.
[102] C. Li *et al.*, “Piezo1 forms mechanosensitive ion channels in the human MCF-7 breast cancer cell line,” *Scientific Reports*, vol. 5, no. 1, p. 8364, Jul. 2015, doi: 10.1038/srep08364.
[103] C. Pardo-Pastor *et al.*, “Piezo2 channel regulates RhoA and actin cytoskeleton to promote cell mechanobiological responses,” *Proceedings of the National Academy of Sciences*, vol. 115, no. 8, pp. 1925–1930, Feb. 2018, doi: 10.1073/pnas.1718177115.
[104] W. Lou *et al.*, “Five miRNAs-mediated PIEZO2 downregulation, accompanied with activation of Hedgehog signaling pathway, predicts poor prognosis of breast cancer,” *Aging*, vol. 11, no. 9, pp. 2628–2652, May 2019, doi: 10.18632/aging.101934.
[105] M. Weller *et al.*, “Glioma,” *Nature Reviews Disease Primers*, vol. 1, no. 1, p. 15017, Dec. 2015, doi: 10.1038/nrdp.2015.17.
[106] X. Chen *et al.*, “A Feedforward Mechanism Mediated by Mechanosensitive Ion Channel PIEZO1 and Tissue Mechanics Promotes Glioma Aggression,” *Neuron*, vol. 100, no. 4, pp. 799-815.e7, Nov. 2018, doi: 10.1016/j.neuron.2018.09.046.
[107] R. Emig *et al.*, “Piezo1 Channels Contribute to the Regulation of Human Atrial Fibroblast Mechanical Properties and Matrix Stiffness Sensing,” *Cells*, vol. 10, no. 3, p. 663, Mar. 2021, doi: 10.3390/cells10030663.
[108] K. T. Chan, D. A. Bennin, and A. Huttenlocher, “Regulation of Adhesion Dynamics by Calpain-mediated Proteolysis of Focal Adhesion Kinase (FAK),”

Journal of Biological Chemistry, vol. 285, no. 15, pp. 11418–11426, Apr. 2010, doi: 10.1074/jbc.M109.090746.
[109] H. Yang *et al.*, "Piezo2 protein: A novel regulator of tumor angiogenesis and hyperpermeability," *Oncotarget*, vol. 7, no. 28, pp. 44630–44643, Jul. 2016, doi: 10.18632/oncotarget.10134.
[110] J. Mo, H. W. Park, and K. Guan, "The Hippo signaling pathway in stem cell biology and cancer," *EMBO Rep*, vol. 15, no. 6, pp. 642–656, Jun. 2014, doi: 10.15252/embr.201438638.
[111] R. Johnson and G. Halder, "The two faces of Hippo: targeting the Hippo pathway for regenerative medicine and cancer treatment," *Nature Reviews Drug Discovery*, vol. 13, no. 1, pp. 63–79, Jan. 2014, doi: 10.1038/nrd4161.
[112] S. Dupont *et al.*, "Role of YAP/TAZ in mechanotransduction," *Nature*, vol. 474, no. 7350, pp. 179–183, 2011, doi: 10.1038/nature10137.
[113] S. Dupont *et al.*, "Role of YAP/TAZ in mechanotransduction," *Nature*, vol. 474, no. 7350, pp. 179–183, Jun. 2011, doi: 10.1038/nature10137.
[114] S. Piccolo, S. Dupont, and M. Cordenonsi, "The biology of YAP/TAZ: Hippo signaling and beyond," *Physiological Reviews*, vol. 94, no. 4, pp. 1287–1312, 2014, doi: 10.1152/physrev.00005.2014.
[115] F. Zanconato, M. Cordenonsi, and S. Piccolo, "YAP/TAZ at the Roots of Cancer," *Cancer Cell*, vol. 29, no. 6, pp. 783–803, Jun. 2016, doi: 10.1016/j.ccell.2016.05.005.
[116] C. Peng *et al.*, "Regulation of the Hippo-YAP Pathway by Glucose Sensor O-GlcNAcylation," *Molecular Cell*, vol. 68, no. 3, pp. 591-604.e5, Nov. 2017, doi: 10.1016/j.molcel.2017.10.010.
[117] E. Kim *et al.*, "*O* -GlcNAcylation on LATS2 disrupts the Hippo pathway by inhibiting its activity," *Proceedings of the National Academy of Sciences*, vol. 117, no. 25, pp. 14259–14269, Jun. 2020, doi: 10.1073/pnas.1913469117.
[118] K.-I. Wada, K. Itoga, T. Okano, S. Yonemura, and H. Sasaki, "Hippo pathway regulation by cell morphology and stress fibers," *Development*, vol. 138, no. 18, pp. 3907 LP – 3914, Sep. 2011, doi: 10.1242/dev.070987.
[119] S. Tavares *et al.*, "Actin stress fiber organization promotes cell stiffening and proliferation of pre-invasive breast cancer cells," *Nature Communications*, vol. 8, no. 1, p. 15237, 2017, doi: 10.1038/ncomms15237.
[120] J. Du *et al.*, "Extracellular matrix stiffness dictates Wnt expression through integrin pathway," *Scientific Reports*, vol. 6, no. 1, p. 20395, Apr. 2016, doi: 10.1038/srep20395.
[121] D. Buechel *et al.*, "Parsing β-catenin's cell adhesion and Wnt signaling functions in malignant mammary tumor progression," *Proceedings of the National Academy of Sciences*, vol. 118, no. 34, Aug. 2021, doi: 10.1073/pnas.2020227118.
[122] J. Wang, J. Jiang, X. Yang, G. Zhou, L. Wang, and B. Xiao, "Tethering Piezo channels to the actin cytoskeleton for mechanogating via the cadherin-β-catenin mechanotransduction complex," *Cell Reports*, vol. 38, no. 6, p. 110342, Feb. 2022, doi: 10.1016/j.celrep.2022.110342.

[123] B. T. MacDonald, K. Tamai, and X. He, “Wnt/β-Catenin Signaling: Components, Mechanisms, and Diseases,” *Developmental Cell*, vol. 17, no. 1, pp. 9–26, Jul. 2009, doi: 10.1016/j.devcel.2009.06.016.
[124] K. S. Kang and A. G. Robling, “New Insights into Wntâ€“Lrp5/6â€“Î²-Catenin Signaling in Mechanotransduction,” *Frontiers in Endocrinology*, vol. 5, Jan. 2015, doi: 10.3389/fendo.2014.00246.
[125] B. W. Benham-Pyle, B. L. Pruitt, and W. J. Nelson, “Mechanical strain induces E-cadherin–dependent Yap1 and β-catenin activation to drive cell cycle entry,” *Science (1979)*, vol. 348, no. 6238, pp. 1024–1027, May 2015, doi: 10.1126/science.aaa4559.
[126] V. Tajadura *et al.*, “β-catenin promotes endothelial survival by regulating eNOS activity and flow-dependent anti-apoptotic gene expression,” *Cell Death & Disease*, vol. 11, no. 6, p. 493, Jun. 2020, doi: 10.1038/s41419-020-2687-6.
[127] W.-K. Yu *et al.*, “Targeting β-Catenin Signaling by Natural Products for Cancer Prevention and Therapy,” *Frontiers in Pharmacology*, vol. 11, Jun. 2020, doi: 10.3389/fphar.2020.00984.
[128] H. Yamaguchi *et al.*, “Stromal Fibroblasts Mediate Extracellular Matrix Remodeling and Invasion of Scirrhous Gastric Carcinoma Cells,” *PLoS ONE*, vol. 9, no. 1, p. e85485, Jan. 2014, doi: 10.1371/journal.pone.0085485.
[129] T. Liu *et al.*, “The β-catenin/YAP signaling axis is a key regulator of melanoma-associated fibroblasts,” *Signal Transduction and Targeted Therapy*, vol. 4, no. 1, p. 63, Dec. 2019, doi: 10.1038/s41392-019-0100-7.
[130] Z. Wang, J. Ye, Y. Deng, Z. Yan, S. Denduluri, and T.-C. He, “Wnt versus Hippo: A balanced act or dynamic duo?,” *Genes & Diseases*, vol. 1, no. 2, pp. 127–128, Dec. 2014, doi: 10.1016/j.gendis.2014.09.001.
[131] H. W. Park *et al.*, “Alternative Wnt Signaling Activates YAP/TAZ,” *Cell*, vol. 162, no. 4, pp. 780–794, Aug. 2015, doi: 10.1016/j.cell.2015.07.013.
[132] T. Bardelli, C. Marano, and F. Briatico Vangosa, “Polydimethylsiloxane crosslinking kinetics: A systematic study on Sylgard184 comparing rheological and thermal approaches,” *Journal of Applied Polymer Science*, vol. 138, no. 39, p. 51013, Oct. 2021, doi: 10.1002/app.51013.
[133] R. N. Palchesko, L. Zhang, Y. Sun, and A. W. Feinberg, “Development of Polydimethylsiloxane Substrates with Tunable Elastic Modulus to Study Cell Mechanobiology in Muscle and Nerve,” *PLoS ONE*, vol. 7, no. 12, p. e51499, Dec. 2012, doi: 10.1371/journal.pone.0051499.
[134] T. C. T. Ting and T. Chen, “Poisson’s ratio for anisotropic elastic materials can have no bounds,” *The Quarterly Journal of Mechanics and Applied Mathematics*, vol. 58, no. 1, pp. 73–82, Feb. 2005, doi: 10.1093/qjmamj/hbh021.
[135] W. Zhang, D. S. Choi, Y. H. Nguyen, J. Chang, and L. Qin, “Studying Cancer Stem Cell Dynamics on PDMS Surfaces for Microfluidics Device Design,” *Scientific Reports*, vol. 3, no. 1, p. 2332, Dec. 2013, doi: 10.1038/srep02332.
[136] A. A. Narkhede, J. H. Crenshaw, R. M. Manning, and S. S. Rao, “The influence of matrix stiffness on the behavior of brain metastatic breast cancer cells in a biomimetic hyaluronic acid hydrogel platform,” *Journal of Biomedical Materials*

Research Part A, vol. 106, no. 7, pp. 1832–1841, Jul. 2018, doi: 10.1002/jbm.a.36379.
[137] C. Peng *et al.*, "Regulation of the Hippo-YAP Pathway by Glucose Sensor O-GlcNAcylation," *Molecular Cell*, vol. 68, no. 3, pp. 591-604.e5, Nov. 2017, doi: 10.1016/j.molcel.2017.10.010.
[138] E. Kima *et al.*, "O-GlcNAcylation on LATS2 disrupts the Hippo pathway by inhibiting its activity," *Proc Natl Acad Sci U S A*, vol. 117, no. 25, pp. 14259–14269, 2020, doi: 10.1073/pnas.1913469117.
[139] A. Choudhury, N. C. Das, R. Patra, and S. Mukherjee, "In silico analyses on the comparative sensing of SARS-CoV-2 mRNA by the intracellular TLRs of humans," *Journal of Medical Virology*, vol. 93, no. 4, pp. 2476–2486, Apr. 2021, doi: 10.1002/jmv.26776.
[140] J. Sandholm and K. S. Selander, "Toll-Like Receptor 9 in Breast Cancer," *Frontiers in Immunology*, vol. 5, Jul. 2014, doi: 10.3389/fimmu.2014.00330.
[141] W. Yu, Y. Bai, A. Raha, Z. Su, and F. Geng, "Integrative In Silico Investigation Reveals the Host-Virus Interactions in Repurposed Drugs Against SARS-CoV-2," *Frontiers in Bioinformatics*, vol. 1, Jan. 2022, doi: 10.3389/fbinf.2021.763540.
[142] M. Liu, J. Sun, Y. Sun, C. Bock, and Q. Chen, "Thickness-dependent mechanical properties of polydimethylsiloxane membranes," *Journal of Micromechanics and Microengineering*, vol. 19, no. 3, p. 035028, Mar. 2009, doi: 10.1088/0960-1317/19/3/035028.
[143] K. Pogoda *et al.*, "Soft Substrates Containing Hyaluronan Mimic the Effects of Increased Stiffness on Morphology, Motility, and Proliferation of Glioma Cells," *Biomacromolecules*, vol. 18, no. 10, pp. 3040–3051, Oct. 2017, doi: 10.1021/acs.biomac.7b00324.
[144] L. Wullkopf *et al.*, "Cancer cells' ability to mechanically adjust to extracellular matrix stiffness correlates with their invasive potential," *Molecular Biology of the Cell*, vol. 29, no. 20, pp. 2378–2385, Oct. 2018, doi: 10.1091/mbc.E18-05-0319.
[145] W. J. Ashby and A. Zijlstra, "Established and novel methods of interrogating two-dimensional cell migration," *Integrative Biology*, vol. 4, no. 11, p. 1338, 2012, doi: 10.1039/c2ib20154b.
[146] J. M. Franklin, R. P. Ghosh, Q. Shi, M. P. Reddick, and J. T. Liphardt, "Concerted localization-resets precede YAP-dependent transcription," *Nature Communications*, vol. 11, no. 1, p. 4581, Dec. 2020, doi: 10.1038/s41467-020-18368-x.
[147] N. O. Deakin, J. Pignatelli, and C. E. Turner, "Diverse Roles for the Paxillin Family of Proteins in Cancer," *Genes & Cancer*, vol. 3, no. 5–6, pp. 362–370, May 2012, doi: 10.1177/1947601912458582.
[148] X. Zhang *et al.*, "The essential role of YAP O-GlcNAcylation in high-glucose-stimulated liver tumorigenesis," *Nature Communications*, vol. 8, no. 1, p. 15280, Aug. 2017, doi: 10.1038/ncomms15280.
[149] X. Li *et al.*, "OGT regulated O-GlcNAcylation promotes papillary thyroid cancer malignancy via activating YAP," *Oncogene*, vol. 40, no. 30, pp. 4859–4871, Jul. 2021, doi: 10.1038/s41388-021-01901-7.

[150] R. Friedman, K. Boye, and K. Flatmark, “Molecular modelling and simulations in cancer research,” *Biochimica et Biophysica Acta (BBA) - Reviews on Cancer*, vol. 1836, no. 1, pp. 1–14, Aug. 2013, doi: 10.1016/j.bbcan.2013.02.001.
[151] B. L. Doss *et al.*, “Cell response to substrate rigidity is regulated by active and passive cytoskeletal stress,” *Proceedings of the National Academy of Sciences*, vol. 117, no. 23, p. 12817, Jun. 2020, doi: 10.1073/pnas.1917555117.
[152] N. M. E. Ayad, S. Kaushik, and V. M. Weaver, “Tissue mechanics, an important regulator of development and disease,” *Philosophical Transactions of the Royal Society B: Biological Sciences*, vol. 374, no. 1779, p. 20180215, Aug. 2019, doi: 10.1098/rstb.2018.0215.
[153] T. A. Ulrich, E. M. de Juan Pardo, and S. Kumar, “The mechanical rigidity of the extracellular matrix regulates the structure, motility, and proliferation of glioma cells,” *Cancer Res*, vol. 69, no. 10, pp. 4167–4174, May 2009, doi: 10.1158/0008-5472.CAN-08-4859.
[154] W. J. Tyler, “The mechanobiology of brain function,” *Nature Reviews Neuroscience*, vol. 13, no. 12, pp. 867–878, 2012, doi: 10.1038/nrn3383.
[155] S. Chatelin, A. Constantinesco, and R. Willinger, “Fifty years of brain tissue mechanical testing: From in vitro to in vivo investigations,” *Biorheology*, vol. 47, pp. 255–276, 2010, doi: 10.3233/BIR-2010-0576.
[156] G. Franceschini, D. Bigoni, P. Regitnig, and G. A. Holzapfel, “Brain tissue deforms similarly to filled elastomers and follows consolidation theory,” *Journal of the Mechanics and Physics of Solids*, vol. 54, no. 12, pp. 2592–2620, Dec. 2006, doi: 10.1016/j.jmps.2006.05.004.
[157] F. Pervin and W. W. Chen, “Dynamic mechanical response of bovine gray matter and white matter brain tissues under compression,” *Journal of Biomechanics*, vol. 42, no. 6, pp. 731–735, Apr. 2009, doi: 10.1016/j.jbiomech.2009.01.023.
[158] S. Budday *et al.*, “Mechanical properties of gray and white matter brain tissue by indentation,” *Journal of the Mechanical Behavior of Biomedical Materials*, vol. 46, pp. 318–330, 2015, doi: https://doi.org/10.1016/j.jmbbm.2015.02.024.
[159] I. Sack *et al.*, “The impact of aging and gender on brain viscoelasticity,” *Neuroimage*, vol. 46, no. 3, pp. 652–657, Jul. 2009, doi: 10.1016/j.neuroimage.2009.02.040.
[160] L. Alhalhooly, B. Mamnoon, J. Kim, S. Mallik, and Y. Choi, “Dynamic cellular biomechanics in responses to chemotherapeutic drug in hypoxia probed by atomic force spectroscopy,” *Oncotarget*, vol. 12, no. 12, pp. 1165–1177, Jun. 2021, doi: 10.18632/oncotarget.27974.
[161] S. Chatelin, J. Vappou, S. Roth, J. S. Raul, and R. Willinger, “Towards child versus adult brain mechanical properties,” *Journal of the Mechanical Behavior of Biomedical Materials*, vol. 6, pp. 166–173, Feb. 2012, doi: 10.1016/j.jmbbm.2011.09.013.
[162] J. Weickenmeier, R. de Rooij, S. Budday, P. Steinmann, T. C. Ovaert, and E. Kuhl, “Brain stiffness increases with myelin content,” *Acta Biomaterialia*, vol. 42, pp. 265–272, 2016, doi: 10.1016/j.actbio.2016.07.040.

[163] H. Atcha *et al.*, “Mechanically activated ion channel Piezo1 modulates macrophage polarization and stiffness sensing,” *Nature Communications*, vol. 12, no. 1, p. 3256, Dec. 2021, doi: 10.1038/s41467-021-23482-5.
[164] A. Nukuda *et al.*, “Stiff substrates increase YAP-signaling-mediated matrix metalloproteinase-7 expression,” *Oncogenesis*, vol. 4, no. July, pp. 1–11, 2015, doi: 10.1038/oncsis.2015.24.
[165] J. Du *et al.*, “Extracellular matrix stiffness dictates Wnt expression through integrin pathway,” *Scientific Reports*, vol. 6, no. 1, p. 20395, Apr. 2016, doi: 10.1038/srep20395.
[166] K. Hasegawa, S. Fujii, S. Matsumoto, Y. Tajiri, A. Kikuchi, and T. Kiyoshima, “<scp>YAP</scp> signaling induces <scp>PIEZO1</scp> to promote oral squamous cell carcinoma cell proliferation,” *The Journal of Pathology*, vol. 253, no. 1, pp. 80–93, Jan. 2021, doi: 10.1002/path.5553.
[167] W. Zhou *et al.*, “Identification of PIEZO1 as a potential prognostic marker in gliomas,” *Scientific Reports*, vol. 10, no. 1, p. 16121, 2020, doi: 10.1038/s41598-020-72886-8.
[168] M. Javier-Torrent, G. Zimmer-Bensch, and L. Nguyen, “Mechanical Forces Orchestrate Brain Development,” *Trends in Neurosciences*, Dec. 2020, doi: 10.1016/j.tins.2020.10.012.
[169] D. E. Koser *et al.*, “Mechanosensing is critical for axon growth in the developing brain,” *Nature Neuroscience*, vol. 19, no. 12, pp. 1592–1598, Dec. 2016, doi: 10.1038/nn.4394.
[170] M. M. Pathak *et al.*, “Stretch-activated ion channel Piezo1 directs lineage choice in human neural stem cells.,” *Proc Natl Acad Sci U S A*, vol. 111, no. 45, pp. 16148–53, Nov. 2014, doi: 10.1073/pnas.1409802111.
[171] M. Velasco-Estevez *et al.*, “Infection Augments Expression of Mechanosensing Piezo1 Channels in Amyloid Plaque-Reactive Astrocytes,” *Frontiers in Aging Neuroscience*, vol. 10, Oct. 2018, doi: 10.3389/fnagi.2018.00332.
[172] T. Panciera *et al.*, “Reprogramming normal cells into tumour precursors requires ECM stiffness and oncogene-mediated changes of cell mechanical properties,” *Nature Materials*, vol. 19, no. 7, pp. 797–806, 2020, doi: 10.1038/s41563-020-0615-x.
[173] M. M. Pathak *et al.*, “Stretch-activated ion channel Piezo1 directs lineage choice in human neural stem cells,” *Proceedings of the National Academy of Sciences*, vol. 111, no. 45, pp. 16148–16153, Nov. 2014, doi: 10.1073/pnas.1409802111.
[174] Y. Yu *et al.*, “Piezo1 regulates migration and invasion of breast cancer cells via modulating cell mechanobiological properties,” *Acta Biochimica et Biophysica Sinica*, Nov. 2020, doi: 10.1093/abbs/gmaa112.
[175] J. Seong, N. Wang, and Y. Wang, “Mechanotransduction at focal adhesions: from physiology to cancer development,” *Journal of Cellular and Molecular Medicine*, vol. 17, no. 5, pp. 597–604, May 2013, doi: https://doi.org/10.1111/jcmm.12045.
[176] A. Ray *et al.*, “Anisotropic forces from spatially constrained focal adhesions mediate contact guidance directed cell migration,” *Nature Communications*, vol. 8, no. 1, p. 14923, Apr. 2017, doi: 10.1038/ncomms14923.

[177] V. Gkretsi and T. Stylianopoulos, “Cell Adhesion and Matrix Stiffness: Coordinating Cancer Cell Invasion and Metastasis,” *Frontiers in Oncology*, vol. 8, May 2018, doi: 10.3389/fonc.2018.00145.
[178] L. Neufeld *et al.*, “Microengineered perfusable 3D-bioprinted glioblastoma model for in vivo mimicry of tumor microenvironment,” *Science Advances*, vol. 7, no. 34, Aug. 2021, doi: 10.1126/sciadv.abi9119.
[179] B. Zhao *et al.*, “Inactivation of YAP oncoprotein by the Hippo pathway is involved in cell contact inhibition and tissue growth control,” *Genes & Development*, vol. 21, no. 21, pp. 2747–2761, Nov. 2007, doi: 10.1101/gad.1602907.
[180] “Cell Scale Biomaterials Testing,” 2022. https://www.cellscale.com/products/microtester/ (accessed Apr. 20, 2022).

Supplemental Figures

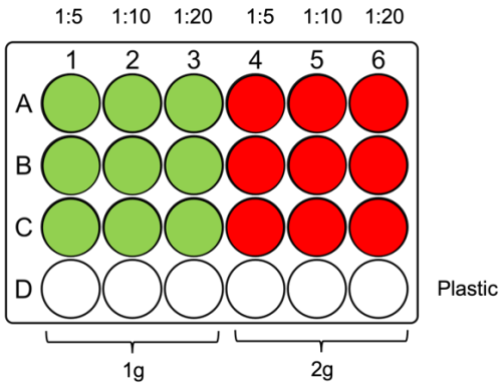

Figure S1: PDMS plate design for substrate characterization

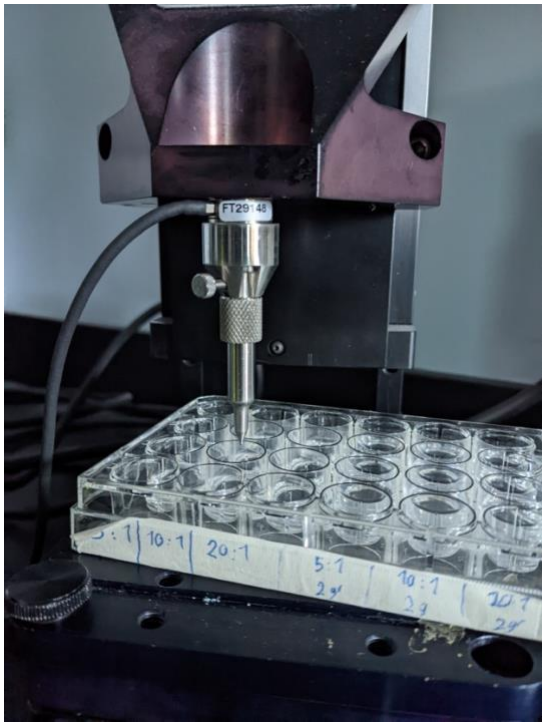

Figure S2: Picture of Biomomentum mechanical testing set-up with spherical indenter attachment

Table S1: Stiffness values of different PDMS formulations

Stiffness of PDMS (MPa)		
Ratio	**1g of PDMS**	**2g of PDMS**
1:5	1.47	1.26
1:10	2.30	1.89
1:20	0.48	0.57

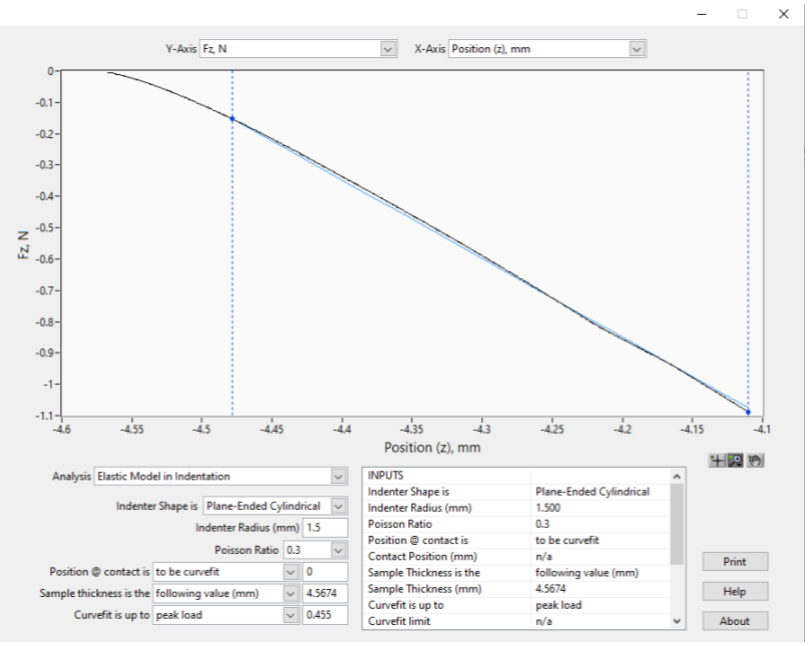

Figure S3: Biomomentum raw data force vs displacement graph for PDMS testing. Data fitted to bounds highlighted in blue dashed lines corresponding to the linear region of the curve.

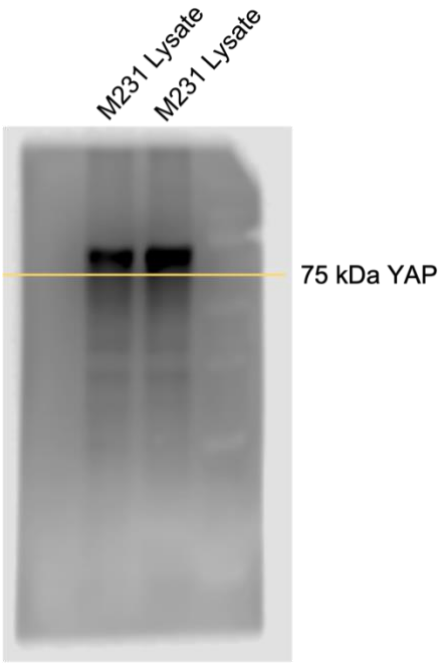

Figure S4: Positive control Immunoblot for YAP using MDA-MB-231 cell lines with high expression of YAP

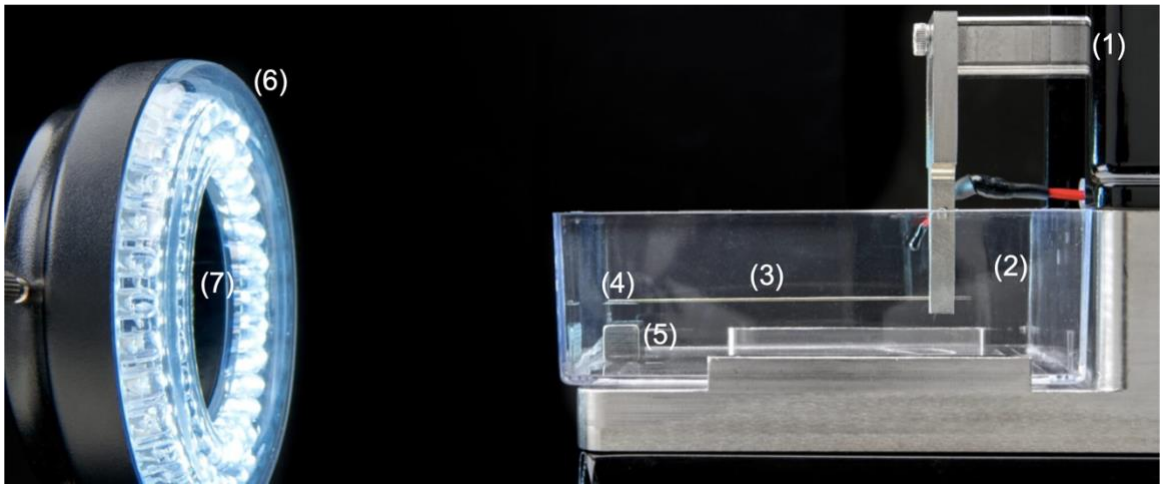

Figure S5: Microtester compression testing setup. (1) Piezo-electric actuator. (2) Fluid bath. (3) Cantilever. (4) 6x6mm platen. (5) Sample (example specimen). (6) Ring light. (7) CCD Camera housed in the center of the ring light [180].

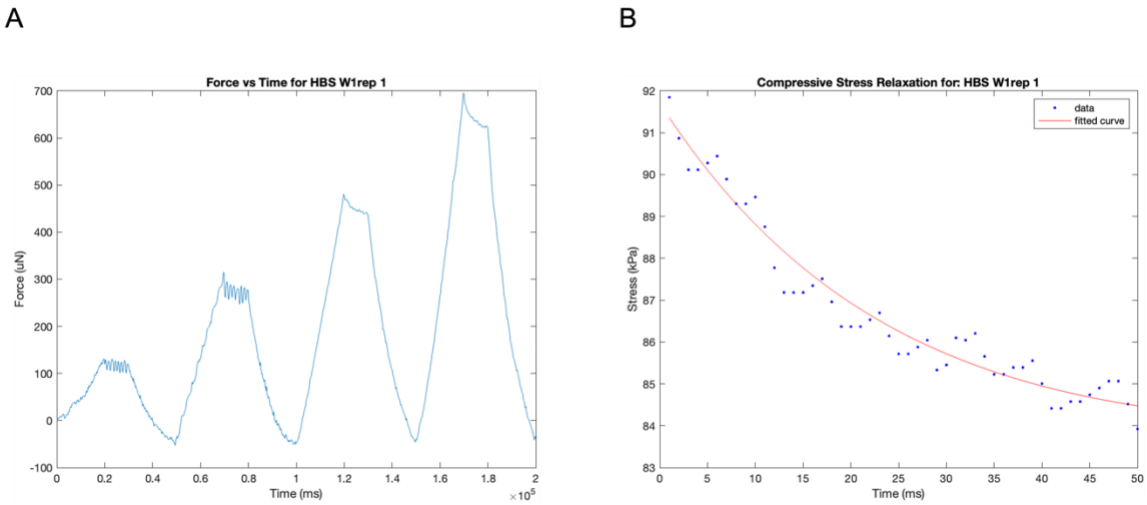

Figure S6: Isolating viscoelastic response in brain tissue from stepwise ramp compression of human brain specimen. (A) Initial stepwise compression profile. (B) stress relaxation curve isolated from third cyclic loading cycle at 7.5% strain with curve fitting applied using Zener model.

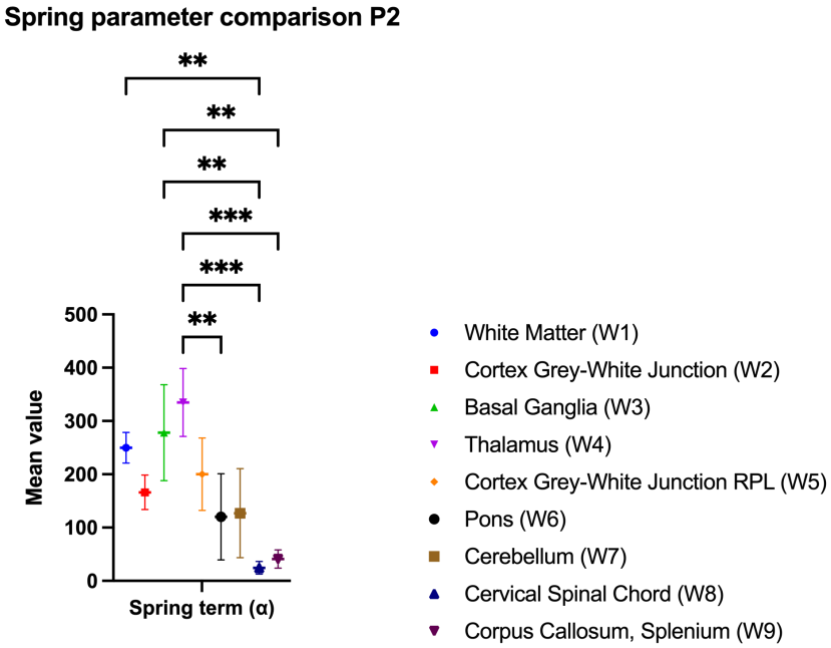

Figure S7: Spring parameter significant pairwise comparisons based on one-way ANOVA

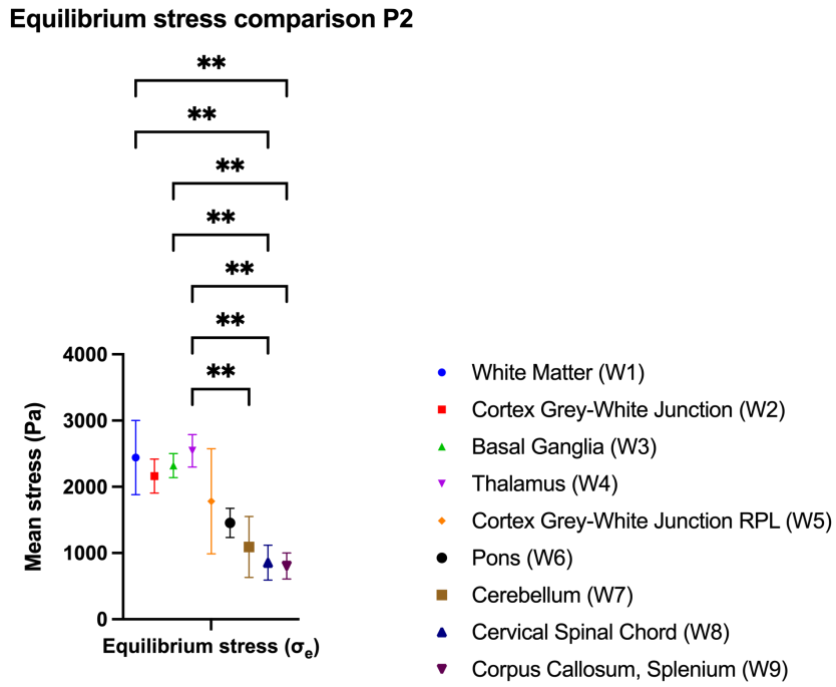

Figure S8: Equilibrium stress parameter significant pairwise comparisons based on one-way ANOVA

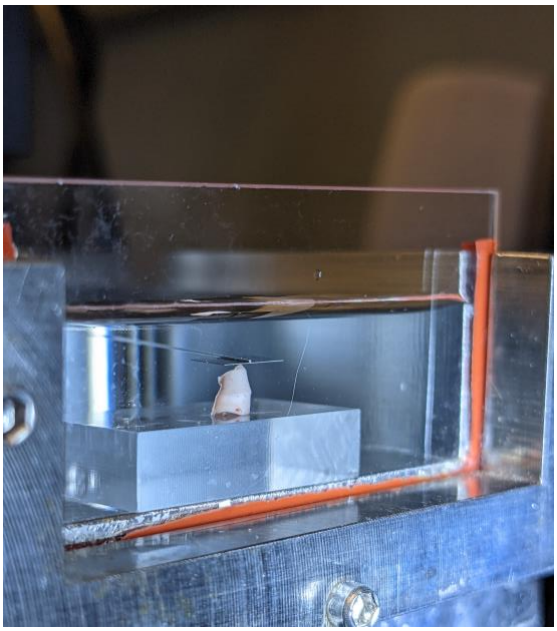

Figure S9: Brain sample submerged in PBS to prevent osmotic degradation during compression testing.

Table S2: Patient 1 - Coefficient Determination from Zener Model curve fitting

Brain Region	Replicates	α	b	σ_e	r-squared value
	rep1	91.41165	-0.05135	964.8255	0.959
	rep2	136.1192	-0.03898	1460.181	0.7884
W1	rep3	381.9289	-0.04803	2252.516	0.9787
	rep1	435.3257	-0.04281	1973.992	0.9789
	rep2	316.5571	-0.04731	2126.828	0.9128
W2 Grey Matter	rep3	649.734	-0.05468	3389.798	0.9893
	rep1	105.4231	-0.03824	1017.205	0.7695
	rep2	79.99644	-0.04333	992.0801	0.8456
W2 White Matter	rep3	149.3454	-0.04785	1131.39	0.7132
	rep1	240.9061	-0.05037	1055.954	0.8245
	rep2	249.7659	-0.05868	1393.826	0.9875
W2 G/W Junction	rep3	177.4251	-0.04423	1560.301	0.9478
	rep1	743.636	-0.05192	3743.988	0.9736
	rep2	347.5703	-0.05818	2081.369	0.9678
W3	rep3	319.4722	-0.0574	2166.949	0.9651
	rep1	54.39773	-0.00663	1312.603	0.0343
	rep2	654.1276	-0.08226	1818.181	0.9781
W4	rep3	89.72309	-0.04174	1047.829	0.71
	rep1	281.5067	-0.04702	2250.093	0.9721
	rep2	410.9429	-0.05882	2941.758	0.9771
W5	rep3	416.6448	-0.04888	2313.493	0.964
	rep1	111.6971	-0.00918	1571.441	0.0854
	rep2	459.8523	-0.00308	3319.127	0.0088
W6	rep3	175.9518	-0.05254	1785.331	0.8882
	rep1	164.4616	-0.05156	1394.135	0.8596
	rep2	53.34803	-0.00493	954.1258	0.0151
W7	rep3	177.0611	-0.01827	2008.309	0.3893
	rep1	125.5705	-0.04968	1594.692	0.8736
	rep2	281.5771	-0.04511	2134.946	0.9084
W8	rep3	433.0057	-0.04388	1702.141	0.8569

Table S3: Patient 2 - Coefficient Determination from Zener Model curve fitting

Brain Region	Replicates	α	b	σ_e	r-sqrd value	
	rep1	259.751	-0.03512	3089.0387	0.5999	
	rep2	217.5146	-0.01605	2136.4908	0.1847	
W1	rep3	272.3917	-0.03492	2100.1946	0.7917	
	rep1	154.5964	-0.04078	2380.0552	0.8859	
	rep2	141.3836	-0.0472	2229.2765	0.9038	
W2	rep3	202.582	-0.03239	1879.2266	0.82	
	rep1	277.8734	-0.05355	2519.4977	0.9803	
	rep2	188.0985	-0.04434	2168.5778	0.6753	
W3	rep3	368.3398	-0.02218	2272.0556	0.2469	
	rep1	262.7411	-0.04566	2268.7062	0.9733	
	rep2	358.6463	-0.04076	2735.2432	0.8385	
W4	rep3	383.3643	-0.02214	2629.8606	0.5304	
	rep1	272.9859	-0.03851	1789.6778	0.7496	
	rep2	138.6988	-0.02432	985.56361	0.556	
W5	rep3	188.9532	-0.0381	2572.9292	0.7222	
	rep1	151.4573	-0.04189	1613.1747	0.8187	
	rep2	28.29546	0.021154	1204.5635	0.228	**overfit
W6	rep3	180.6558	-0.04356	1550.2716	0.7914	
	rep1	34.14437	-0.02725	928.67464	0.582	
	rep2	150.8122	-0.04015	735.53412	0.8173	
W7	rep3	196.2419	-0.05004	1610.659	0.8581	
	rep1	24.27678	-0.00977	1122.734	0.0221	
	rep2	12.82488	-0.02617	844.11179	0.3457	
W8	rep3	36.50286	-0.04397	597.0587	0.7822	
	rep1	34.40851	-0.02696	856.88477	0.4418	
	rep2	60.25951	-0.02352	587.45805	0.7451	
W9	rep3	28.42702	-0.03072	972.15351	0.6235	